1 OF 1

N82-20143 UNCLAS

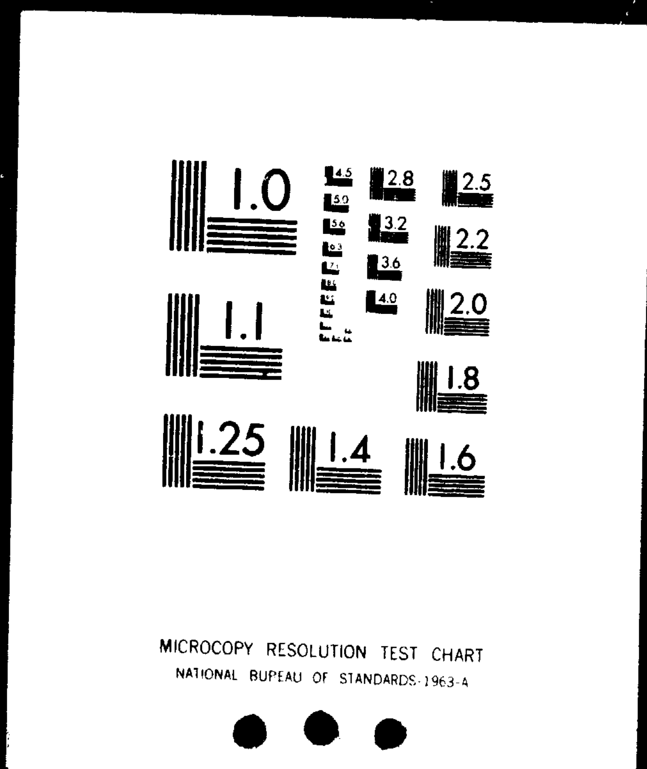

NASA CONTRACTOR REPORT 166279

(NASA-CR-166279) TESTS AND ANALYSIS OF A VENTED D THRUST DEFLECTING NOZZLE ON A TURBOFAN ENGINE Final Report, Mar. 1980 - Mar. 1982 (McDonnell Aircraft Co.) 78 p HC A05/MF A01 CSCL 21E G3/02

N82-20143

Unclas 09297

Test and Analysis of a Vented "D" Thrust Deflecting Nozzle on a Turbofan Engine

E. W. Rosenberg

CONTRACT NAS2-10564
March 1982

NASA

NASA CONTRACTOR REPORT 166279

Test and Analysis of a Vented "D" Thrust Deflecting Nozzle on a Turbofan Engine

E. W. Rosenberg
McDonnell Aircraft Company
P.O. Box 516
St. Louis, Missouri 63166

Prepared for
Ames Research Center
under Contract NAS2-10564

National Aeronautics and
Space Administration

Ames Research Center
Moffett Field, California 94035

SUMMARY

Static tests of a large scale "D" vented thrust deflecting nozzle were conducted at the Outdoor Aerodynamic Research Facility of the NASA-Ames Research Center. The overall objective of the test program was to demonstrate the capabilities of a "D" vented nozzle with a high bypass ratio turbofan engine. Specific objectives were to (1) obtain nozzle performance characteristics "in" and "out" of ground effects; (2) demonstrate the compatibility of the nozzle with a turbofan engine; (3) obtain pressure and temperature distributions on the surface of the "D" vented nozzle and (4) establish a correlation of the nozzle performance between small scale and large scale models.

The test nozzle was a "boilerplate" model of the MCAIR "D" vented nozzle configured for operation with a General Electric YTF-34-F5 turbofan engine. Calibration of the engine with a simple convergent nozzle was performed with three different nozzle exit areas to establish reference thrust, nozzle pressure ratio, and nozzle corrected flow characteristics for comparison with the thrust vectoring data. The "D" vented nozzle was configured to provide (1) a thrust vectoring range of 0° to 115°; (2) a yaw vectoring range of 0° to 10°; (3) variable nozzle area control; and (4) variable spacing between the core exit and nozzle entrance station. Extensive pressure and temperature instrumentation was installed throughout the model.

SIGNIFICANT TEST RESULTS

- Compatibility between the YTF-34-F5 turbofan engine and the "D" vented nozzle was demonstrated. There were no significant effects of nozzle vectoring on engine operation.

- Velocity coefficients of 0.96 and greater were obtained for 90° of thrust vectoring. These levels verify that the "D" vented nozzle is a highly efficient thrust vectoring device for subsonic V/STOL aircraft applications.

- Measurement of nozzle wall temperatures showed that the walls remained cool ($\leq$ 50°C) during all test conditions. This means that production nozzles will not require high temperature materials.

- Good agreement was achieved between the current large scale (72%) and previous small scale (10%) data in the operating range of interest.

- In ground effect, the vented nozzle design was found to maintain thrust and airflow as the ratio of ground height to nozzle diameter was reduced to 1.03. No performance deterioration or engine/nozzle compatibility problems occurred at VTOL conditions.

TABLE OF CONTENTS

List of Pages

LIST OF FIGURES

LIST OF SYMBOLS

A	Physical area, cm^2
AE	Effective area, cm^2
CD	Circumferential distortion based on average rake leg differences $[(\text{RAKE AVG})_{HI}-(\text{RAKE AVG})_{LO}]$/AVG OF ALL PROBES
C_V	Velocity coefficient
C_W	Flow coefficient
D	Nozzle equivalent exit diameter, cm
D_7	Nozzle entrance diameter, cm
F_G	Gross thrust, newtons
F_{G_I}	Ideal gross thrust, newtons
g	Gravitational constant, 980.6 cm/sec^2
H	Ground plane height
L_T	Thrust moment arm, cm
M	Mach number
N_F	Fan speed, RPM
NPR	Nozzle pressure ratio
P_a	Ambient pressure, $newtons/cm^2$
P_s	Static pressure, $newtons/cm^2$
P_{std}	Standard pressure, 10.13 $newtons/cm^2$
P_T	Total pressure, $newtons/cm^2$
R	Gas constant, 2.8696×10^6 cm^2/sec^2 °K
RD	Radial distortion based on average ring differences $[(\text{RING AVG})_{HI}-(\text{RING AVG})_{LO}]$/AVG OF ALL PROBES
T_T	Total temperature, °C
T_{std}	Standard temperature, 15.0°C
W	Flow rate, kg/sec
β	Nozzle hood deflection angle, degrees
γ	Ratio of specific heats
δ	Relative absolute pressure ratio, ambient pressure/standard pressure
δ_t	Relative total pressure ratio, total pressure/standard pressure
θ	Longitudinal thrust vector angle, degrees
θ_t	Relative total temperature ratio, total temperature/standard temperature
ψ	Lateral thrust vector angle, degrees
ψ_{GEO}	Yaw vane deflection angle, degrees

SUBSCRIPTS

7	Nozzle entrance
8	Nozzle exit
13	Fan stream fan exit
16	Fan stream nozzle entrance
56	Core stream nozzle entrance

ABBREVIATIONS

cm	Centimeters
kg	Kilograms
°C	Degrees Centigrade
N	Newtons
in	Inches
lb	Pounds
°F	Degrees Fahrenheit

CONVERSIONS

Newtons	= 4.4482 pounds force
Kilograms	= .4536 pounds mass
Centimeter	= .3937 inches
°Centigrade	= (°Fahrenheit -32)/1.8

1. INTRODUCTION

The "D" vented nozzle is a lift/cruise thrust vectoring system designed for operation with low pressure ratio, high bypass ratio propulsion systems. The nozzle is a multi-function hood deflector which can be configured for either a conventional turbofan engine or a tip turbine fan system. It is shown installed in a typical subsonic V/STOL aircraft configuration in Figure 1-1. This aircraft employs two conventional high bypass turbofan engines in an under-the-wing nacelle arrangement. The "D" vented thrust vectoring nozzle is attached to the nacelle immediately downstream of the engine. These nozzles vector thrust from vertical to horizontal as the aircraft progresses from vertical takeoff (VTO) through transition to conventional flight.

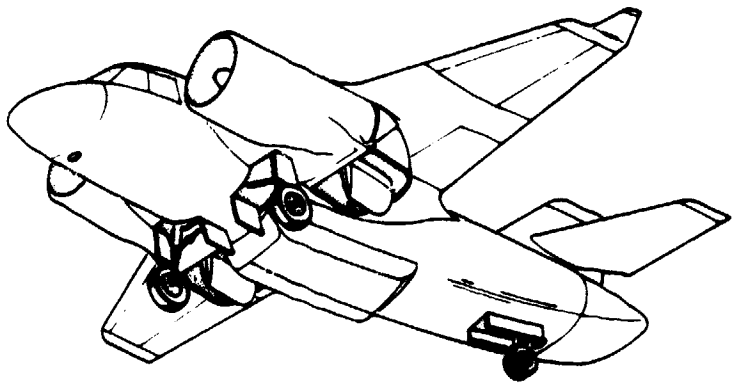

Figure 1-1. Typical Subsonic V/STOL Configuration

The performance of thrust vectoring nozzles in the 90° vectored position for VTO operation is extremely critical to overall aircraft performance, since a 1% reduction in VTO thrust vectoring efficiency results in a 1% loss in aircraft takeoff gross weight capability. This corresponds to a 5 to 10% reduction in aircraft payload/range capability. Thus, particular attention must be focused on thrust vectoring nozzle performance in the design of V/STOL aircraft.

MCAIR has carried out extensive investigations of thrust vectoring, lift/cruise nozzle systems starting in 1971. Experimental tests have been carried out on a continuing basis up to the present, with a cumulative total of over 1800 test occupancy hours. This effort has included screening tests of various nozzle concepts, and detailed parametric studies of circular, rectangular and "D" shaped deflector nozzles. The current "D" vented nozzle configuration has been shaped primarily by the results of a series of small scale model test programs which are described in References 1 and 2.

To demonstrate the capabilities of a large scale "D" vented thrust deflecting system coupled with a high bypass ratio engine, the NASA Ames Research Center contracted with MCAIR to design and test a "boilerplate" version

of the nozzle under static ground conditions. A large scale "D" vented nozzle and a calibration nozzle were fabricated and mounted behind a General Electric YTF-34-F5 turbofan engine. Specific objectives of the test program were to (1) obtain nozzle performance characteristics "in" and "out" of ground effects; (2) demonstrate the compatibility of the nozzle with a turbofan engine; (3) obtain pressure and temperature distributions on the surface of the "D" vented nozzle and (4) establish a correlation of the nozzle performance between small scale and large scale models.

The overall program was conducted under Contract NAS2-10564 with Mr. Richard Christiansen of NASA Ames Research Center serving as Technical Monitor. MCAIR established the design configuration of the test nozzles and provided detailed drawings of the test apparatus. Fabrication and assembly of the test nozzles and associated test hardware were accomplished at NASA Ames.

The experimental test program was carried out by NASA Ames personnel with MCAIR support. The tests were conducted at the Ames Outdoor Aerodynamic Research Facility during the period between 28 July and 1 September 1981. Data reduction and analysis of the test results were performed by MCAIR, and are documented in this report.

The "D" vented nozzle design concept is described in Section 2. A description of the model and instrumentation is provided in Section 3. Test procedures and data accuracy are discussed in Section 4. Section 5 presents a discussion of the test results and large scale/small scale data comparisons. Data are presented for a range of vector angles and exit areas, for variations in core nozzle geometry, and for operation in and out of ground proximity. Conclusions derived from the test program are discussed in Section 6.

2. "D" VENTED NOZZLE DESIGN

2.1 GEOMETRIC DESIGN

The "D" vented nozzle is a thrust vectoring, lift/cruise system designed for low pressure, high bypass ratio propulsion systems. The nozzle can be configured for either a conventional turbofan engine or a tip turbine fan. Figure 2-1 shows the nozzle in both cruise and VTOL modes, installed with a turbofan engine. The nozzle assembly consists of a fan duct, a fixed asymmetric structure, movable deflector hoods, and a split yaw vane/closure door assembly attached to a single support beam, centrally located on the bottom of the nozzle structure. In the cruise mode, the yaw vane doors are closed to form a flat bottom duct and a "D" shaped exit area. For transition to vertical flight, the closure doors are each rotated 90° to form a single split yaw vane after which longitudinal thrust vector is accomplished by rotation of the deflector hood elements. Lateral vectoring is obtained by deflection of the split yaw vane.

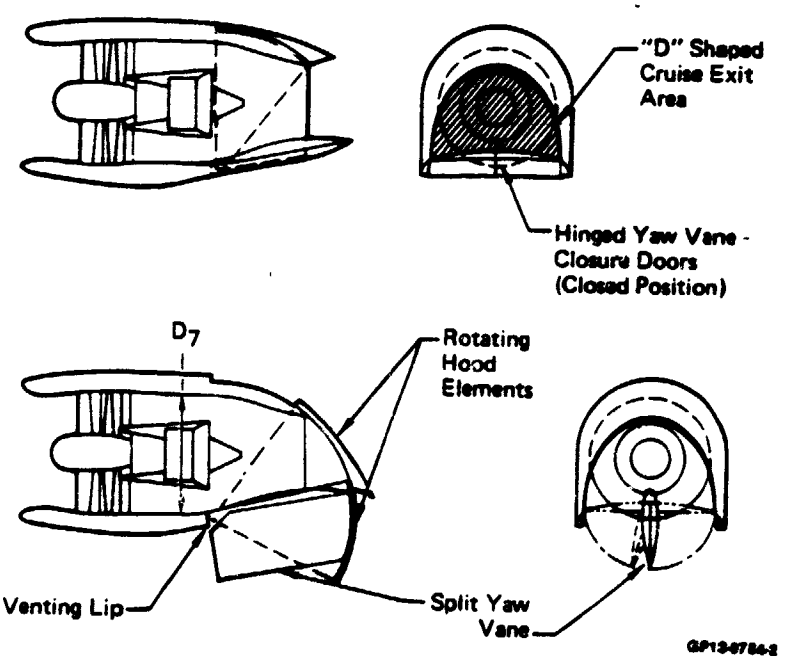

Figure 2-1. "D" Vented Nozzle Geometry

The "D" vented nozzle utilizes a concept called "venting". "Venting" a deflector nozzle serves to improve the 90 degree vectoring performance and is accomplished by removing the inside wall of the elbow turn of a conventional deflector nozzle design. A comparison of the flow characteristics of unvented and vented nozzles is presented in Figure 2-2. In an unvented deflector, the pressure on the outer wall increases, peaks, and then decreases to match ambient pressure at the nozzle exit. In the elbow inner corner, static pressure decreases to a sub-ambient minimum and then rises to match ambient at the exit.

The local flow near the inner wall increases in velocity through the turn and then decreases in the "adverse" pressure region near the exit. For short radius elbows (unvented nozzle), the boundary layer flow can not negotiate the adverse pressure region, separates from the wall, and introduces a total pressure loss. In a vented nozzle, the static pressure in the elbow inner corner is constrained to near ambient and the static pressure on the outer wall increases to maintain the required static pressure gradient to balance the centrifugal forces in the turn. Since no elbow inner wall surface is present, separation does not occur and the corresponding total pressure loss is avoided. A 2% velocity coefficient advantage for the "D" vented nozzle over an unvented design is typical.

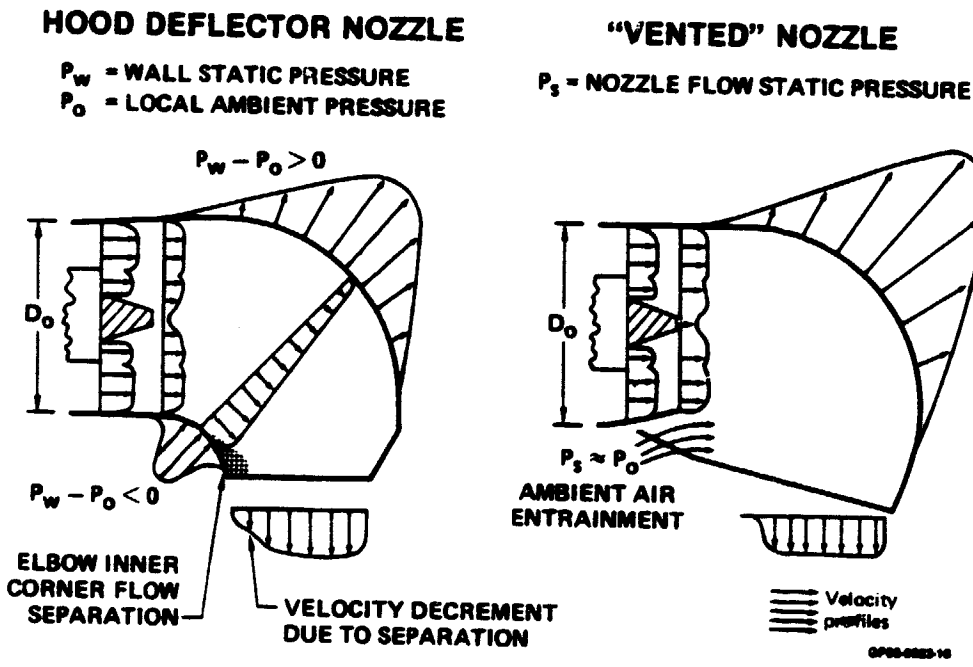

Figure 2-2. Nozzle Flow and Pressure Distributions

2.2 ENGINE/NOZZLE MATCHING

Proper aerodynamic matching of the engine and nozzle is critical to achieving high nozzle performance and maintaining efficient engine operation. This high bypass ratio, normally separated flow engine was run in the mixed flow mode for this application. The engine has a fan diameter of 111.76 cm (44 in.) and an aerodynamic fan pressure ratio of 1.5.

The optimum fan pressure ratio or VTO nozzle pressure ratio for subsonic, long endurance V/STOL missions usually falls between 1.3 and 1.6. Fan discharge or nozzle entrance Mach number is typically about 0.5 for these applications. In addition, results from previous nozzle testing indicate that maximum vectoring performance is achieved with equal or nearly equal fan and core stream total pressures. Using the above guidelines, the engine mixing plane areas for this test program were sized to provide a nozzle

entrance Mach number of 0.5 and a core to fan stream total pressure ratio of 0.98. This results in an engine bypass ratio of 6.60 with a total flow of 141.5 kg/sec (312 lb/sec), a fan pressure ratio of 1.41, and a maximum thrust of approximately 35,500 N (8000 lb). This occurred at a fan speed of approximately 93%, which was the maximum speed limit imposed on the test engine. A schematic of the engine along with a summary of engine operating conditions at the engine/nozzle match point is presented in Figure 2-3.

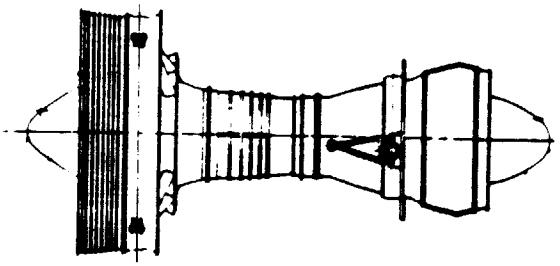

AIRFLOW	kg/sec (lb/sec)	
TOTAL		141.7 (312.3)
CORE ENGINE		18.64 (41.1)
BYPASS RATIO		6.60
FAN PRESSURE RATIO		1.41
FAN TURBINE INLET TEMPERATURE	°C (°F)	813 (1,495)
FAN ROTOR SPEED	RPM	6,442
CORE ENGINE ROTOR SPEED	RPM	16,610
THRUST*	N (lb)	36,866 (8,288)
MIXING PLANE TOTAL PRESSURE	N/cm^2 ($lb/in.^2$)	
FAN STREAM		13.94 (20.22)
CORE STREAM		13.66 (19.81)

*$C_V = 1.0$

GP13-1010-1

Figure 2-3. YTF-34-F5 Engine Operating Conditions at Engine/Nozzle Match Point

3. TEST APPARATUS

3.1 MODEL DESCRIPTION

The test model consisted of a bellmouth inlet, a General Electric YTF-34-F5 turbofan engine, and a "D" vented thrust deflecting nozzle mounted on a metric test stand, as shown schematically in Figure 3-1. The nozzle contained provisions for (1) a thrust vectoring range of 0° to 115°, (2) a yaw vectoring range of 0° to 10°, (3) variable nozzle area control, and (4) variable spacing between the core exit and nozzle entrance stations. Extensive pressure and temperature instrumentation was installed throughout the model. The nozzle was mounted inverted to prevent hot gas reingestion. The test stand hardware included frames for mounting the bellmouth, engine, and nozzle, as well as a metric platform. A raised ground plane was used to determine nozzle characteristics in close proximity to the ground. Nozzle thrust loads were measured by three component loads cells located between the metric platform and a nonmetric frame. The nonmetric frame was securely attached to the ground through three large struts. Figure 3-2 through 3-7 are photographs of the installed "D" vented nozzle at each of the geometric hood rotation angles, 35°, 60°, 100°, 110°, 120°, and 130°, respectively. A description of each of the model components is given below.

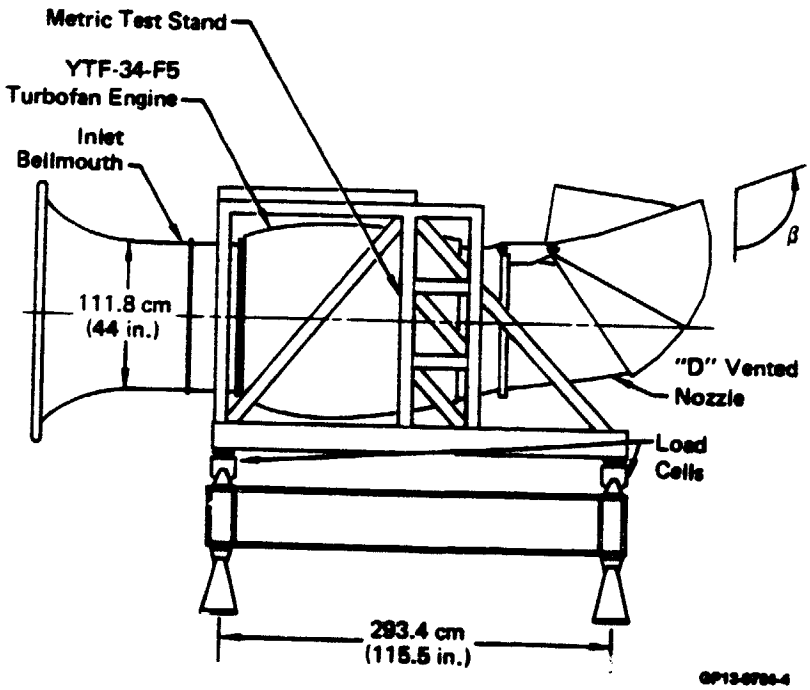

Figure 3-1. TF34/"D" Vented Nozzle Test Aparatus

ORIGINAL PAGE
BLACK AND WHITE PHOTOGRAPH

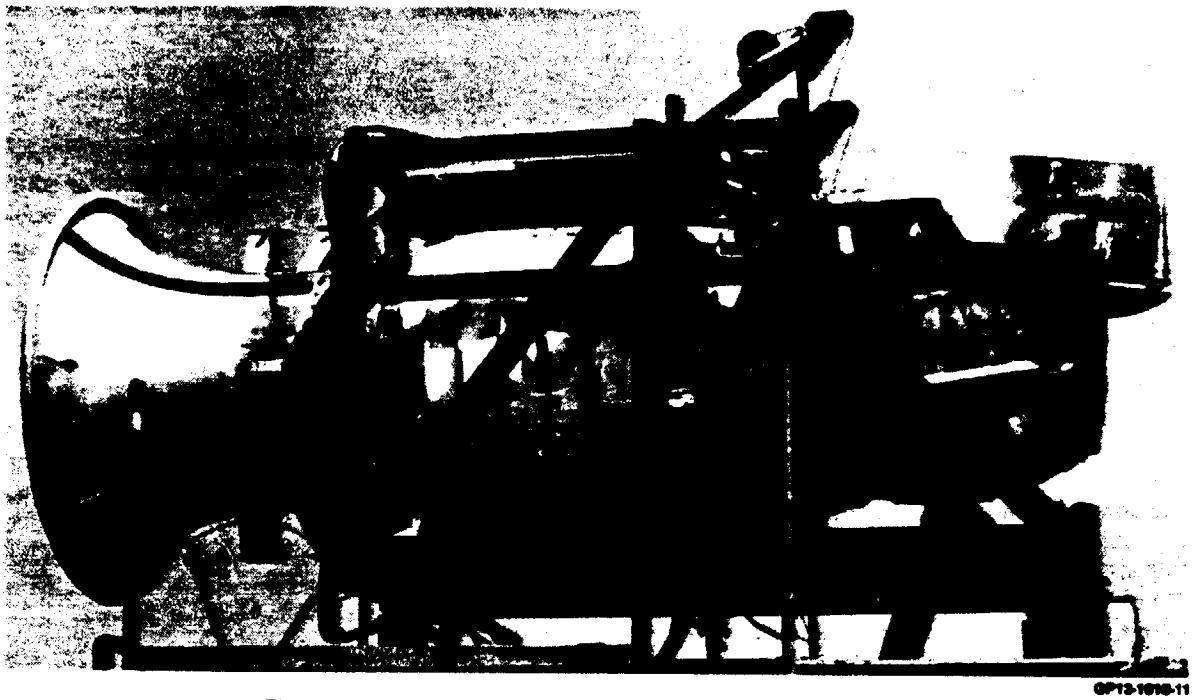

GP13-1018-11

Figure 3-2. "D" Vented Nozzle Installed on Test Stand
Hood Rotation Angle = 35°

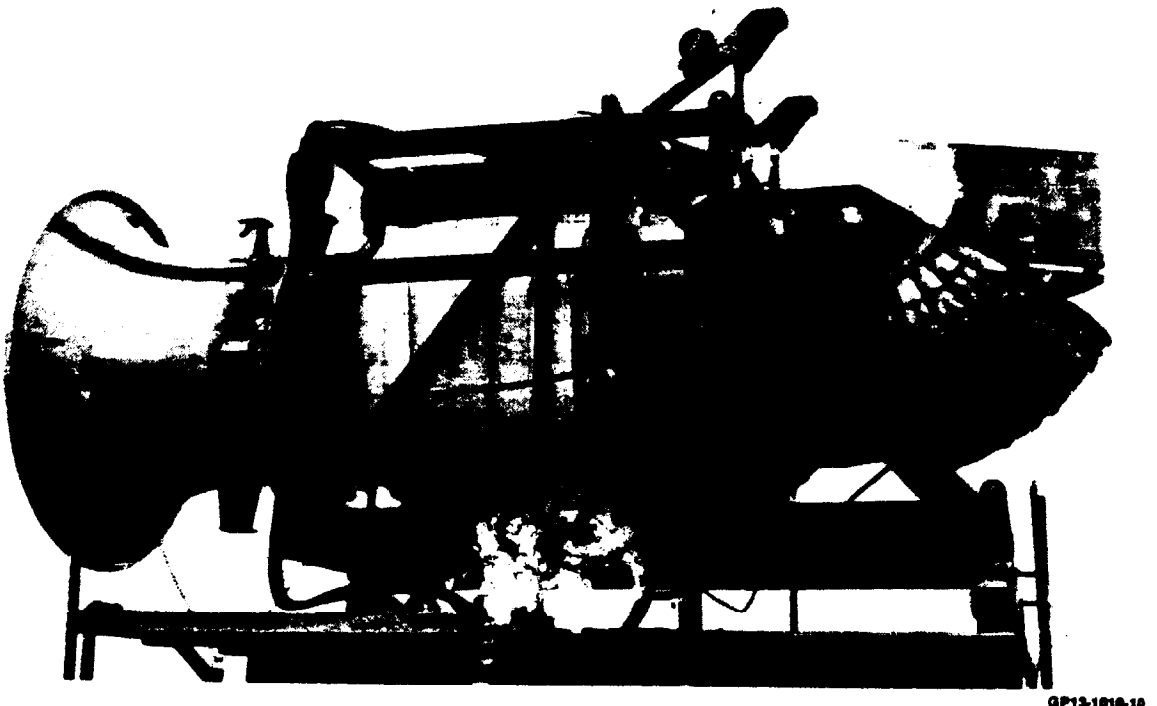

GP13-1018-10

Figure 3-3. "D" Vented Nozzle Installed on Test Stand
Hood Rotation Angle = 60°

ORIGINAL PAGE
BLACK AND WHITE PHOTOGRAPH

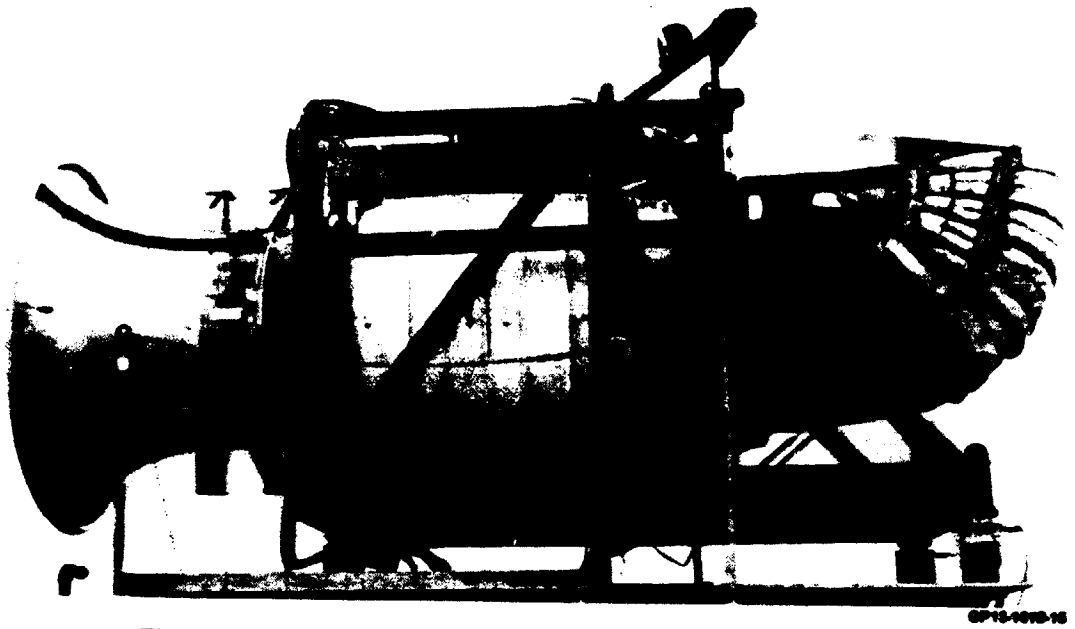

Figure 3-4. "D" Vented Nozzle Installed on Test Stand
Hood Rotation Angle = 100°

Figure 3-5. "D" Vented Nozzle Installed on Test Stand
Hood Rotation Angle = 110°

ORIGINAL PAGE
BLACK AND WHITE PHOTOGRAPH

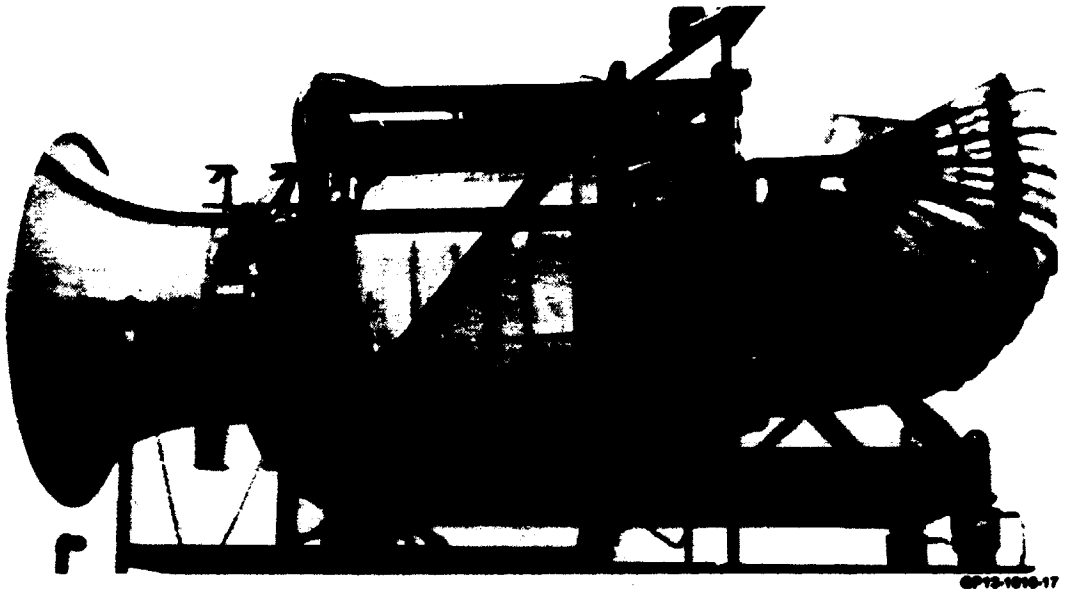

Figure 3-6. "D" Vented Nozzle Installed on Test Stand
Hood Rotation Angle = 120°

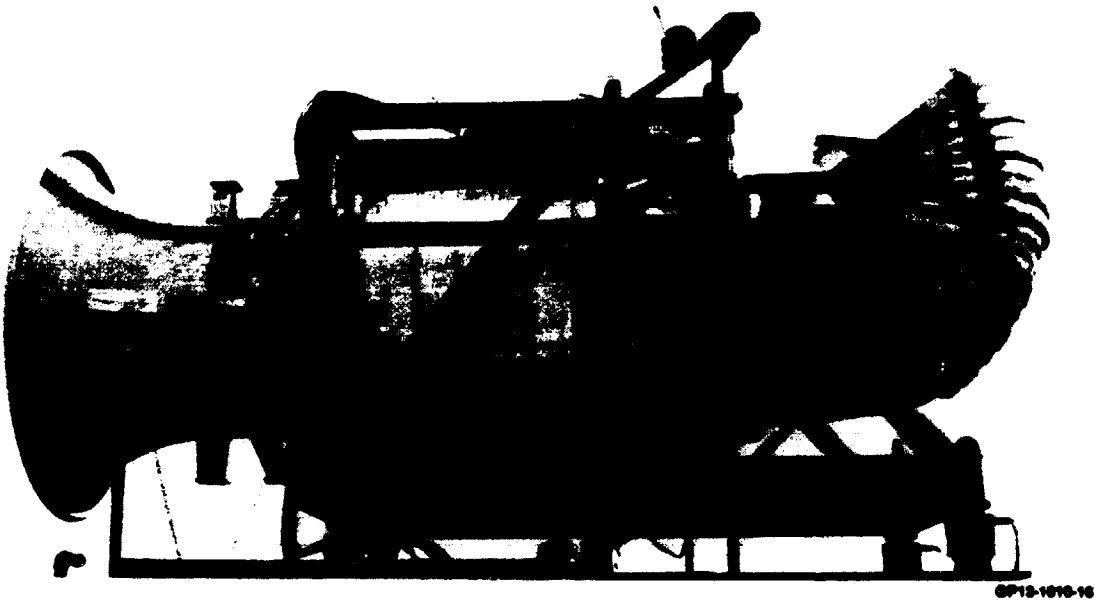

Figure 3-7. "D" Vented Nozzle Installed on Test Stand
Hood Rotation Angle = 130°

The engine and bellmouth were supported as one unit and the boilerplate "D" vented nozzle was supported as a separate unit. This arrangement was chosen to prevent transference of the nozzle vectoring loads into the engine. The thrust and weight of the engine/bellmouth assembly were supported through the engine mounts. Flexible seals between the engine fan duct and the "D" vented nozzle were used to prevent gas leakage. The core nozzle was mounted directly to the turbine case of the engine.

In addition to the "D" vented nozzle hardware, a thrust calibration nozzle with three different exit areas was constructed to establish baseline engine performance with a near ideal nozzle. A schematic of the calibration nozzle is presented in Figure 3-8, and a photograph of the nozzle installed at the test site is shown in Figure 3-9. The three nozzles provided an exit area variation of approximately $\pm 5\%$, and each consisted of a forward assembly and an aft cone. Only one forward assembly was required and one new aft cone was fabricated. Existing hardware from the 1976 NASA Ames large scale "D" vented nozzle test, Reference 3, was utilized for the two additional aft cones.

The thrust vectoring nozzle system hardware consisted of a "D" vented nozzle, a core nozzle, adapter sections for both the "D" vented nozzle and the core nozzle, and a nozzle entrance rake as shown in Figure 3-10. The "D" vented nozzle provided thrust vectoring in both the longitudinal and lateral directions. The core nozzle geometry controlled the flow matching relationship between the core flow and the fan duct flow and also controlled the distance between the core exit and nozzle hood segments. The adapter sections provided a transition of the fan duct from non-circular to circular at the nozzle entrance station and served for mounting of the nozzle entrance rake. The nozzle entrance rake measured total and static pressures and total temperatures of both the fan and the core streams entering the nozzles.

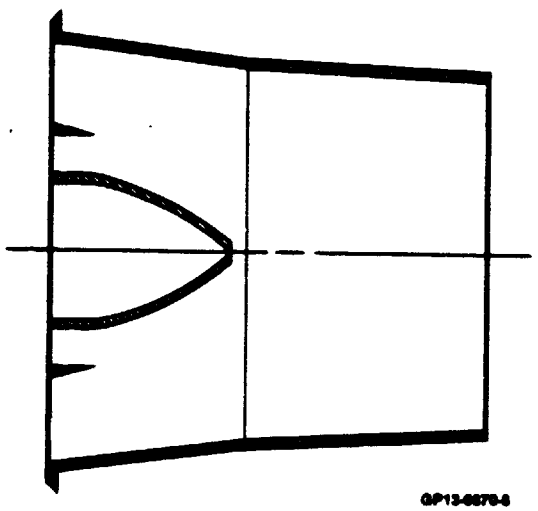

Figure 3-8. Calibration Nozzle

ORIGINAL PAGE
BLACK AND WHITE PHOTOGRAPH

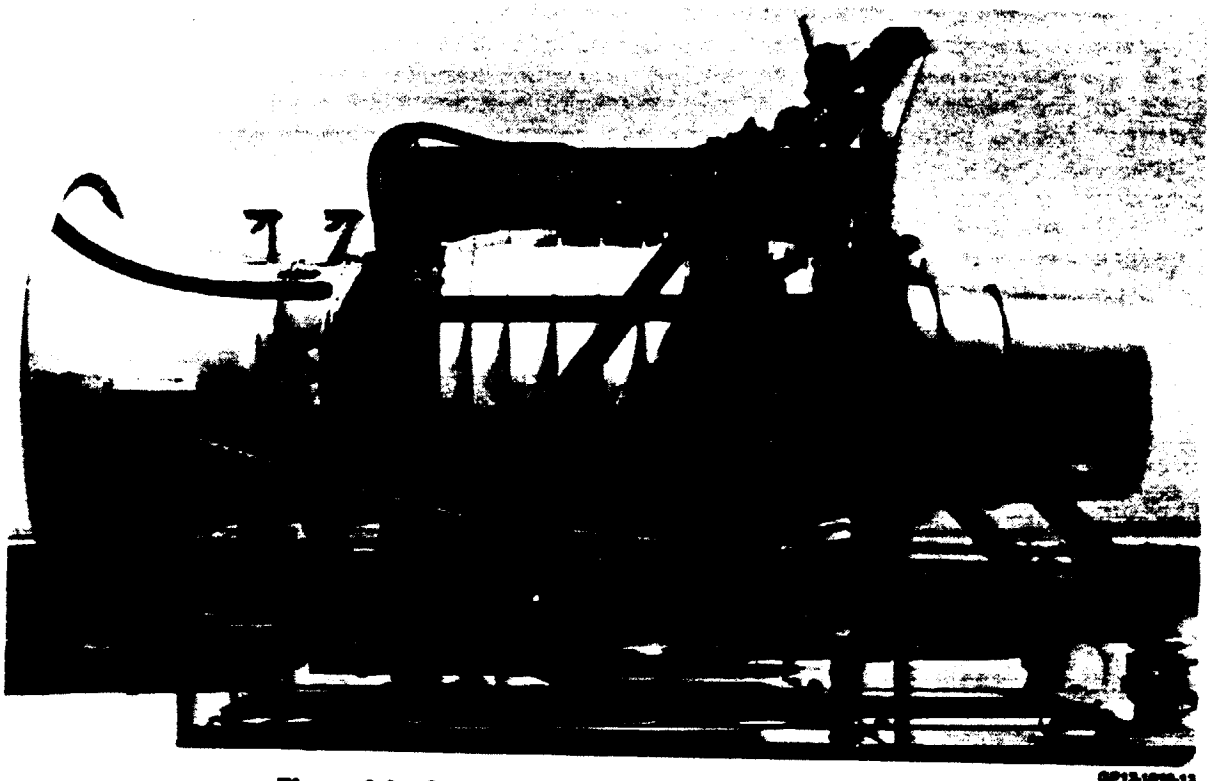

Figure 3-9. Calibration Nozzle Installed on Test Stand

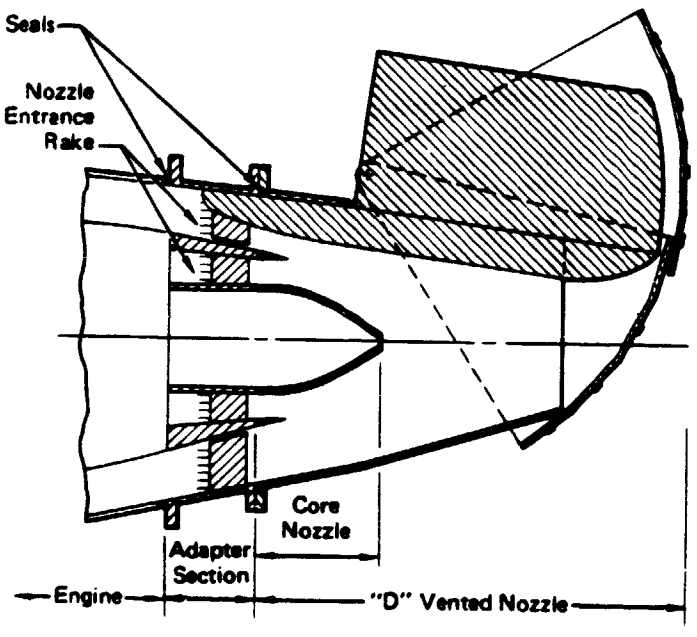

Figure 3-10. Thrust Vectoring Nozzle Assembly

The "D" vented nozzle, illustrated in Figure 3-11, was comprised of a fixed hood, two rotating hoods, a yaw vane/closure door assembly, and a venting lip which controlled the nozzle exit area. The fixed hood was mounted by a flange to the adapter section and provided the cross sectional shape transition from circular to the "D" shaped cruise exit. Two rotating hoods provided the required longitudinal thrust deflection and were stowed externally around the fixed hood for axial thrust operation. The contoured nozzle parts were constructed of rolled steel plate segments welded together to minimize cost and simplify fabrication techniques. The yaw vane was suspended from a beam in the center of the vertical thrust exit area. The vane was deflected to provide a lateral component to the thrust. A split yaw vane would normally serve as a closure door for the nozzle in the cruise mode. However, for the boilerplate hardware in this test, a separate closure door was manufactured to simplify the design. The closure door is shown installed in Figure 3-12. The venting lip was a flat plate attached to the bottom of the fixed hood, Figure 3-11. Five lip elements of varying length were fabricated to provide a means to trim the engine and also to obtain nozzle performance as a function of exit area.

There were six core nozzle configurations fabricated for the test program. Five of the six configurations were designed, as illustrated in Figure 3-13, to provide variations in length and exit area. These variations included three different nozzle lengths; and, at the mid length, three different core exit areas. Each core nozzle configuration consisted of a hub and a shroud; and each of these was attached separately to the adapter section hardware. Cylindrical extensions were used to move the hub to alternate axial locations. The baseline shroud was the shortest, with the alternate length shrouds providing the same nozzle shape, but extended further aft. Alternate core nozzle areas were obtained from two additional shrouds located at the intermediate axial position. The shrouds were fabricated from steel plates rolled to cylindrical and conical shapes. The hub, a smooth body of revolution, was spin fabricated.

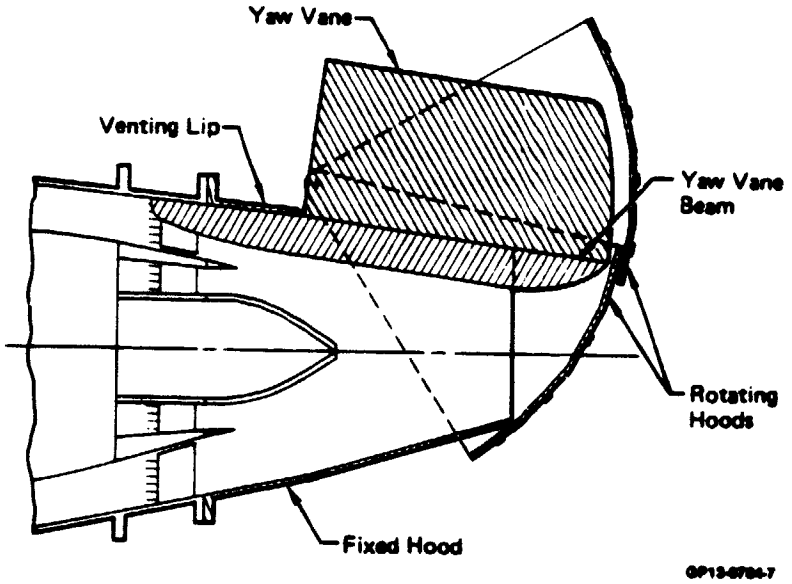

Figure 3-11. "D" Vented Nozzle Schematic

ORIGINAL PAGE
BLACK AND WHITE PHOTOGRAPH

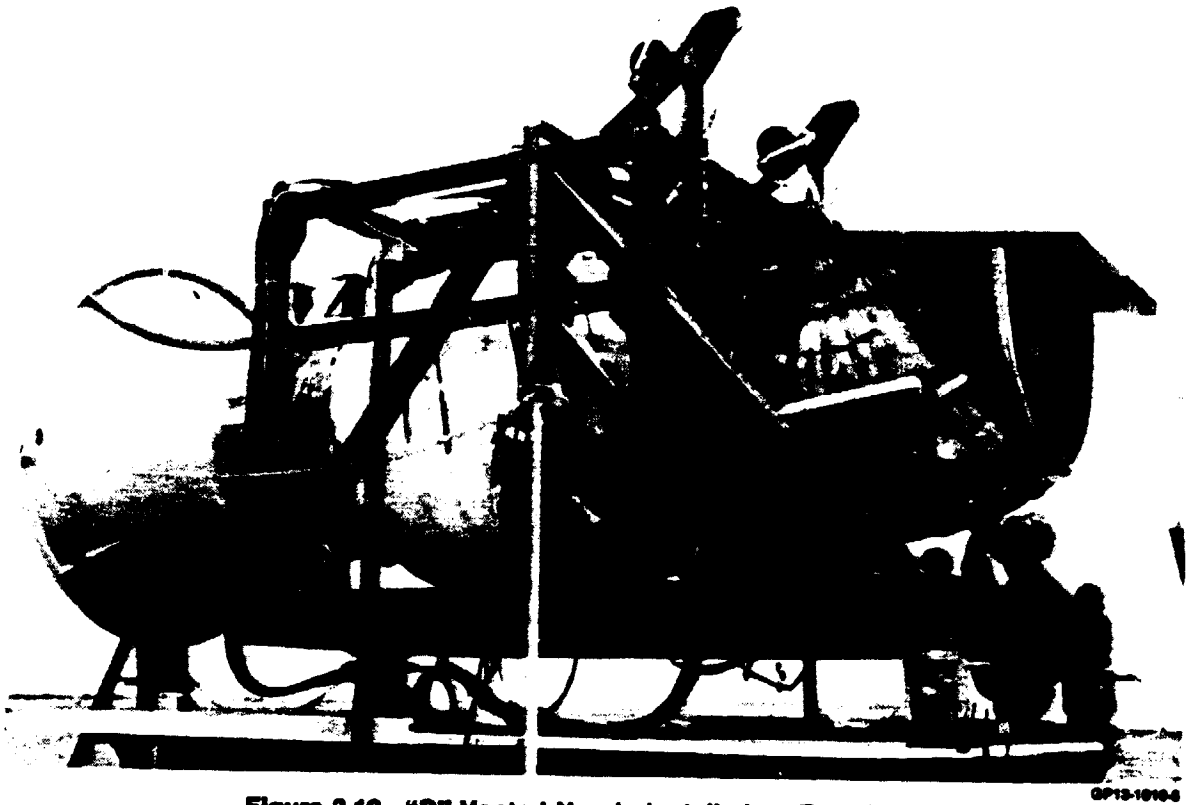

Figure 3-12. "D" Vented Nozzle Installed on Test Stand
Cruise Configuration

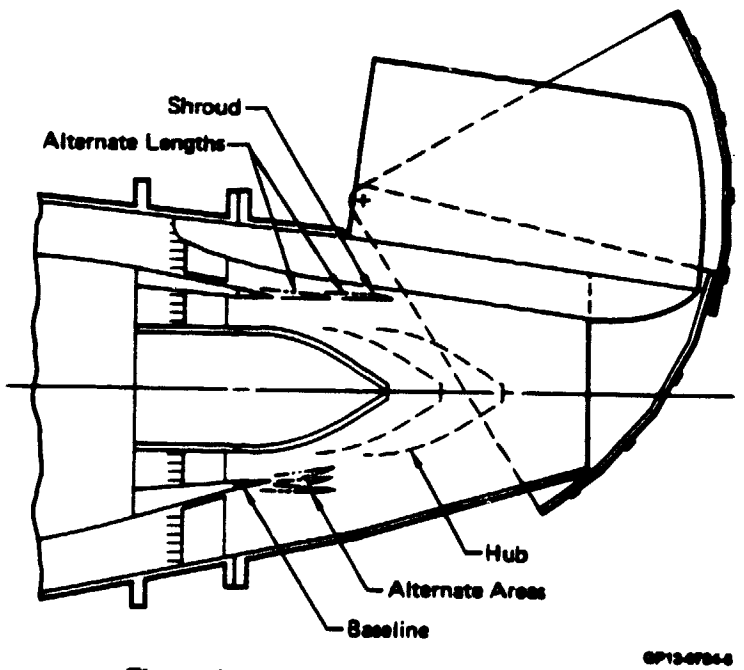

Figure 3-13. Core Nozzle Configurations

The sixth core nozzle configuration was a slotted mixer nozzle, shown schematically in Figure 3-14. This nozzle was included because a similar design showed promise in a previous small scale test, Reference 2. The nozzle was fabricated from two steel plates rolled into a cylinder and a conical section and then welded together.

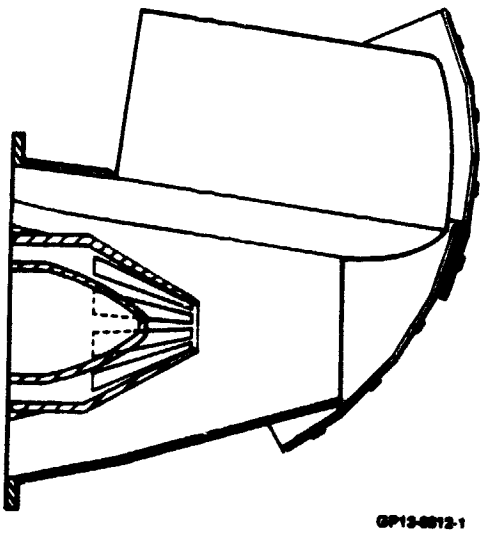

GP13-0012-1

Figure 3-14. Slotted Mixer Core Nozzle

The adapter section provided a transition from the noncircular cross section of the TF34 fan duct to a circular section at the nozzle entrance station. It also accommodated installation of the nozzle entrance rake. Three separate adapter parts were required; one for the "D" vented nozzle, one for the core nozzle shroud and one for the hub. The outer adapter mounted directly to the test stand and became the supporting structure for mounting the "D" vented nozzle. The calibration nozzles also attached directly to this adapter. The other two adapter parts mounted directly to the engine at the turbine case flange and the engine hub. There was a flexible seal between the outer adapter and the outer fan cowling on the engine to allow for some relative motion between the engine and the "D" vented nozzle assembly.

Two six-leg total pressure and temperature rakes were mounted in the core and fan stream adapter sections to measure nozzle entrance pressures and temperatures. The rake legs in the fan stream were each separately attached to the outer adapter wall, and those in the core stream were each mounted between the two inner adapter shells.

Access for core nozzle changes was provided without removal of the "D" nozzle assembly. The changes were made by pivoting the entire "D" vented nozzle assembly upwards after removing the bolts from the fixed hood mounting

flange. This arrangement is illustrated schematically in Figure 3-15. A photograph taken during a core nozzle model change for the slotted mixer nozzle is presented in Figure 3-16.

Ground effects testing was accomplished by erecting a ground plane above the model. The ground plane was an existing NASA structure fabricated of steel plate and I-beams. A deflector was attached to one end to deflect the exhaust flow away from the bellmouth inlet. The ground plane was set at three different positions, corresponding to ratios of height above the nozzle pivot point to nozzle equivalent exit diameter (H/D) of 2.22, 1.70, and 1.03. The 1.03 value is representative of a VTO condition. Photographs of these three configurations are shown in Figures 3-17, 3-18, and 3-19, respectively.

3.2 MODEL INSTRUMENTATION

The "D" vented nozzle test model was instrumented to obtain nozzle loads, engine operating characteristics, and various pressures and temperatures throughout the model. The quantity, type and location of the instrumentation for each model component are described below, and a summary is presented in Figure 3-20.

3.2.1 BELLMOUTH INSTRUMENTATION - The bellmouth contained eight static pressure taps for the purpose of computing airflow. In addition, three total temperature probes were included to permit calculation of corrected engine performance parameters. Location of this instrumentation is illustrated in Figure 3-21.

3.2.2 ENGINE INSTRUMENTATION - The engine instrumentation was selected for two purposes; (1) engine operation monitoring and (2) engine performance. The purpose for each engine measurand is indicated in Figure 3-20. The fan exit total pressure rake was a previously existing device built by Boeing, and is shown in schematic form in Figure 3-22. NASA-Ames received permission from Boeing to borrow the rake for the "D" vented nozzle test.

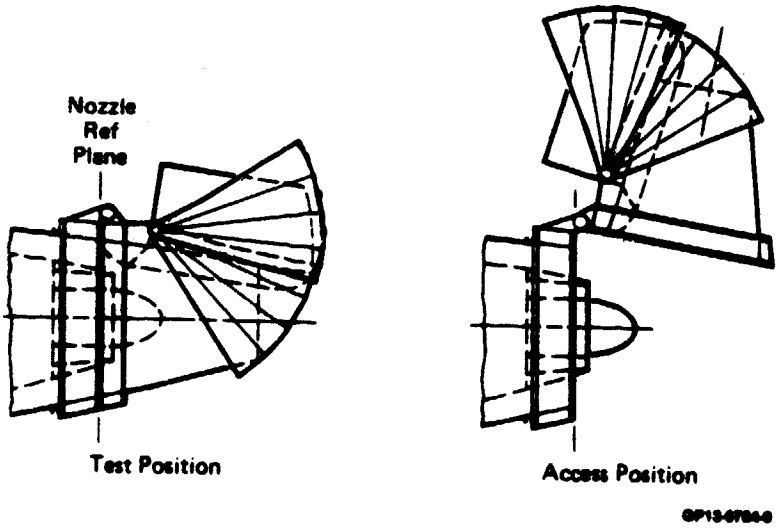

Figure 3-15. Core Nozzle Access

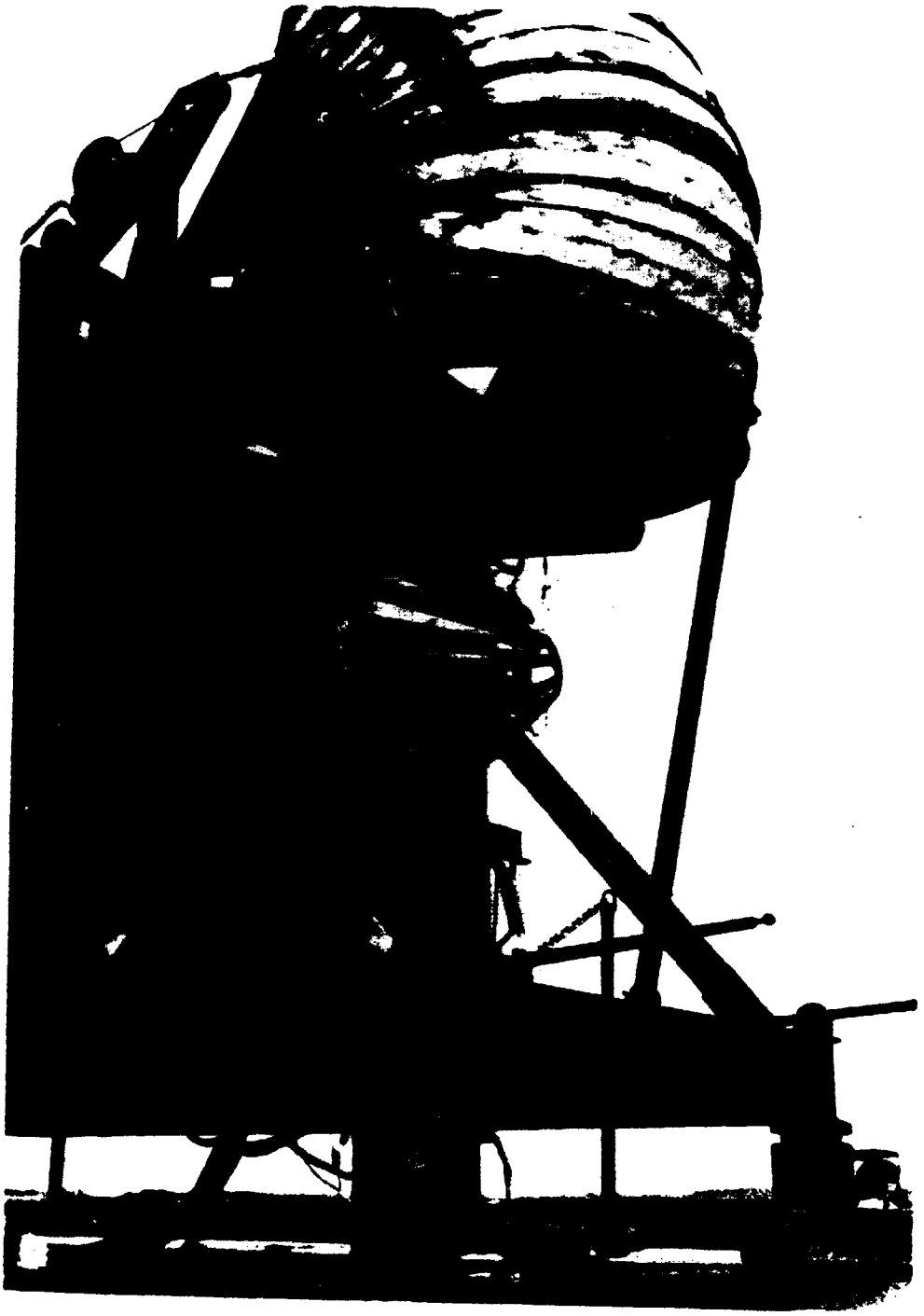

GP15-10156

Figure 3-16. "D" Vented Nozzle Installed on Test Stand
Slotted Mixer Nozzle Installation

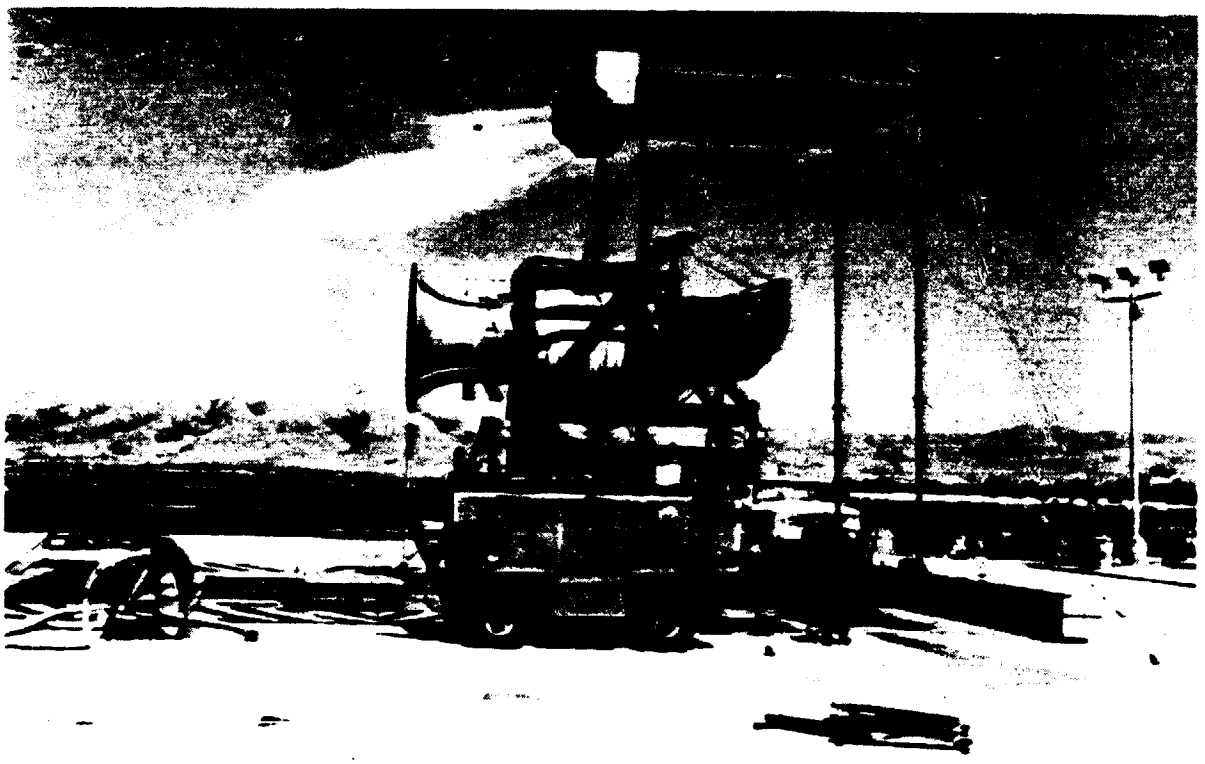

GP13-1016-14

Figure 3-17. "D" Vented Nozzle Installed on Test Stand Ground Plane Installed, H/D = 2.22

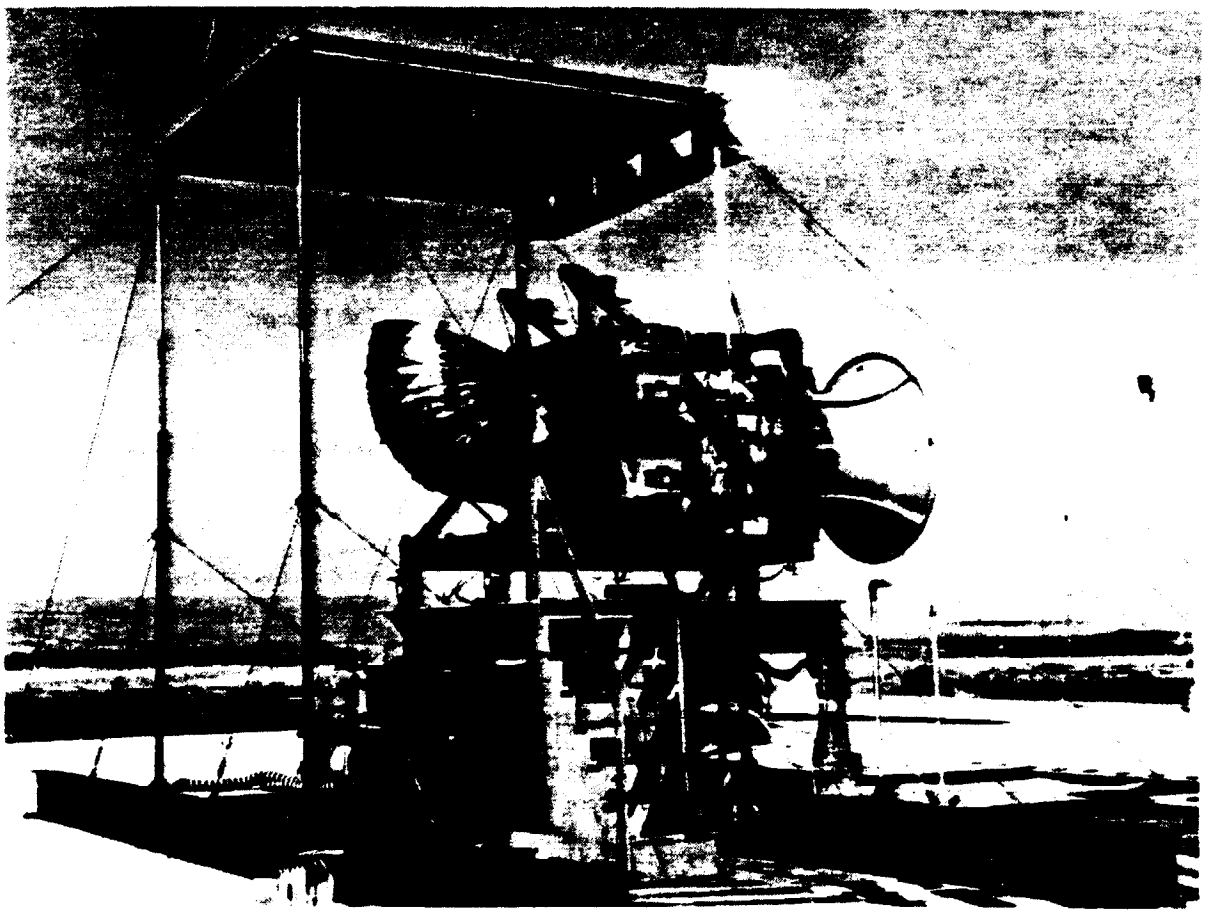

GP13-1010-12

Figure 3-18. "D" Vented Nozzle Installed on Test Stand
Ground Plane Installed, H/D = 1.70

ORIGINAL PAGE
BLACK AND WHITE PHOTOGRAPH

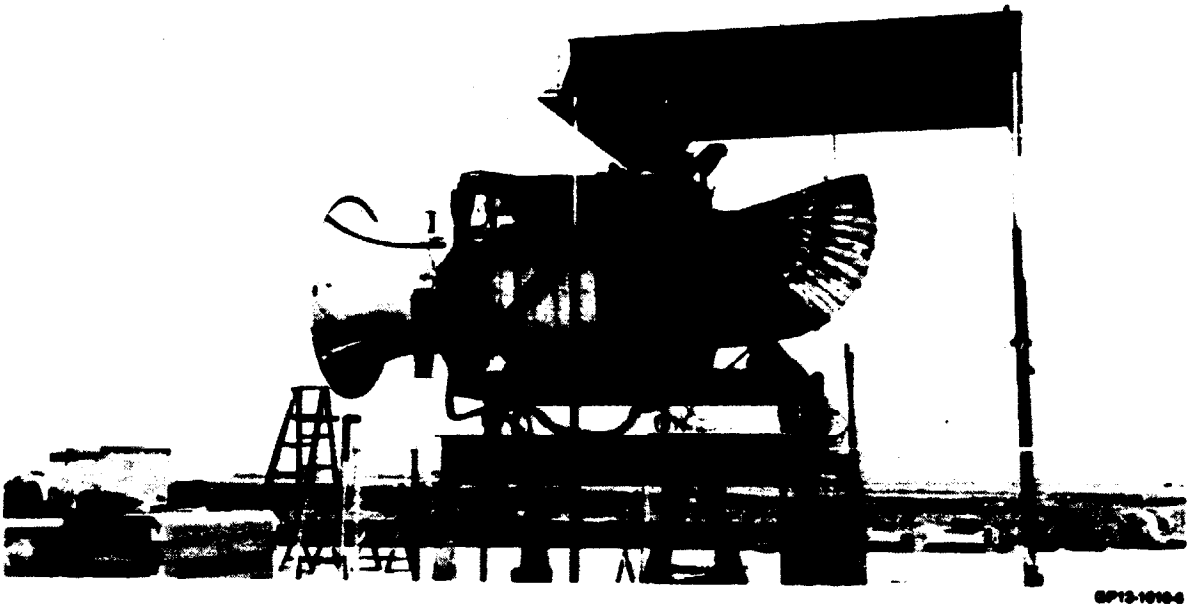

GP13-1010-6

Figure 3-19. "D" Vented Nozzle Installed on Test Stand Ground Plane Installed, H/D = 1.03

Measurand	No.	Purpose	Measuring Device	Recording Mode
Ambient Conditions				
Pressure	1	Reference Pressure	HG Barometer	Hand
Temperature	1	Back-Up for Bellmouth Temperature	HG Thermometer	Hand
Humidity	1	Suitability for Testing	Wet Bulb Thermometer	Hand
Wind Speed	1	Suitability for Testing	Anemometer	Panel Display
Wind Direction	1	Suitability for Testing	Vane	Panel Display
Bellmouth				
Static Pressure	8	Engine Airflow	Scanivalve	ASDAS[1]
Total Temperature	3	Corrected Performance Parameters	Thermocouple	ASDAS
Engine				
LP Rotor Speed	1	Engine Performance and Monitoring	Electromagnetic Pickup	ASDAS, Panel Display
HP Rotor Speed	1	Engine Performance and Monitoring	Tachometer	ASDAS, Panel Display
Fan Exit Total Pressure	20	Fan Pressure Ratio	Scanivalve	ASDAS
Fan Duct Static Pressure	15	Pressure Profiles	Scanivalve	ASDAS
Fuel Flow	1	Nozzle Flow	Flowmeter	ASDAS
Fuel Pressure	1	Engine Operation Monitoring	Pressure Gauge	Panel Display
Fuel Temperature	1	Engine Operation Monitoring	Temperature Gauge	Panel Display
Oil Pressure	1	Engine Operation Monitoring	Pressure Gauge	Panel Display
Oil Temperature	1	Engine Operation Monitoring	Temperature Gauge	Panel Display
LP Turbine Inlet Temperature	1	Engine Operation Monitoring	Thermocouple	Panel Display
Case Vibrations	6	Engine Operation Monitoring	Accelerometer	Panel Display
Fan OGV Stress	12	Incipient Surge Detection	Strain Gauge	Oscillograph
Fuel Filter Pending Bypass ΔP	1	Engine Operation Monitoring	Pressure Gauge	Panel Display
B Sump Aft Scavenge Temperature	1	Engine Operation Monitoring	Thermocouple	Panel Display

1 Ames Standardized Data Acquisition System

Figure 3-20. Summary of Instrumentation

GP13-0010-55

Measurand	No.	Purpose	Measuring Device	Recording Mode
Nozzle Entrance Rake				
Total Pressure	48	Nozzle Performance Parameters	Scanivalve	ASDAS
Total Temperature	30	Nozzle Performance Parameters	Thermocouple	ASDAS
Static Pressure	16	Flow Field Distortion	Scanivalve	ASDAS
Wall Temperature	6	Temperature Profiles	Thermocouple	ASDAS
"D" Vented Nozzle				
Wall Pressure	19	Pressure Profiles	Scanivalve	ASDAS
Wall Temperature	16	Temperature Profiles	Thermocouple	ASDAS
Core Shroud Static Pressure[2]	15	Shroud Aerodynamic Loads	Scanivalve	ASDAS
Yaw Vane Static Pressure	24	Aerodynamic Loads	Scanivalve	ASDAS
Yaw Vane Static Temperature	6	Temperature Profiles	Thermocouple	ASDAS
Closure Door	12	Aerodynamic Loads	Scanivalve	ASDAS
Total Net Loads	7	Aerodynamic Loads	Load Cell	ASDAS
Calibration Nozzle				
Wall Pressure	9	Pressure Profiles	Scanivalve	ASDAS
Wall Temperature	4	Temperature Profiles	Thermocouple	ASDAS
Test Stand				
Normal Force	3	Gross Thrust-Magnitude, Direction and Location	Load Cell	ASDAS
Axial Force	3	Gross Thrust-Magnitude, Direction and Location	Load Cell	ASDAS
Side Force	3	Gross Thrust-Magnitude, Direction and Location	Load Cell	ASDAS
Ground Board				
Total Pressure	24	Velocity Profile	Scanivalve	ASDAS
Total Temperature	24	Temperature Profile	Thermocouple	ASDAS
Static Pressure	30	Impingement Location	Scanivalve	ASDAS

2 Forward shroud has 9 taps, mid shrouds have 12 taps, aft shroud has 15 taps, mixer nozzle has 18 taps.

GP13-0015-31

Figure 3-20. (Continued) Summary of Instrumentation

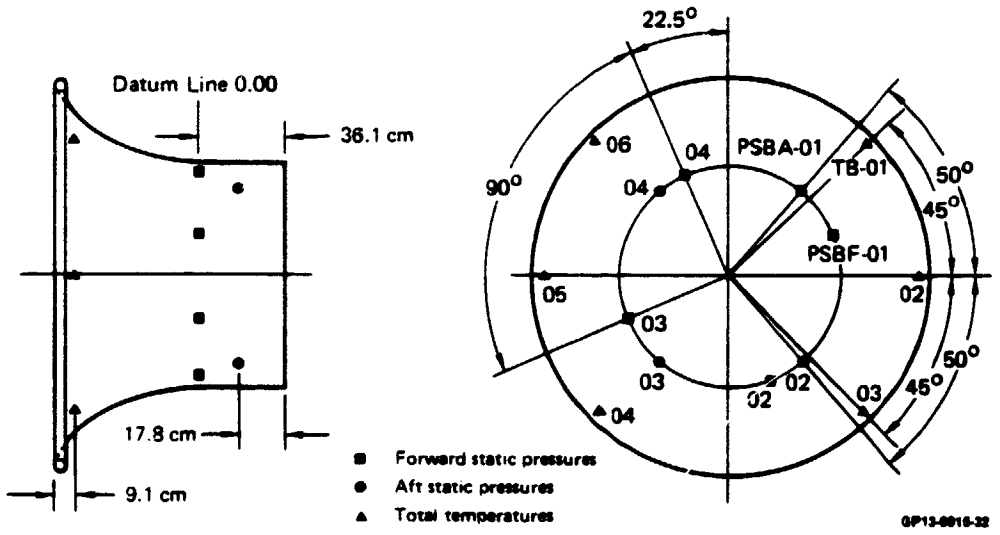

GP13-0015-32

Figure 3-21. Bellmouth Instrumentation

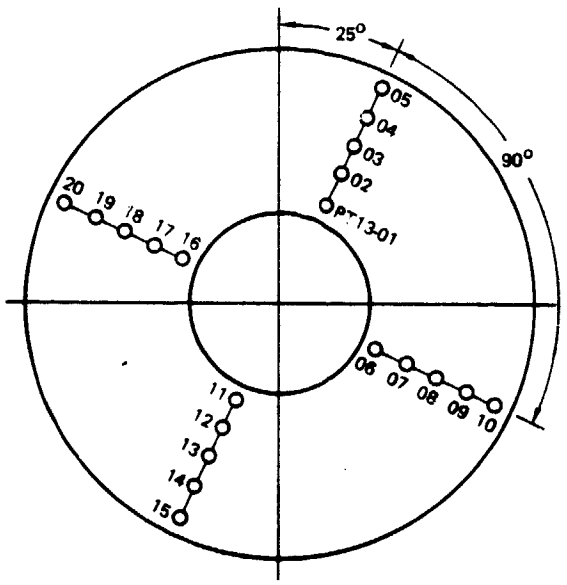

View Forward Looking Aft

Figure 3-22. TF34 Fan Exit Rake

There were fifteen static pressure taps, illustrated in Figure 3-23, located along the fan duct. These were installed to determine the static pressure profiles between the fan exit and nozzle entrance.

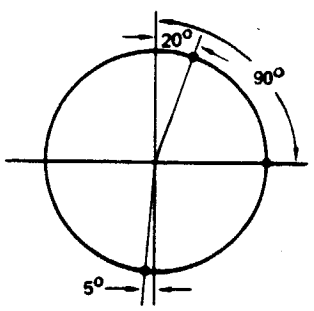

Pressure Tap Orientation
(View Forward Looking Aft)

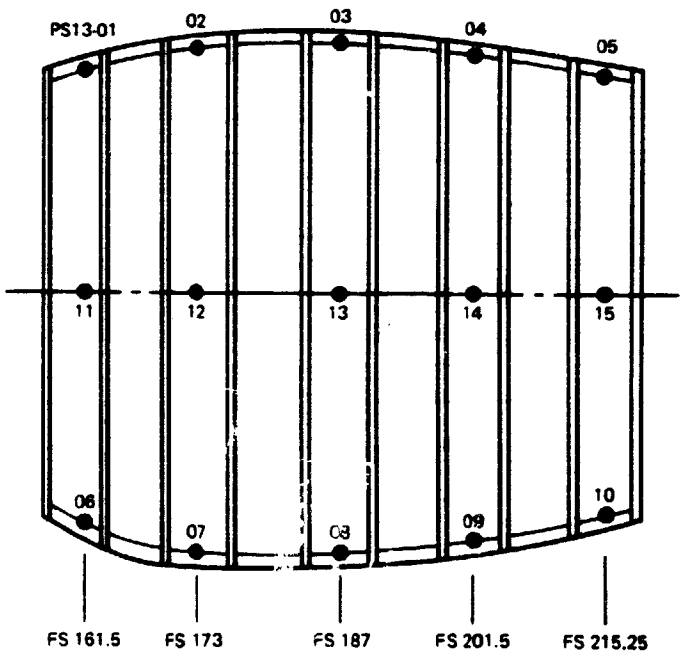

Figure 3-23. Fan Duct Static Pressure Instrumentation

3.2.3 NOZZLE ENTRANCE RAKE - The nozzle entrance instrumentation is shown schematically in Figure 3-24. The rakes extended through both the fan bypass and core streams. The instrumentation consisted of 48 total pressure probes, 30 total temperature probes, 16 wall static pressures, and 6 wall temperature thermocouples.

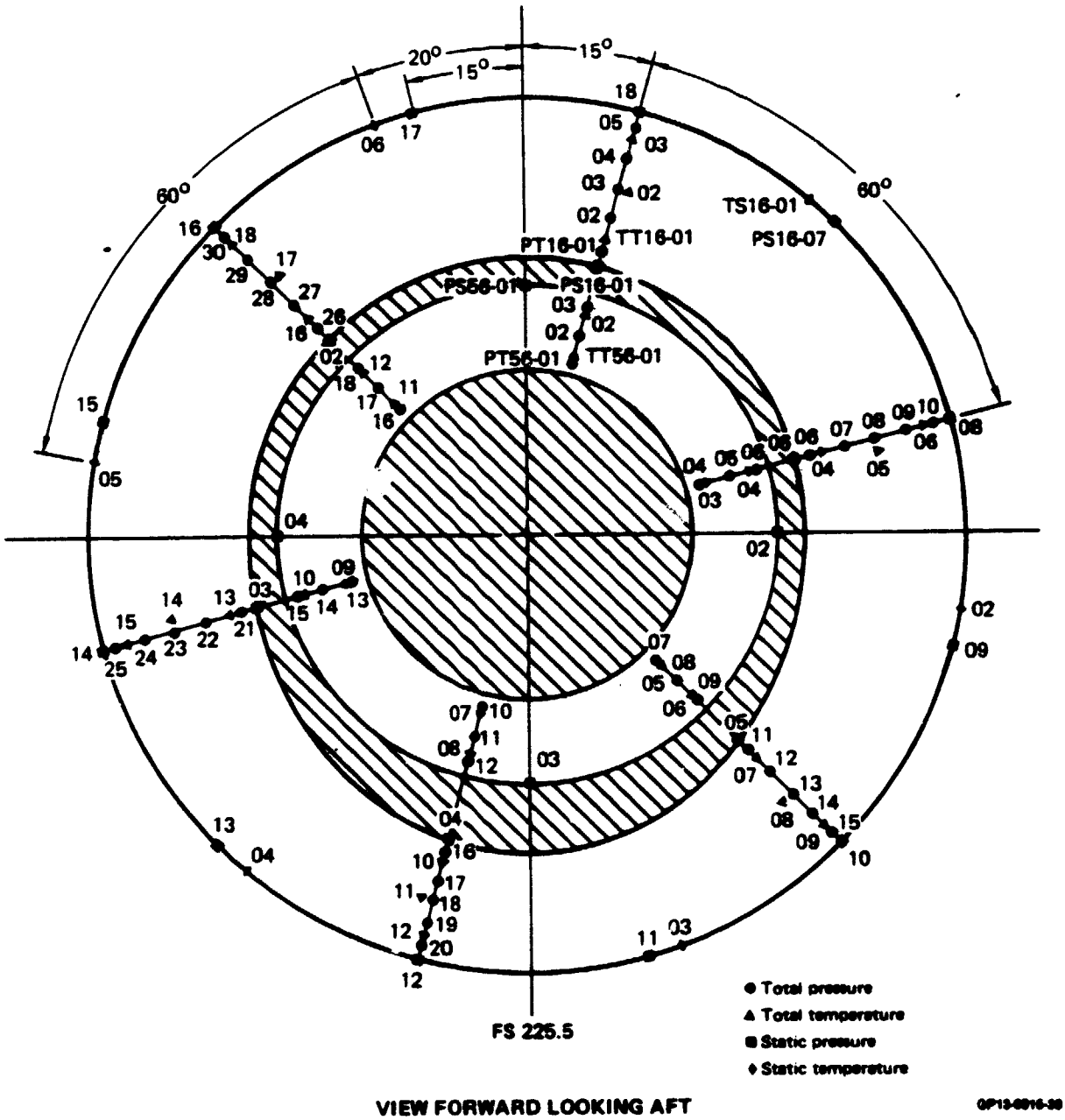

Figure 3-24. Nozzle Entrance Instrumentation

3.2.4 "D" VENTED NOZZLE INSTRUMENTATION - A description of all of the instrumentation installed in the "D" vented nozzle is included below.

"D" Vented Nozzle Walls - Figure 3-25 illustrates the 19 static pressure taps and 16 thermocouples that were located along the nozzle walls.

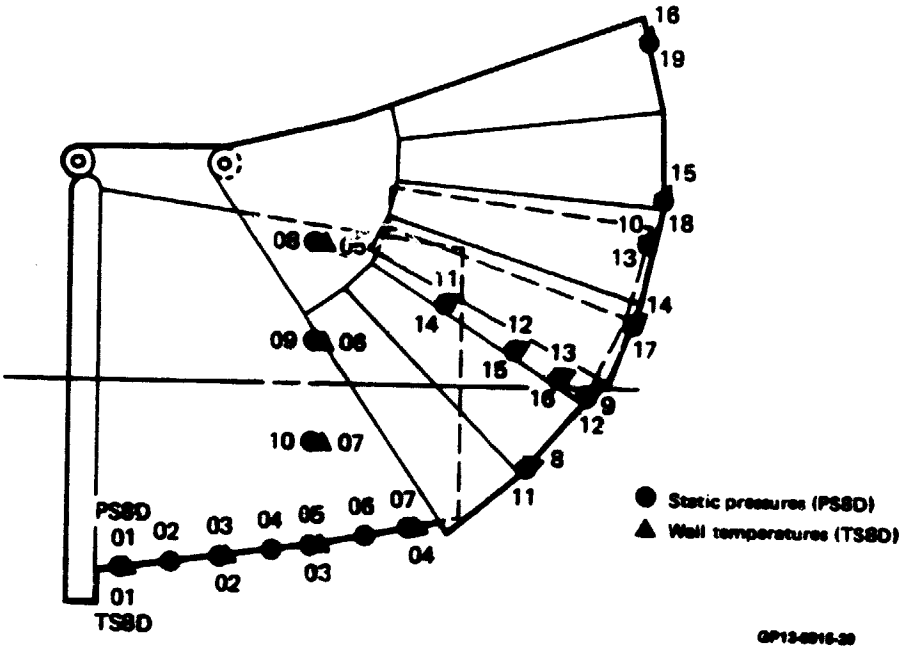

Figure 3-25. "D" Vented Nozzle Hood Instrumentation

Core Nozzles - Each of the core nozzles contained static pressure instrumentation on the outer walls of the nozzles, as illustrated in Figure 3-26. Static pressures were measured at three circumferential positions - top, bottom, and left side. Nine static pressure taps were located on the outer wall of the baseline core shroud. The pressure taps were similarly located for the remaining four core shrouds and the slotted mixer nozzle. There were twelve taps on the mid position shrouds, fifteen taps on the aft shroud, and eighteen taps on the slotted mixer nozzle. The purpose of this instrumentation was to provide data to determine the pressure gradients and aerodynamic loads across the shrouds induced by the vectored "D" vented nozzle.

Yaw Vane - Figure 3-27 shows the yaw vane instrumentation, which includes 24 static pressure taps (12 on each side) and six wall temperatures. The pressure data were integrated to determine the net load on the vane. The thermocouples provided a means to determine the temperature profile across the nozzle.

Closure Door - Twelve static pressure taps were installed in the closure door for the purpose of computing the aerodynamic load on the door. This instrumentation is depicted in Figure 3-28.

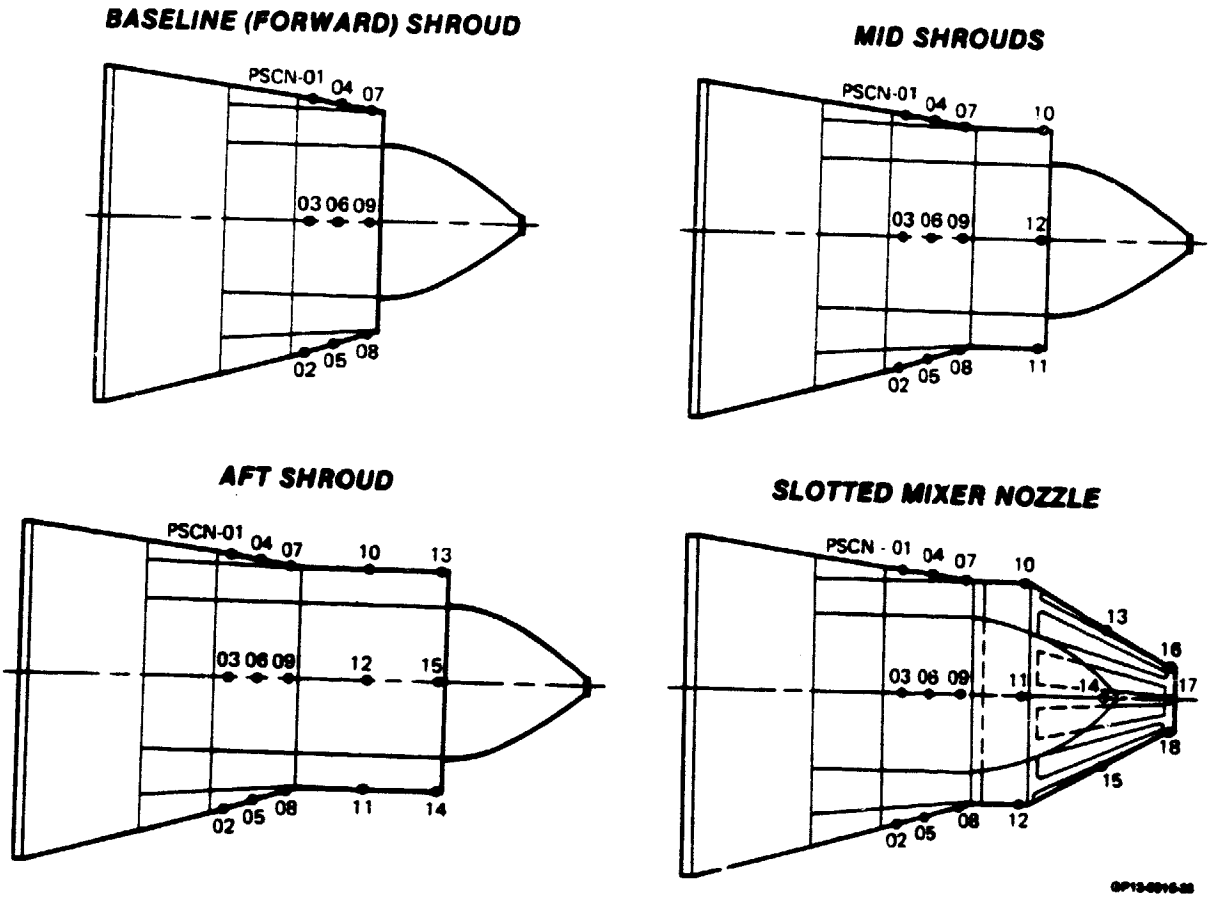

Figure 3-26. Core Nozzle Instrumentation

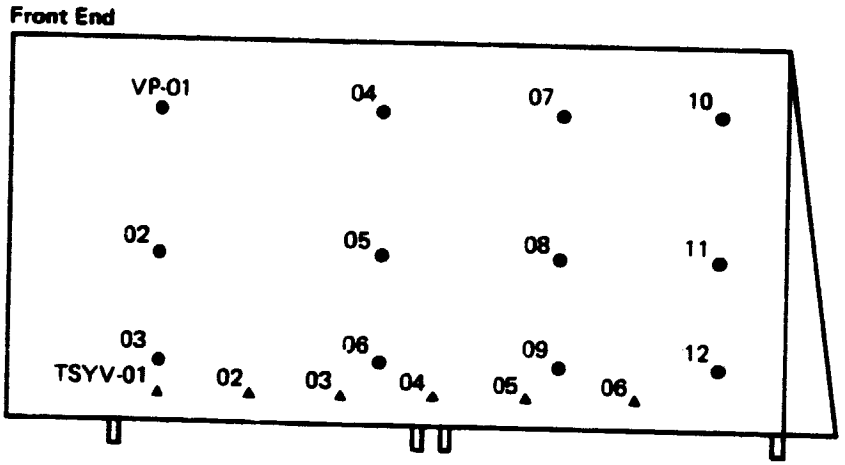

▲ Wall temperature

● Static pressures VP-01 thru VP-12 (VP-13 thru VP-24 are located on opposite side with 13 opposite 01, 14 opposite 02 . . . . .24 opposite 12.)

Figure 3-27. Yaw Vane Instrumentation

GP13-0915-20

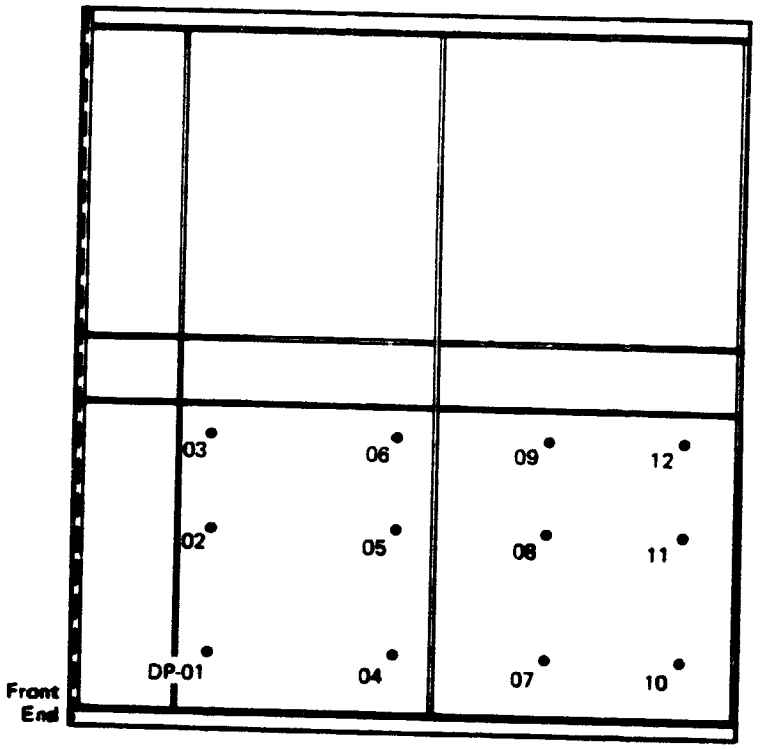

Figure 3-28. Closure Door Instrumentation

Total Net Loads - Vertical, axial, and lateral forces acting on the "D" vented nozzle fixed hood were recorded on seven single-axis load cells located as shown in Figure 3-29. Five load cells were on the vertical and axial load support structs and two were on the side load support struts.

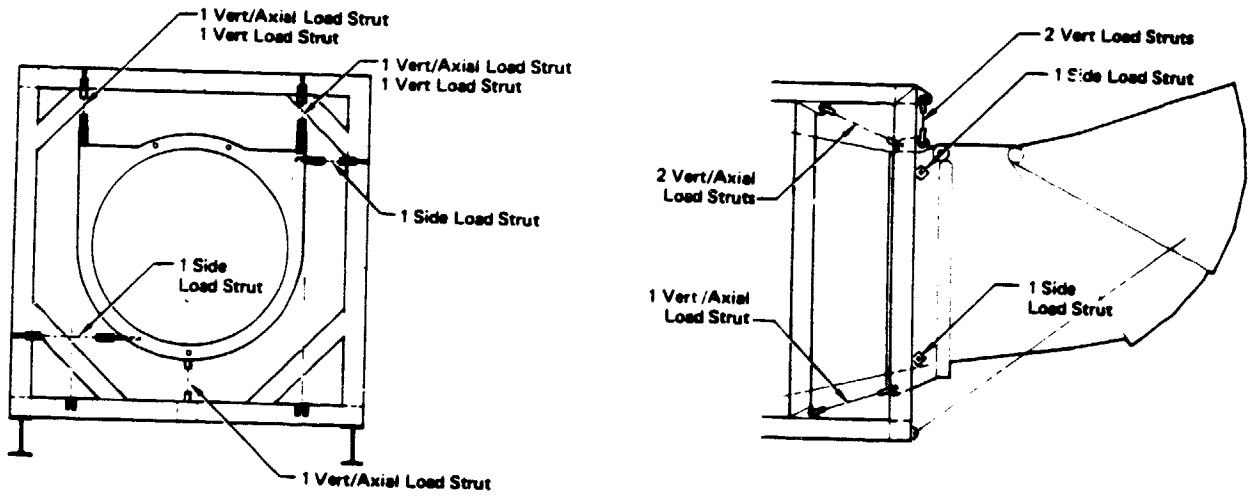

Note: One load cell integrated into each load strut

Figure 3-29. Single-Axis Load Cell Instrumentation

3.2.5 CALIBRATION NOZZLE INSTRUMENTATION - There were nine static pressure taps and four wall temperature thermocouples located along the wall of the calibration nozzle, as illustrated in Figure 3-30.

3.2.6 TEST STAND LOAD CELLS - There were three 3-component load cells on the model to measure axial, side, and normal forces transmitted to the test stand. As shown in Figure 3-31, the cells were arranged in a triangular pattern with one forward and two aft. The selected cells were rated at 26688N (6000 lb) normal force, 17792N (4000 lb) axial force, and 13344N (3000 lb) side force.

3.2.7 GROUND BOARD INSTRUMENTATION - The ground board was equipped with pressure and temperature instrumentation as described below.

Static Pressure Taps - Thirty static pressure taps were arranged in a five-by-six matrix pattern as shown in Figure 3-32. The purpose of this instrumentation was to provide a means to determine the center of impingement of the nozzle flow on the ground plane.

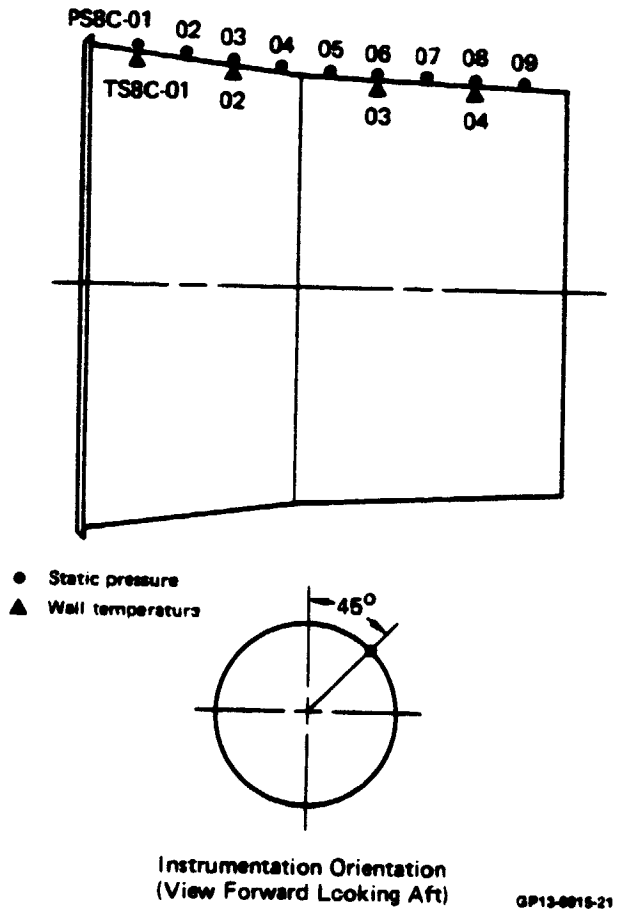

Figure 3-30. Calibration Nozzle Instrumentation

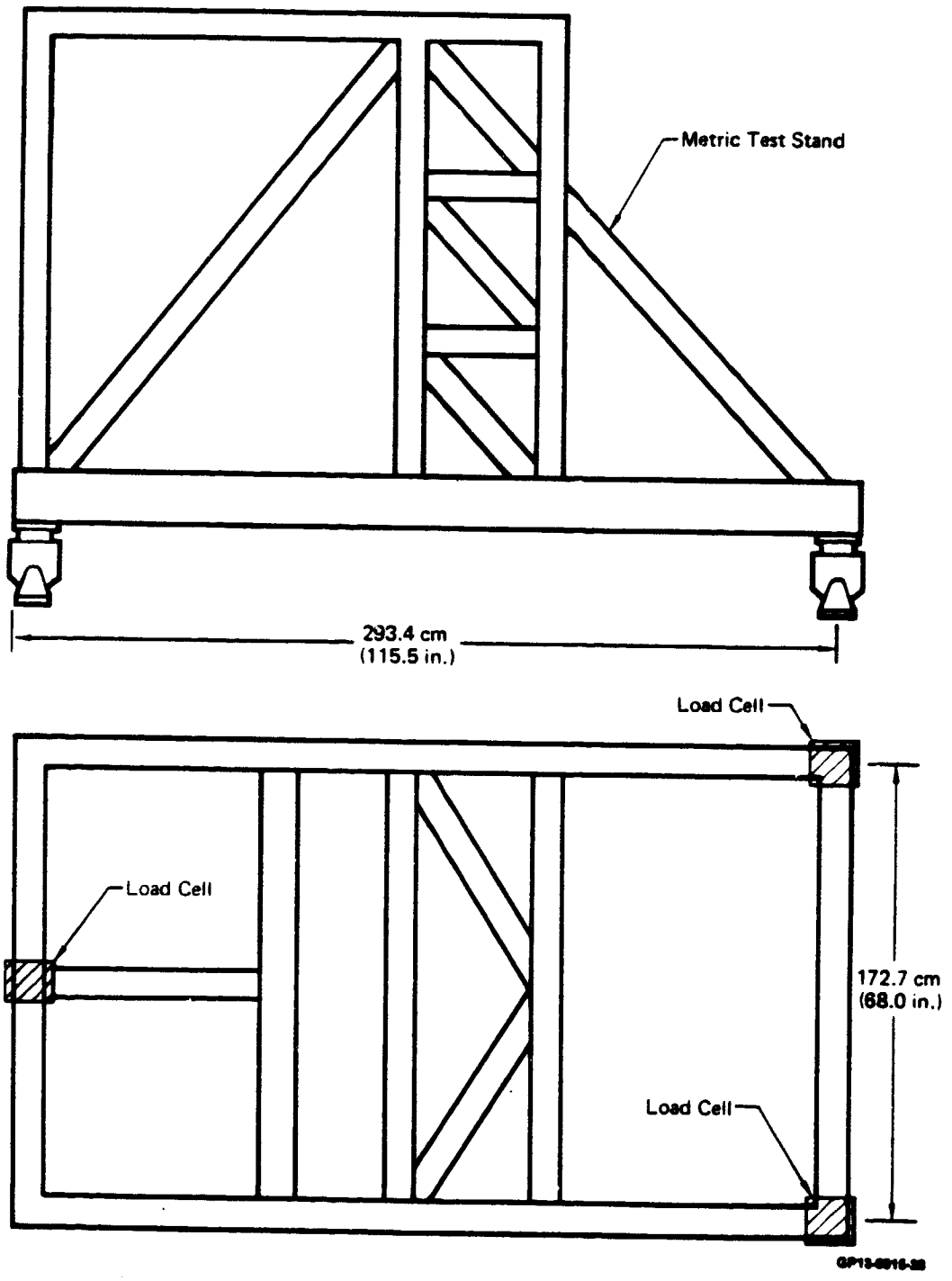

Figure 3-31. Load Cell Arrangement

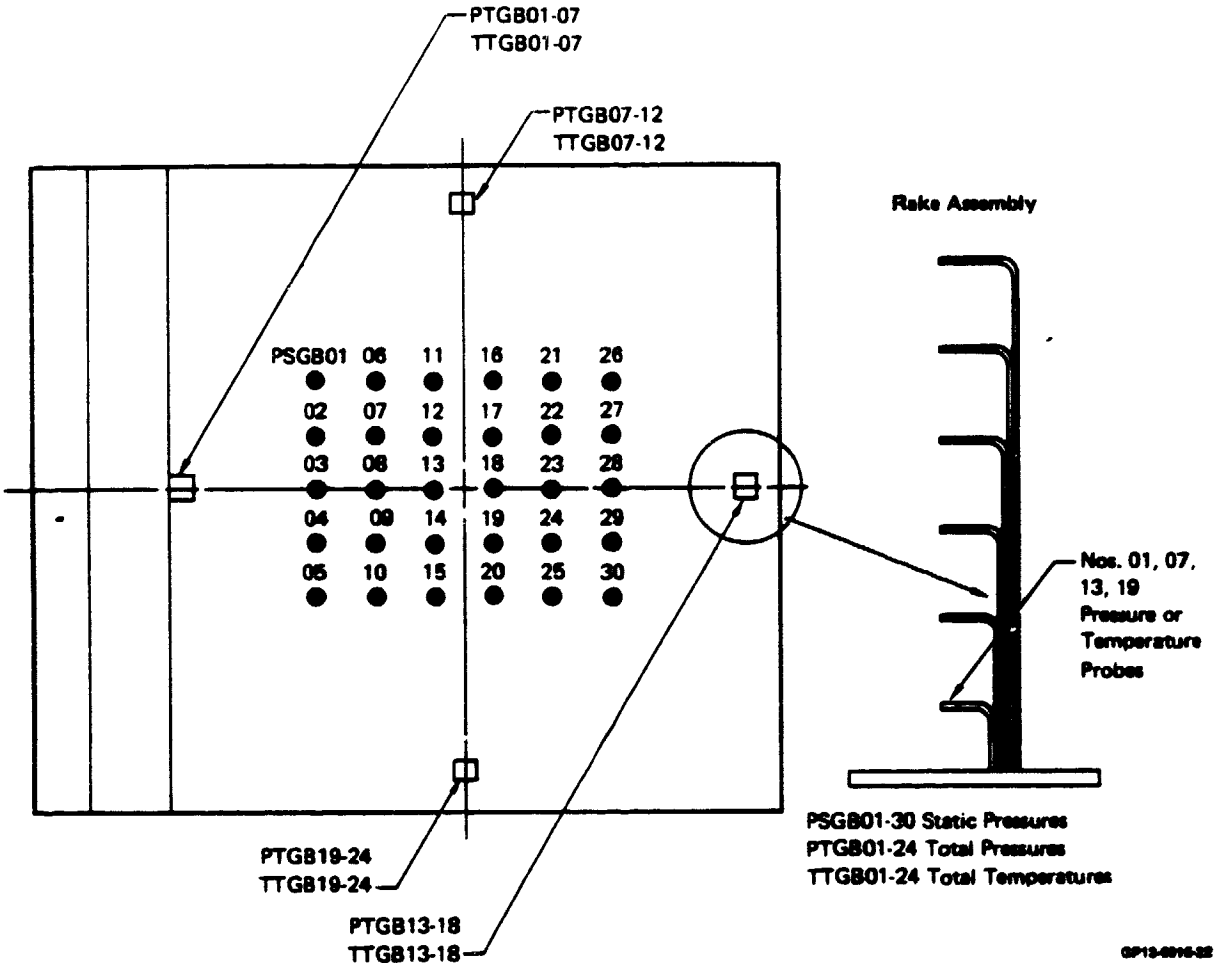

Figure 3-32. Ground Plane Instrumentation

Total Pressure and Temperature Rakes - There were four rakes on the ground board, one at the center of each side of the board. These rakes are also depicted in Figure 3-32. Each rake had six total pressure and six total temperature probes from which the percentage of the total nozzle flow deflected in each direction along the ground plane and the temperature distribution of each component flow could be determined.

3.3 NASA AMES OUTDOOR AERODYNAMIC RESEARCH FACILITY

The nozzle test program was conducted at the Ames Research Center Outdoor Aerodynamic Research Facility (OARF) at Moffett Field, California. The facility is operated and maintained by the Low Speed Wind Tunnel Investigations Branch. Provisions for testing include a permanent data system, a strut support system, a 75-ton gantry crane, a motor generator set, and a weather station. The facility is used primarily for large scale model static testing in the areas of V/STOL fixed wing aircraft, rotorcraft, and acoustics.

4. TEST PROCEDURES AND DATA ACCURACY

The procedures followed during the test program, an assessment of data accuracy and a discussion of data repeatability are presented in this section. The complete test program is summarized in the run schedule shown in Figure 4-1.

RUN NO.	CONFIGURATION	HOOD ANGLE (DEG)	A_8/A_7	OBJECTIVE
1 - 6	TCN	—	—	SYSTEM CHECKOUT
7	TCN, A_8 = 6,071 cm^2	—	0.9973	BASELINE ENGINE PERFORMANCE
8	TCN, A_8 = 6,071 cm^2	—	0.9973	
9	TCN, A_8 = 5,748 cm^2	—	0.9487	
10	TCN, A_8 = 5,748 cm^2	—	0.9487	
11	TCN, A_8 = 5,494 cm^2	—	0.9168	
12	TCN, A_8 = 6,071 cm^2	—	0.9973	
13	DVN, FWD CORE	35	1.7340	ENGINE COMPATIBILITY
14	DVN, FWD CORE	60	1.7340	
15	DVN, MIXER NOZZLE	35	1.7340	
16	DVN, FWD CORE	110	1.7340	EFFECT OF "D" NOZZLE EXIT AREA
17	DVN, FWD CORE	110	1.6662	
18	DVN, FWD CORE	110	1.5828	
19	DVN, FWD CORE	110	1.5280	
20	DVN, MIXER NOZZLE	110	1.5280	ALTERNATE CORE NOZZLE PERFORMANCE
21	DVN, MID CORE, A_{88} = 1,480 cm^2	110	1.5280	
22	DVN, MID CORE, A_{88} = 1,630 cm^2	110	1.5280	
23	DVN, MID CORE, A_{88} = 1,326 cm^2	110	1.5280	
24	DVN, FWD CORE	110	1.5280	REPEATABILITY, RUN 19
25	DVN, FWD CORE, DOORS CLOSED	35	0.9166	BASELINE NOZZLE
26	DVN, MIXER NOZZLE, DOORS CLOSED	35	0.9166	ALTERNATE CORE NOZZLE PERFORMANCE
27	DVN, MID CORE, A_{88} = 1,480 cm^2, DOORS CLOSED	35	0.9166	
28	DVN, MID CORE, A_{88} = 1,630 cm^2, DOORS CLOSED	35	0.9166	
29	DVN, MID CORE, A_{88} = 1,326 cm^2, DOORS CLOSED	35	0.9166	
30	DVN, FWD CORE, DOORS CLOSED	35	0.9166	REPEATABILITY, RUN 25
31	DVN, FWD CORE	35	1.5280	LONGITUDINAL VECTORING PERFORMANCE
32	DVN, FWD CORE	60	1.5280	
33	DVN, FWD CORE	100	1.5280	
34	DVN, FWD CORE	120	1.5280	
35	DVN, FWD CORE	130	1.5280	
36	DVN, FWD CORE, YAW VANE = 10°	110	1.5280	YAW VECTORING PERFORMANCE
37	DVN, FWD CORE, YAW VANE = 15°	110	1.5280	
38	DVN, FWD CORE, YAW VANE = 25°	110	1.5280	
39	DVN, FWD CORE, YAW VANE = 10°	110	1.5280	REPEATABILITY, RUN 36
40	DVN, FWD CORE, BEAM OUT	110	1.7453	PERFORMANCE WITH YAW
41	DVN, FWD CORE, BEAM OUT	110	1.5928	VANE REMOVED
42	DVN, FWD CORE, BEAM OUT	110	1.5280	
43	DVN, FWD CORE, BEAM OUT	110	1.5719	

GP13-0915-14

TCN - Thrust Calibration Nozzle
DVN - "D" Vented Nozzle

Figure 4-1. Run Summary

RUN NO.	CONFIGURATION	HOOD ANGLE (DEG)	A_8/A_7	OBJECTIVE
44	DVN, FWD CORE, BEAM OUT, H/D=2.22	110	1.5828	PERFORMANCE IN GROUND EFFECT
45	DVN, FWD CORE, BEAM OUT, H/D=2.22	110	1.5828	
46	DVN, FWD CORE, BEAM OUT, H/D=1.70	110	1.5828	
47	DVN, FWD CORE, BEAM OUT, H/D=1.03	110	1.5828	
48	DVN, FWD CORE, BEAM OUT	110	1.7453	REPEATABILITY, RUN 40
49	DVN, FWD CORE, BEAM OUT	110	1.5828	REPEATABILITY, RUN 41
50	TCN, A_8=6,871 cm^2	—	0.8973	REPEATABILITY, RUN 7
51	TCN, A_8=5,748 cm^2	—	0.8497	REPEATABILITY, RUN 10
52	TCN, A_8=5,484 cm^2	—	0.8163	REPEATABILITY, RUN 11

TCN - Thrust Calibration Nozzle
DVN - "D" Vented Nozzle

GP13-0816-16

Figure 4-1. (Continued) Run Summary

4.1 TEST PROGRAM PROCEDURE

The outdoor tests were conducted early each morning to take advantage of the low wind conditions which normally existed during this period. The majority of the test runs were made with ambient wind velocities below five knots; and no runs were made with wind velocities above eight knots. For each test run the engine was started and brought to idle speed for a five-minute warm-up period, after which the fan speed was increased in four increments to approximately 93% (6500 RPM). After completion of data acquisition at 93% fan speed, the speed was reduced, again in four increments, to the idle setting for a five-minute cool-down period and then shut down. Engine and nozzle performance data were generally recorded at seven test points during each run.

At each test point, most data were recorded by means of the Ames Standardized Data Acquisition System (ASDAS), while the engine panel instrumentation was manually recorded. The ASDAS data were recorded on magnetic tape and processed through the data reduction program on a PDP 11/70 high speed digital computer. A brief summary of the key portions of the data reduction procedure is included in Appendix A.

4.2 DATA ACCURACY

The overall accuracy of the force measurements is difficult to assess due to the lack of calibration apparatus at the test site and the obvious difficulties in holding environmental conditions constant at an outside facility. Pre-test installed checkouts of the three-component load cell system were performed by applying a horizontal force to the nozzle rig by means of a cable and pulley arrangement with a calibrated single-axis load cell. The results of these tests showed agreement between the applied and measured readings within one-half of one percent.

Due to the presence of two independent sets of load cells installed on this model (single and three-axis) a comparison of the two sets of measurements can be made. Figure 4-2 shows a comparison of vertical thrust between the single and three-axis load cells. Excellent agreement can be seen. This agreement between two independent measuring devices provides a high level of confidence in the test results.

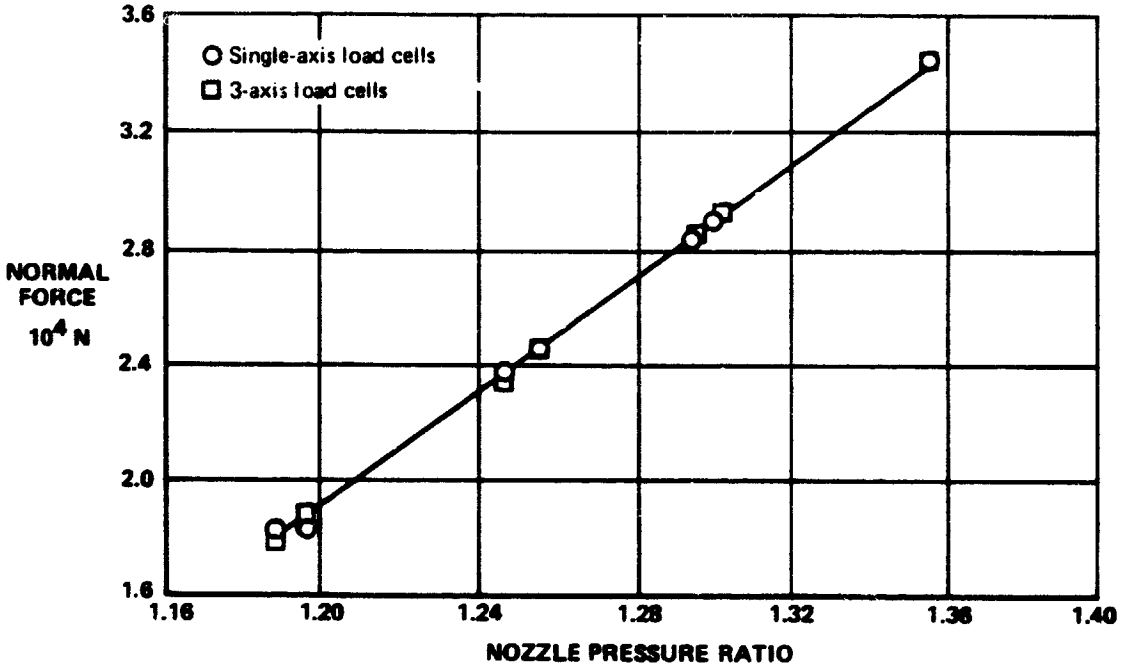

Figure 4-2. Three- Axis and Single-Axis Load Cells Comparison
Hood = 110° $A_8/A_7 = 1.593$

4.3 DATA REPEATABILITY

Several configurations were retested to ensure the repeatability of thrust and mass flow measurements. Repeatability of the data for a typical configuration is shown in Figure 4-3. Based on polynomial curve fits of the data, the velocity coefficient and mass flow repeated within $\pm 1\%$ and $\pm 0.2\%$ respectively. The thrust vector angle repeated within $\pm 1/2$ degree.

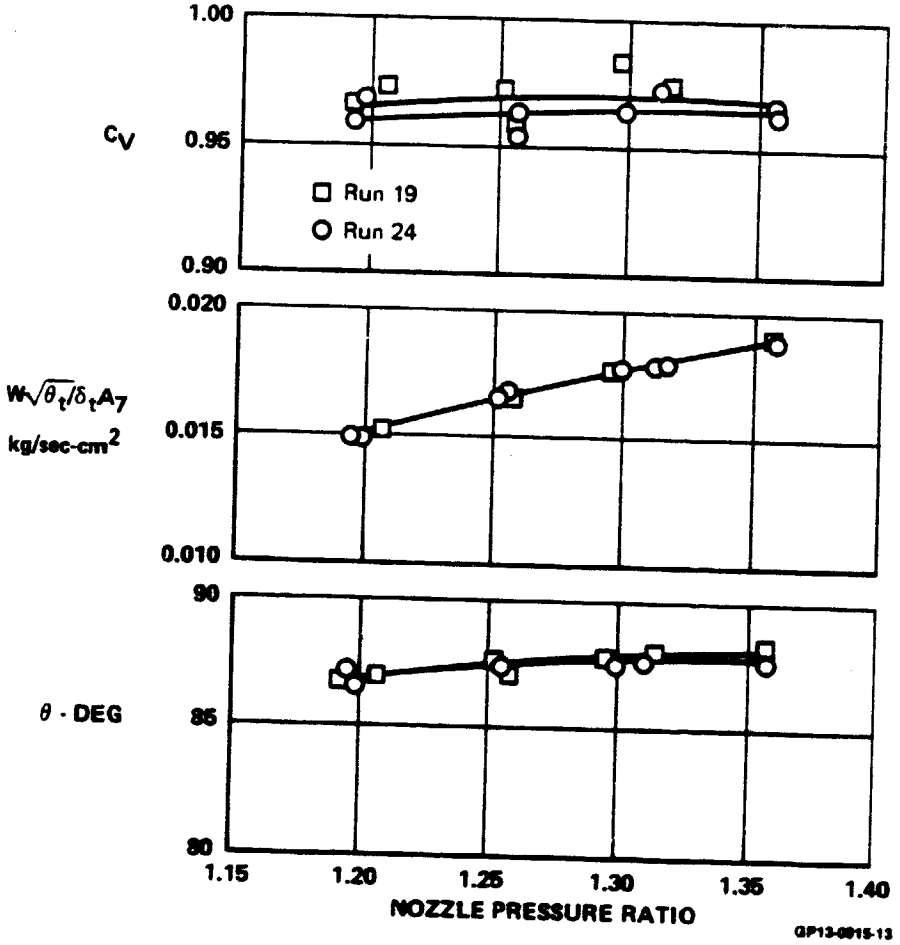

Figure 4-3. Data Repeatability
110° Hood $A_8/A_7 = 1.526$
Runs 19 and 24

5. DISCUSSION OF RESULTS

The experimental data obtained with the calibration and "D" vented nozzles have been reduced primarily in terms of velocity coefficient, C_V, i.e., the ratio of measured thrust to the ideal thrust of the unmixed fan and core streams. These velocity coefficients are presented as a function of either nozzle pressure ratio or specific corrected flow (nozzle entrance Mach number). The equations for these key parameters are defined in Appendix A. The discussion that follows covers engine/nozzle compatibility, the thrust calibration nozzle tests, the "D" vented nozzle tests, and comparison of large scale and small scale test results.

5.1 ENGINE/NOZZLE COMPATIBILITY

The General Electric YTF-34-F5 turbofan engine was run first with a conical calibration nozzle to establish baseline engine performance and then with the "D" vented nozzle. Throughout all of the test conditions, no adverse effects of either type of nozzle on engine operation were observed. An example of this can be seen by examining fan exit total pressure distortion. The values of radial and circumferential distortion measured at the fan exit plane were at the relatively low levels expected from pretest estimates. This was true for engine operation with both the calibration nozzle and the "D" nozzle. As shown in Figure 5-1, the differences in distortion levels between the calibration nozzle and the "D" nozzle vectored to the VTO (110° hood angle, 90° vector angle) position are slight. These characteristics did not change significantly through all of the various nozzle configuration changes.

Additional distortion characteristics for both the calibration and "D" vented nozzles are included in Figures 5-2 and 5-3, respectively. Slightly larger differences in distortion level can be seen between the fan exit and nozzle entrance stations for the vectored "D" vented nozzle than for the calibration nozzle. This larger difference for the "D" nozzle is due to the large static pressure gradient present in the nozzle during vectoring.

The total pressure and temperature distortion characteristics of the installed propulsion system are presented in the form of contour plots in Figures 5-4 through 5-8. The fan stream total pressure contours at the nozzle entrance for the calibration nozzle are shown in Figure 5-4. Figures 5-5 and 5-6 illustrate fan stream total pressure distributions for the "D" vented nozzle at the fan exit and nozzle entrance stations, respectively. Core stream total pressure distortion levels are lower than those in the fan stream as illustrated in Figure 5-7, which presents contours of the core stream at the nozzle entrance. Total temperature distributions of the fan stream at the nozzle entrance plane are shown in Figure 5-8.

5.2 THRUST CALIBRATION NOZZLE TESTS

The thrust calibration nozzle tests were conducted to establish the reference thrust performance levels of the installed YTF-34-F5 engine with near ideal nozzles, and to determine the specific nozzle entrance corrected flow characteristics of the turbofan engine operating with a single nozzle in the confluent (mixed) flow mode.

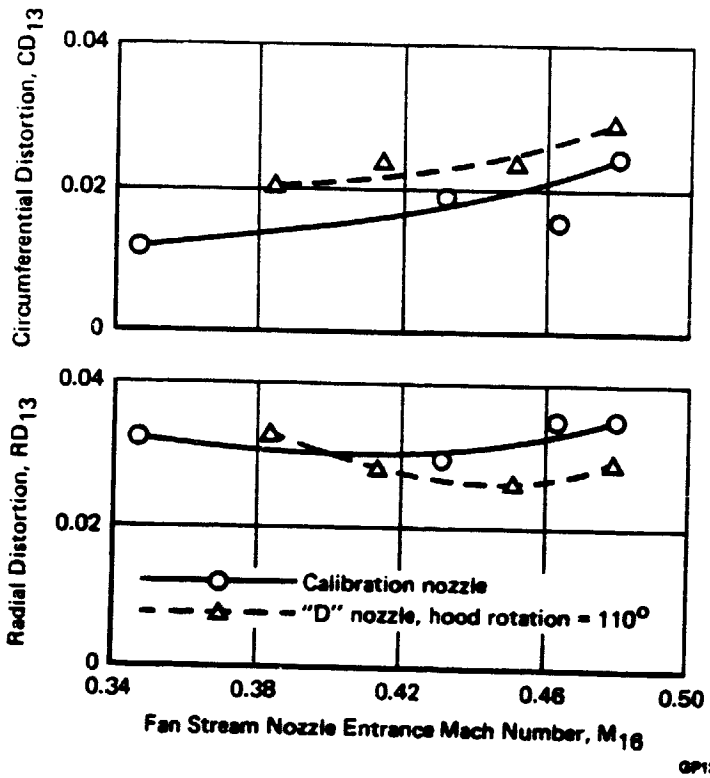

Figure 5-1. Fan Exit Distortion
Calibration Nozzle and "D" Vented Nozzle

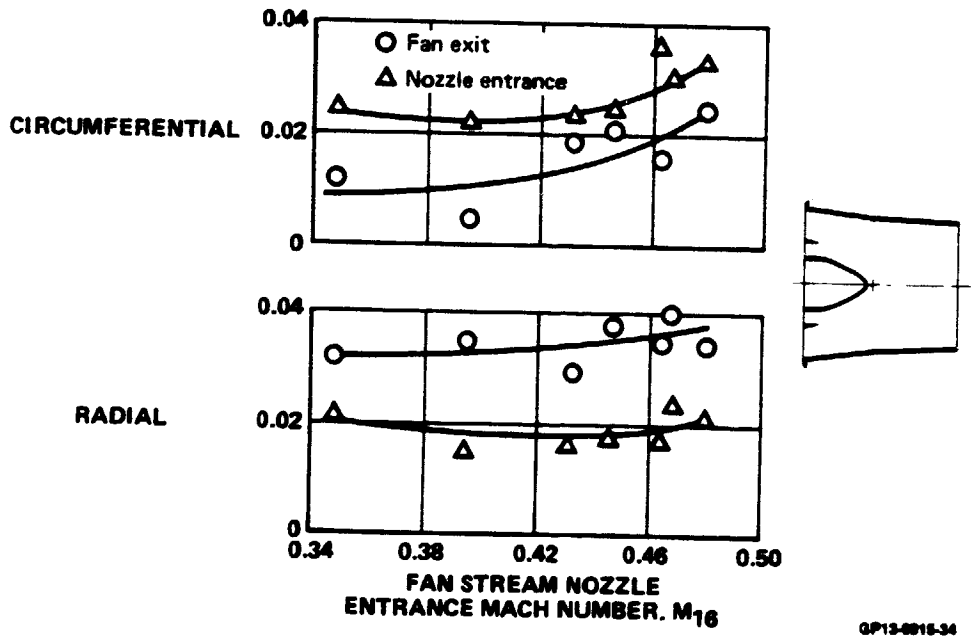

Figure 5-2. Calibration Nozzle Fan Exit and Nozzle Entrance Distortion

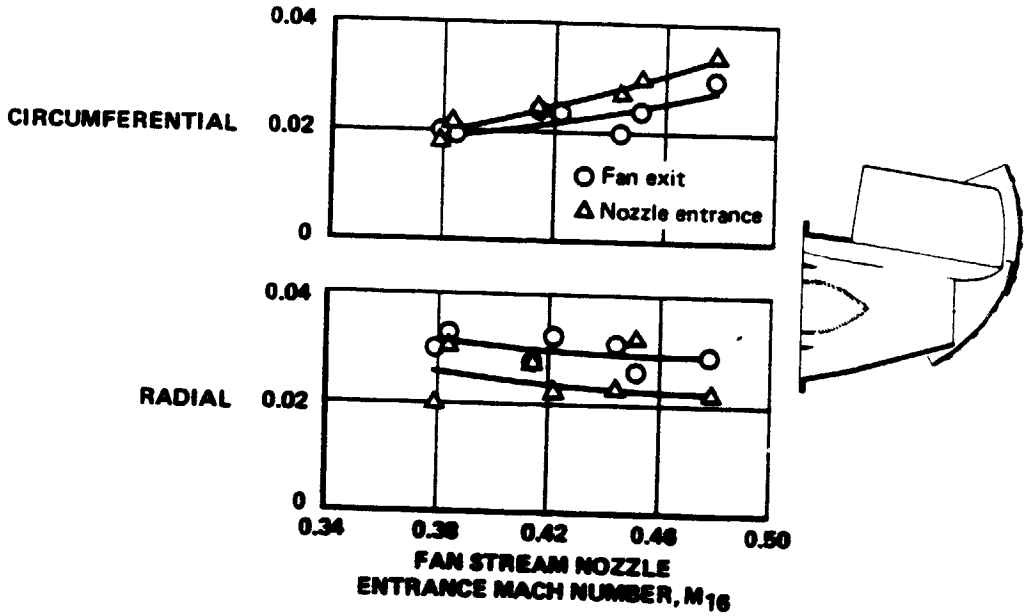

GP13-0015-17

Figure 5-3. "D" Vented Nozzle Fan Exit and Nozzle Entrance Distortion

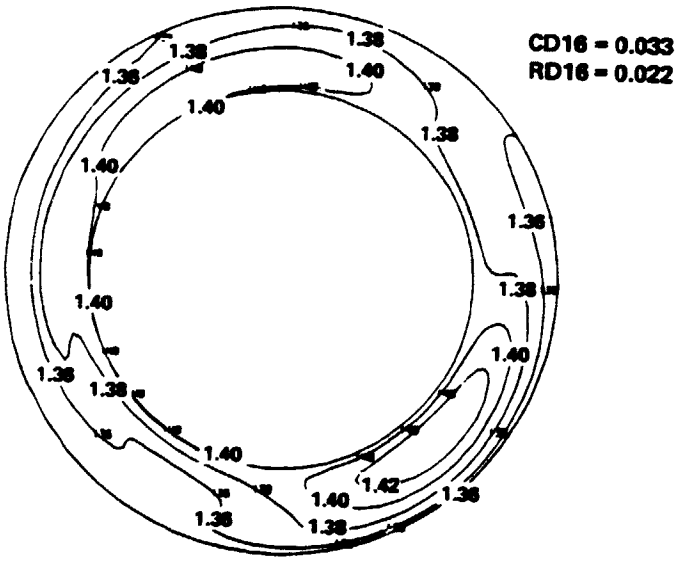

GP13-0015-41

Figure 5-4. Calibration Nozzle $P_{T16}/P_{ambient}$ Contours
Nozzle Entrance Station
$A_8 = 5{,}748\ cm^2$

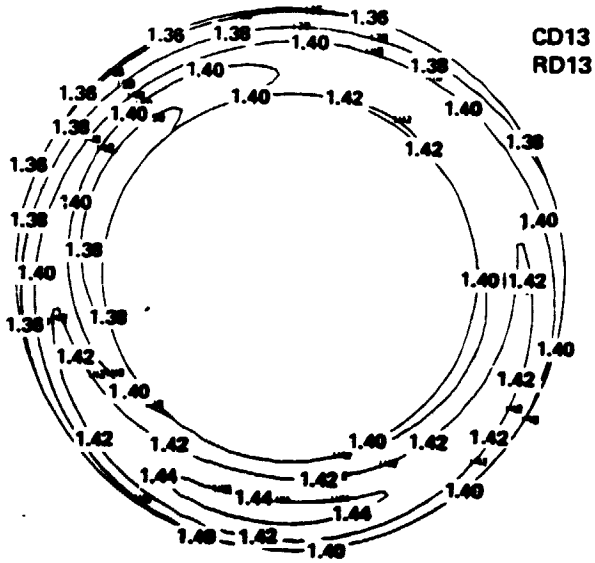

Figure 5-5. "D" Vented Nozzle $P_{T_{13}}/P_{ambient}$ Contours

Fan Exit Station

Hood = 110° $A_8/A_7 = 1.526$

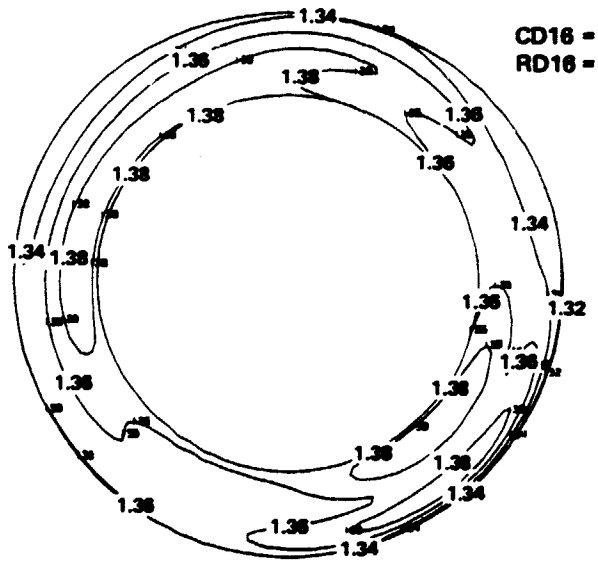

Figure 5-6. "D" Vented Nozzle $P_{T_{16}}/P_{ambient}$ Contours

Nozzle Entrance Station

Hood = 110° $A_8/A_7 = 1.526$

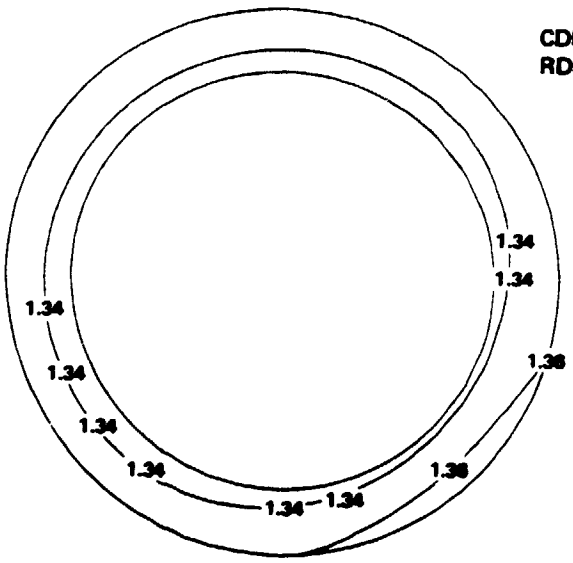

Figure 5-7. "D" Vented Nozzle $P_{T_{56}}/P_{ambient}$ Contours

Nozzle Entrance Station

Hood = 110° $A_8/A_7 = 1.526$

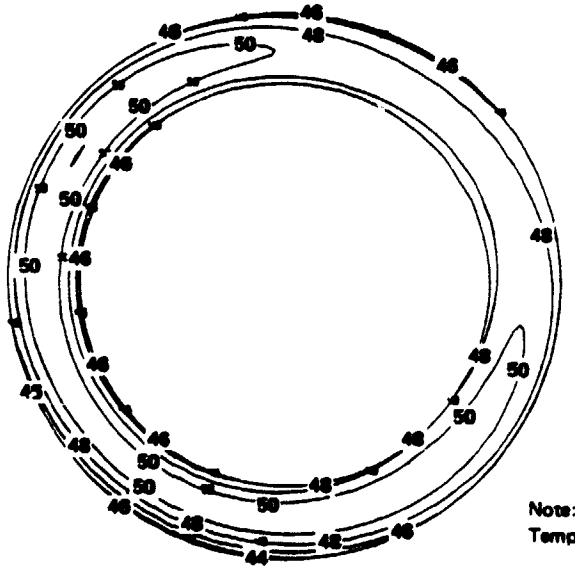

Figure 5-8. "D" Vented Nozzle $T_{T_{16}}/T_{ambient}$ Contours

Nozzle Entrance Station

Hood = 110° $A_8/A_7 = 1.526$

5.2.1 THRUST PERFORMANCE - The fan operating characteristics obtained during the thrust calibration nozzle tests are shown in Figure 5-9. The observed fan operating line for the selected match point exit area (5748 cm^2) was slightly lower than that predicted by GE prior to the test. The GE predictions were based on a computer engine deck simulation of this specific YTF-34-F5 turbofan engine. Apparently, this simulation did not match the actual engine performance precisely. This would explain the differences noted in Figure 5-9 between the predicted and demonstrated fan operating line characteristics.

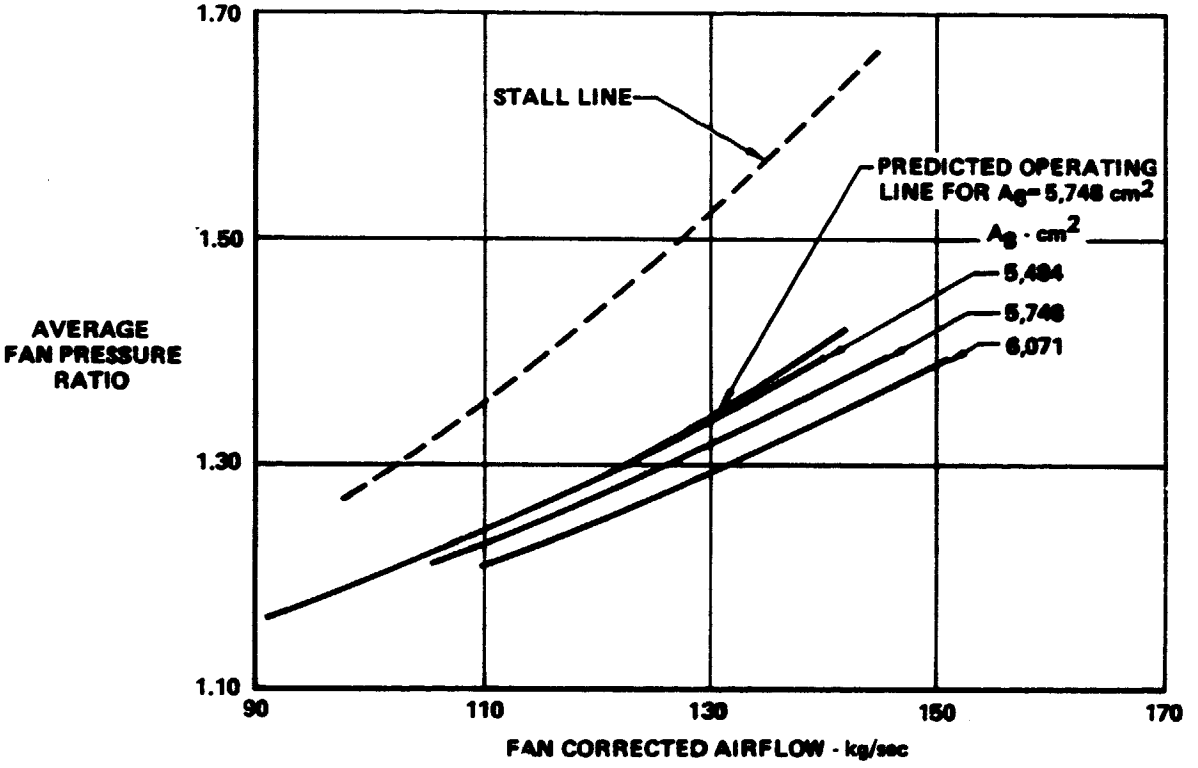

Figure 5-9. Fan Operating Characteristics Calibration Nozzle

Thrust and mass flow characteristics for the three nozzle areas tested are presented in Figures 5-10 and 5-11, respectively. The corrected thrust increased and the corrected fan flow decreased, as expected, as nozzle exit area was reduced.

5.2.2 WALL PRESSURE AND TEMPERATURE MEASUREMENTS - Figures 5-12 and 5-13 show a typical set of internal pressure measurements for the calibration nozzle. The data plotted are for the middle exit area, 5748 cm^2, at a corrected fan speed ($N_F \sqrt{\theta_t}$) of 93 percent. The circumferential static pressures in the fan and core ducts, presented in Figure 5-12, are relatively independent of the angle, ϕ. Figure 5-13 illustrates the radial static pressure distributions from the fan exit through to the nozzle exit. The static pressure increases and then decreases in the fan duct as the flow diffuses and then accelerates. Then the pressure decreases through the nozzle toward ambient at the nozzle exit.

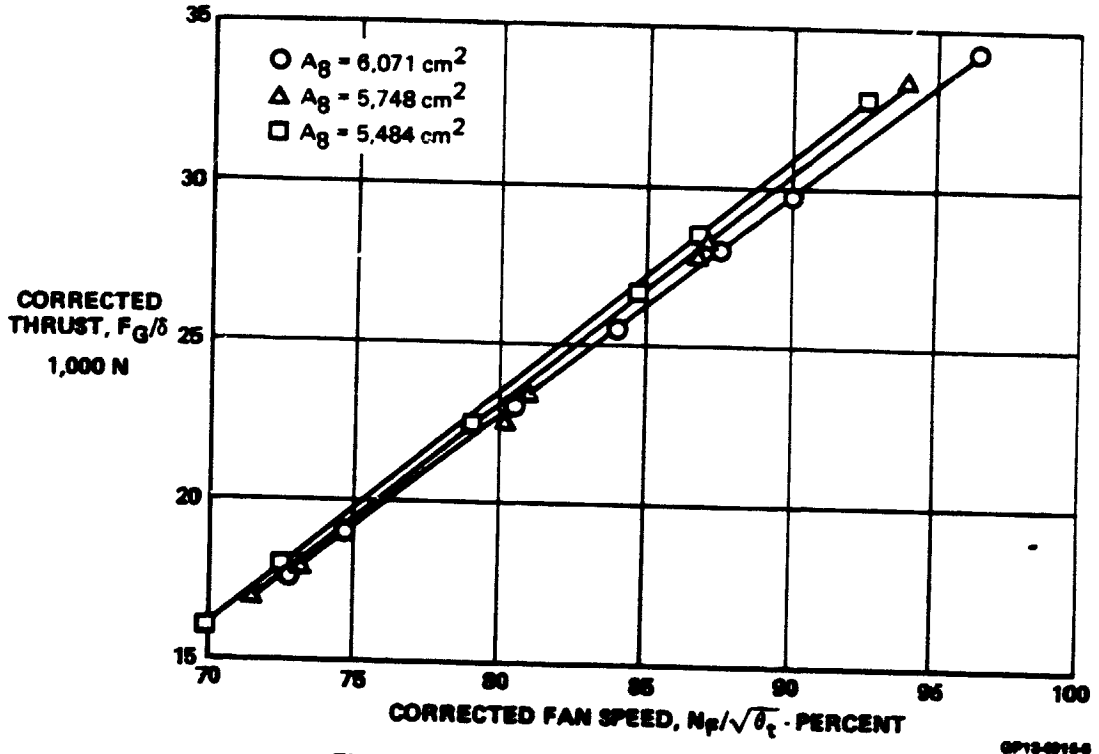

Figure 5-10. Thrust vs Fan Speed
Calibration Nozzle Performance

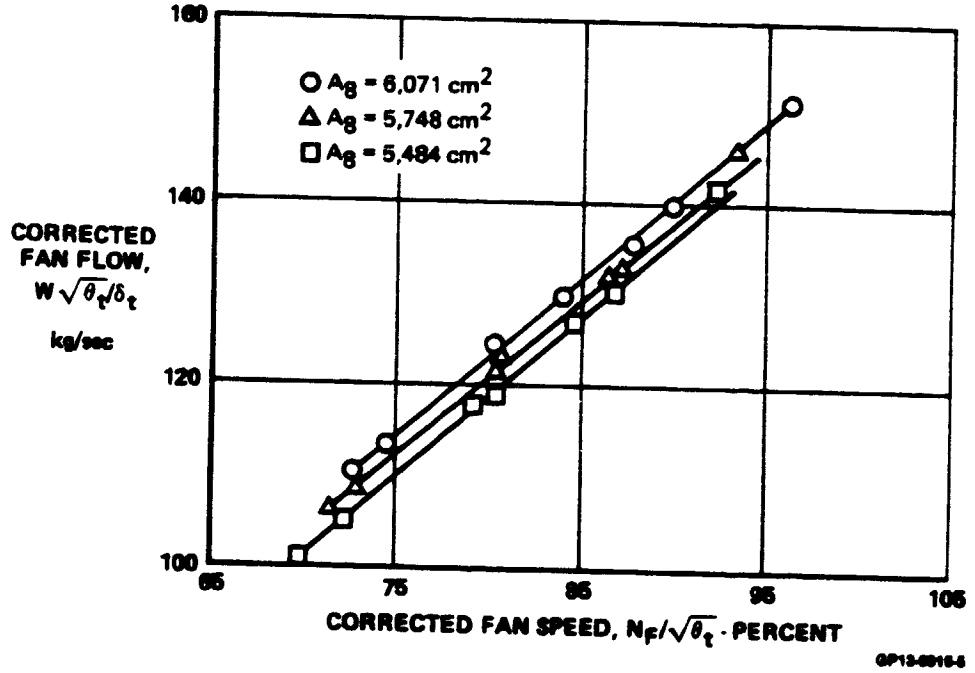

Figure 5-11. Fan Flow vs Fan Speed
Calibration Nozzle Performance

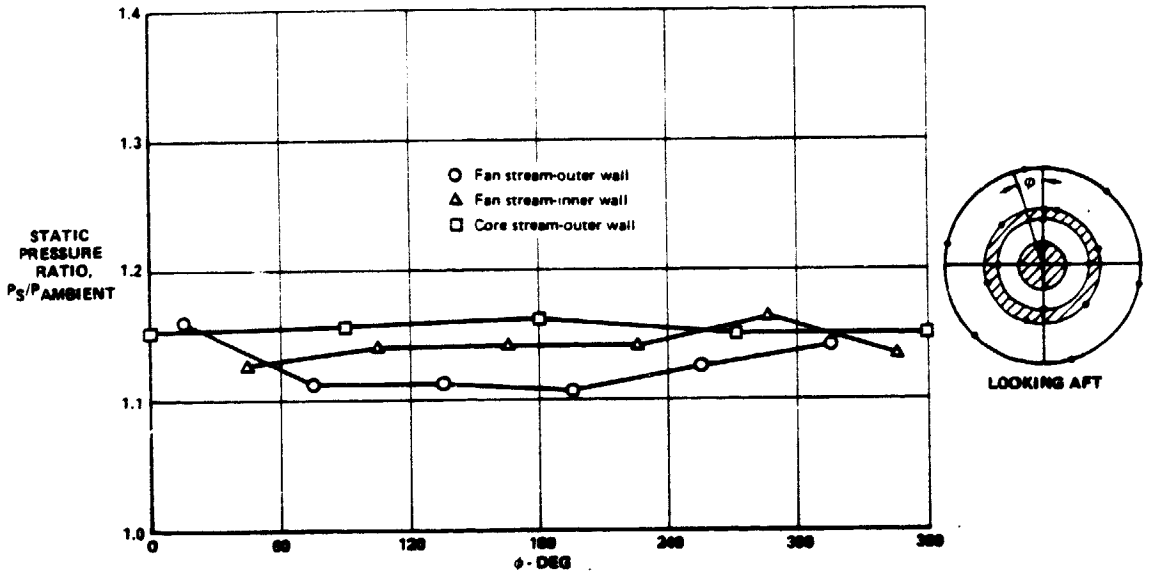

Figure 5-12. Circumferential Wall Pressure Distributions
Calibration Nozzle $A_8 = 6{,}071\ cm^2$ Nozzle Entrance Station

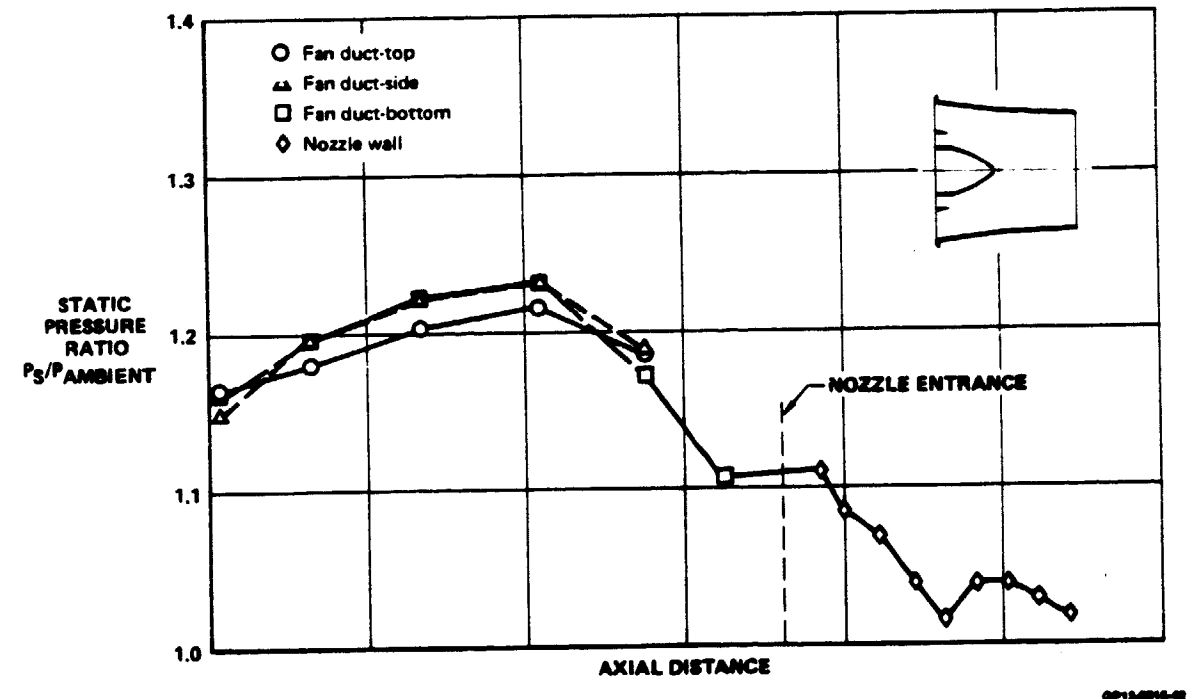

Figure 5-13. Radial Wall Pressure Distributions
Calibration Nozzle $A_8 = 6{,}071\ cm^2$

Wall temperature measurements for a typical calibration nozzle run are included in Figure 5-14. The temperatures along the nozzle wall are essentially constant at approximately the same value as the fan air. This indicates that mixing of the fan and core streams is incomplete.

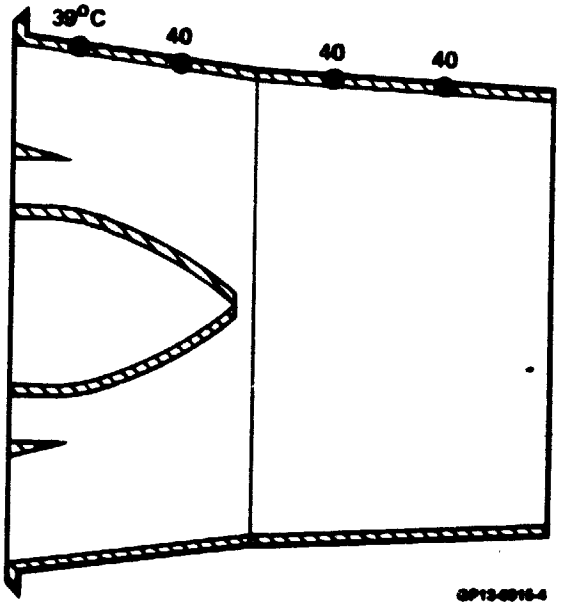

Figure 5-14. Wall Temperature Distributions Calibration Nozzle

5.3 "D" VENTED NOZZLE TESTS

The tests with the "D" vented nozzle were conducted to evaluate exit area variations, alternate core nozzles, longitudinal and yaw vectoring, wall pressure and temperature distributions, performance "in" and "out" of ground effect, and several other nozzle characteristics. A discussion of the results obtained for these parametric investigations is presented in this section.

5.3.1 EXIT AREA VARIATIONS - Previous tests of the "D" vented nozzle, described in References 1 and 2, indicate that the velocity coefficient is strongly dependent on exit area variation, particularly in the vectored mode. In this test program, exit area was varied parametrically for the baseline (forward core) configuration. Four areas were tested by employing different size venting lips. These provided nozzle exit to entrance area ratios of 1.526, 1.593, 1.666, and 1.735. The effect of variations in exit area on the fan operating line is shown in Figure 5-15. An exit area of 10,323 cm^2, corresponding to an area ratio of 1.526, was selected for the majority of test configurations because it produced the operating line closest to the desired engine/nozzle match during 90° thrust vector operation.

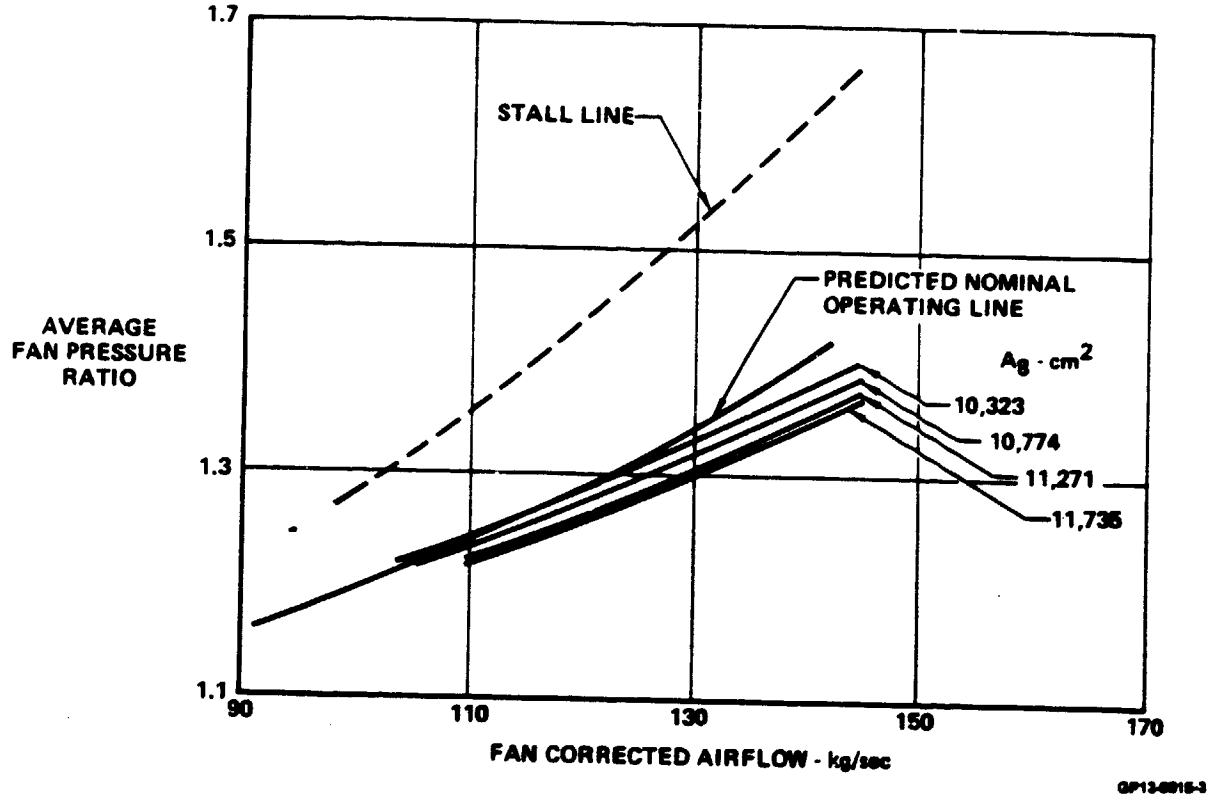

Figure 5-15. Fan Operating Characteristics
"D" Vented Nozzle Hood Rotation Angle = 110°

Vectored "D" vented nozzle performance for variations in exit area is presented in the form of the map shown in Figure 5-16 for the forward core nozzle configuration. Velocity coefficient is depicted as a function of nozzle entrance specific corrected flow, nozzle pressure ratio, and nozzle exit-to-entrance area ratio. In this manner, both the nozzle performance, C_V, and the nozzle sizing parameter, specific corrected flow, are presented on the same map. In addition, specific corrected flow can be converted to Mach number, which has the advantage of being a nondimensional parameter. The performance shown on this map includes the detrimental effects of boilerplate irregularities, non-production seals, and instrumentation. These effects would not be present in a production nozzle.

5.3.2 CORE NOZZLE COMPARISONS - Three basic comparisons with the baseline can be made from the different core configurations tested. These include the effect of core exit location, the effect of core exit area, and the performance of the slotted mixer nozzle.

The effect of core exit location on velocity coefficient can be seen in Figure 5-17. The performance with the mid core is substantially lower, 1.5 to 3.5 percent, than that for the forward core configuration, depending on the nozzle pressure ratio. The aft core configuration was not tested due to time constraints. However, based on previous test data, References 2 and 4, the performance for the aft position would be expected to be lower than that for the mid position.

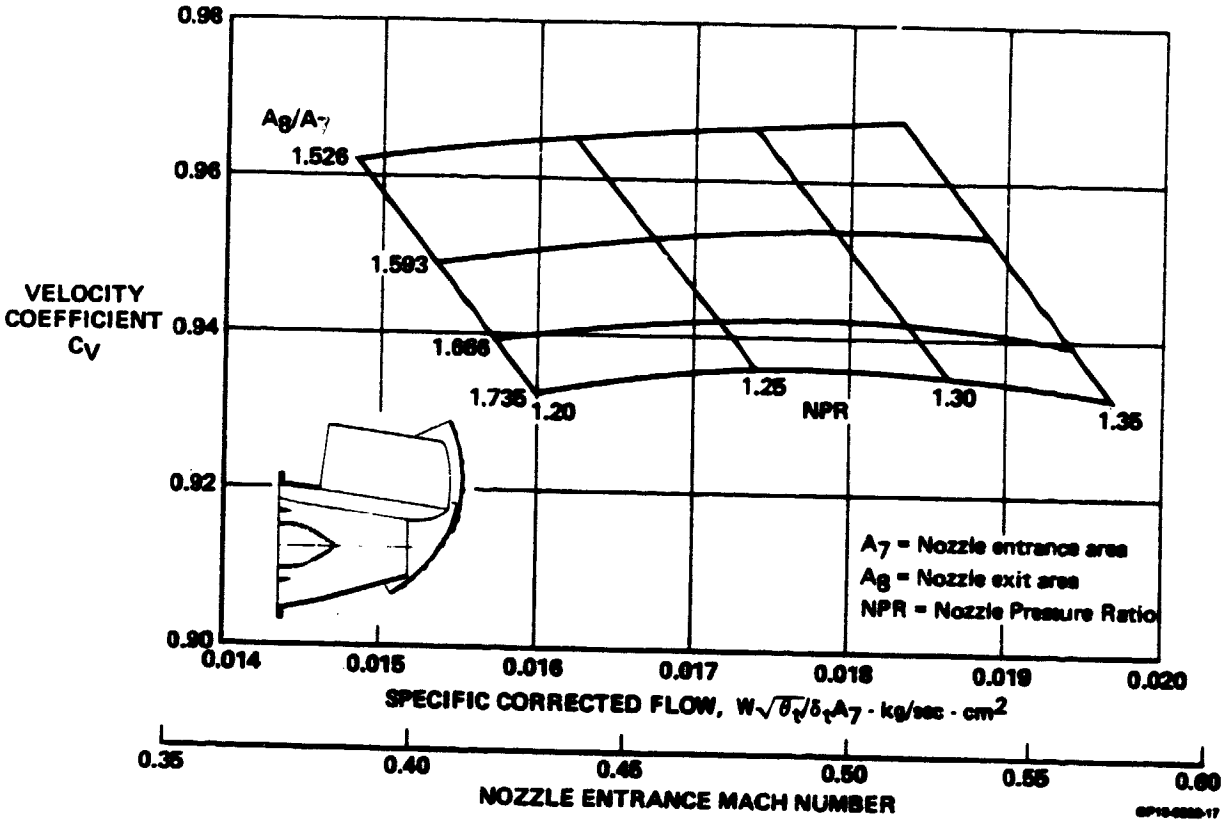

Figure 5-16. TF34/"D" Vented Nozzle VTO Performance Map
90° Thrust Vector Angle

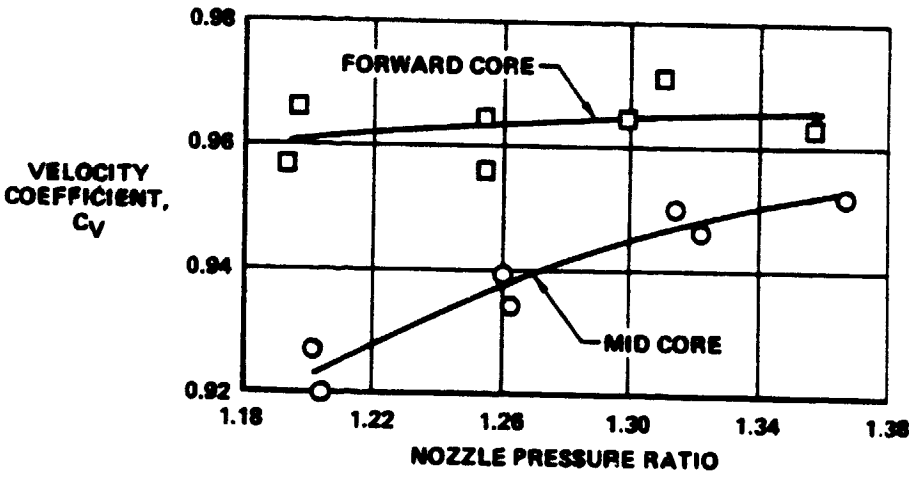

Figure 5-17. Effect of Core Axial Location
Hood = 110° $A_8/A_7 = 1.526$

The effect of core exit area on nozzle performance was examined by testing three different areas at the mid core position. A comparison of the vectored performance for the three areas is shown in Figure 5-18. In general, the middle area, which is the same as that of the forward core, is slightly higher in performance than the smallest area and significantly higher than the largest area. Cruise nozzle performance was approximately the same for all three configurations.

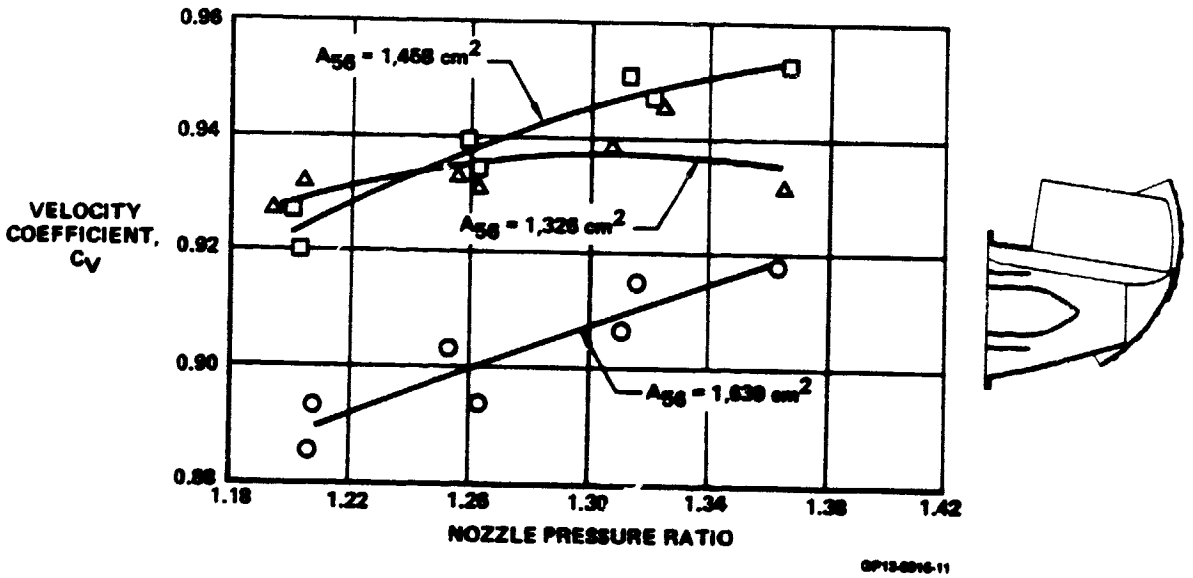

Figure 5-18. Effect of Core Exit Area
Mid Core Position
Hood = 110° $A_8/A_7 = 1.526$

The slotted mixer was designed to improve nozzle performance at the engine out condition. The slotted, conical shaped surface was intended to aid in the control of the diffusion of the fan stream with the core not flowing. This is contrasted with the sudden diffusion of the fan stream that would take place at the nozzle entrance with the baseline core configuration at the engine out condition. While the engine out condition could not be simulated in this test, it was hoped that equal or better performance could be achieved with the slotted mixer nozzle during normal engine operation. This would result if the nozzle induced substantial mixing of the high temperature core and low temperature fan streams. The performance obtained with the mixer nozzle is compared with that for the forward core nozzle in Figure 5-19, for a hood rotation angle of 110°. The measured velocity coefficients are one-half to one percent lower for the mixer nozzle over the NPR range tested. This is apparently an indication that the slotted mixer nozzle does not promote sufficient additional mixing of the two streams to compensate for slot exit pressure losses. Performance in the cruise mode was approximately equal for the two core nozzles. A large scale test of the slotted mixer nozzle at the engine out condition would be required to completely judge the merits of this core exit configuration.

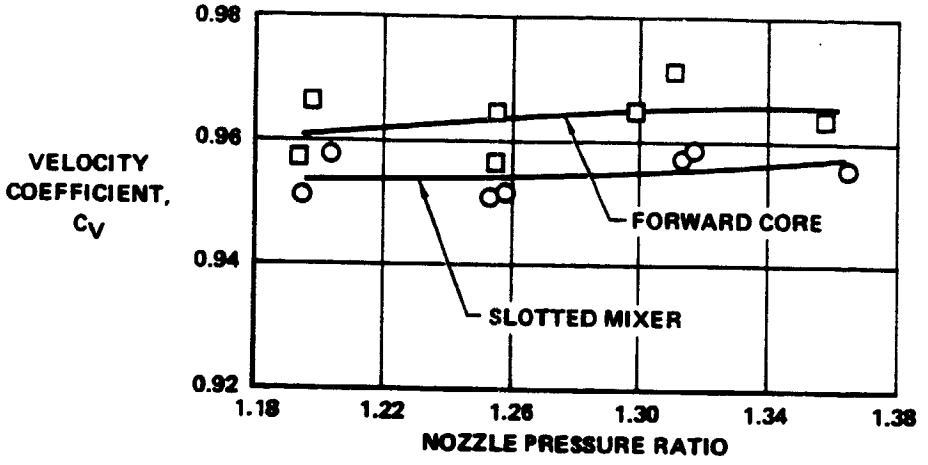

Figure 5-19. Forward Core and Slotted Mixer Comparison GP13-0015-0
Hood = 110° $A_8/A_7 = 1.526$

5.3.3 LONGITUDINAL VECTORING - The "D" vented nozzle was tested at hood deflection angles of 35°, 60°, 100°, 120° and 130°. The variations of velocity coefficient, specific corrected flow, and hood rotation angle with longitudinal vector angle are shown in Figure 5-20. In general, the vector angle, θ, trails the hood rotation angle, β, by approximately 20 degrees. As can be seen θ increases from 0 to 8 degrees as the closure doors are opened. In addition, opening the doors results in a substantial increase in effective exit area. This results in an increase in nozzle flow rate and entry Mach number and a corresponding decrease in velocity coefficient. Testing constraints did not permit testing of different venting lips (exit areas) at each vector angle. However, if the nozzle exit area were variable, as it would be on a production nozzle, the "dip" in the velocity coefficient curve could be eliminated. This is also illustrated in Figure 5-20.

5.3.4 THRUST MOMENT ARM - The distance between the gross thrust vector line of action and the aircraft center of gravity is important in the design of V/STOL aircraft, in terms of both balance and control. The thrust moment arm is defined in Figure 5-21 as the distance measured along the engine centerline between the hood rotation point and the point where the gross thrust vector line of action and the engine centerline intersect. Variations of the thrust moment arm with nozzle pressure ratio and nozzle exit area are presented in Figure 5-22, where the thrust moment arm, L_T, has been normalized to the nozzle entrance diameter, D_7. The data indicate that the thrust vector moves aft slightly with both increasing nozzle pressure ratio and decreasing exit area.

Variation of the thrust moment arm is also shown as a function of thrust vector angle in Figure 5-23. The thrust vector moves aft as the longitudinal vector angle increases, as expected.

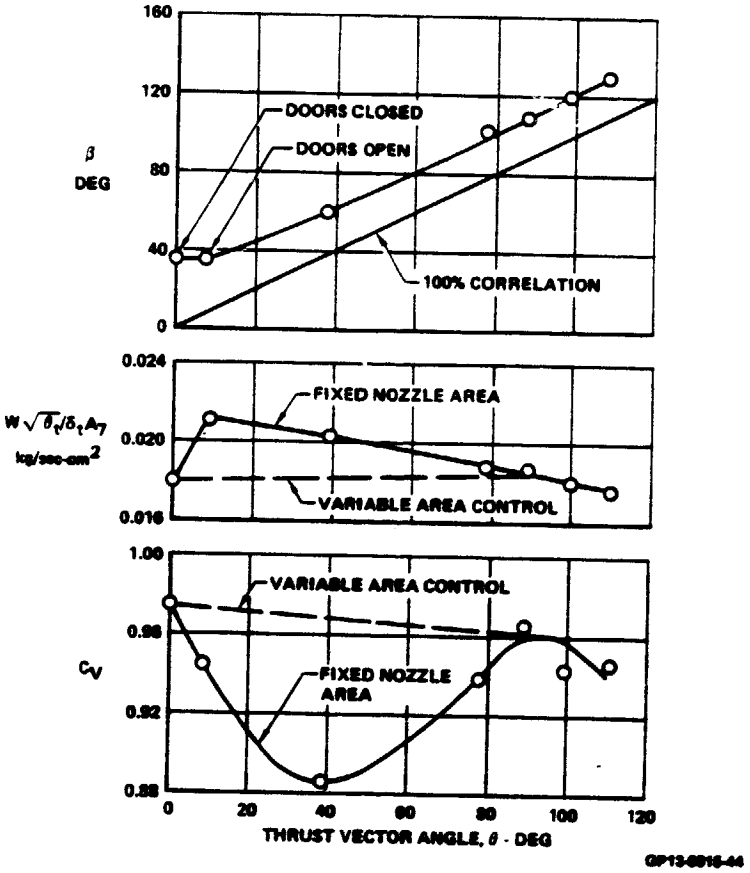

Figure 5-20. "D" Vented Nozzle Vectoring Performance
NPR = 1.35

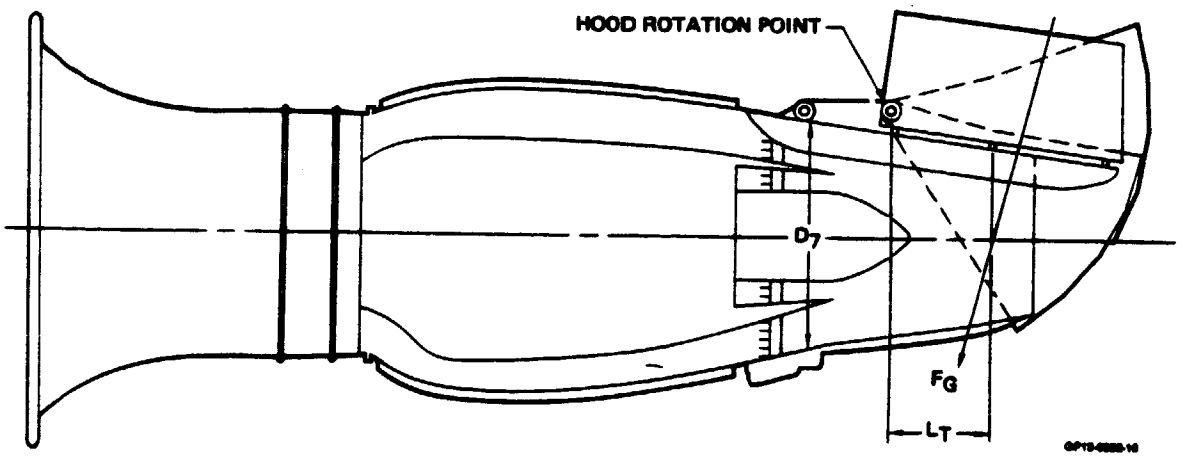

Figure 5-21. Definition of Thrust Moment Arm

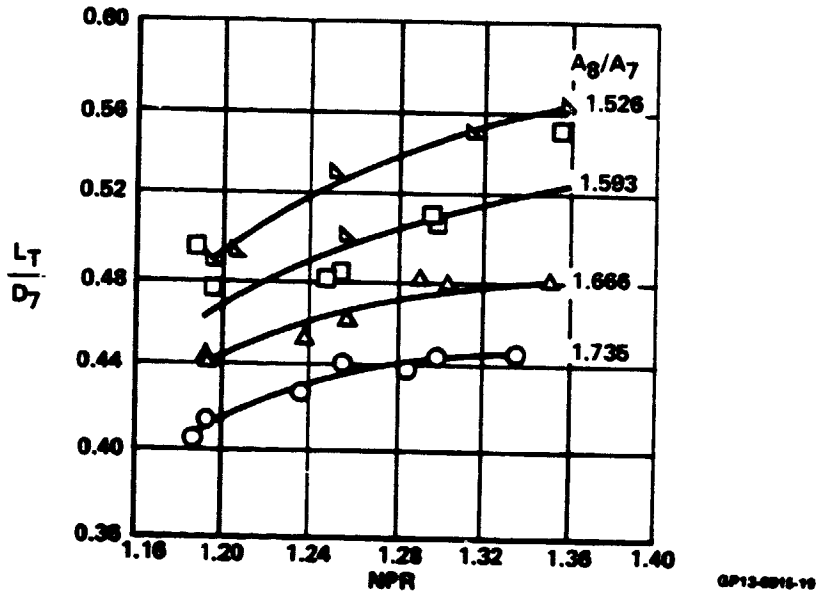

Figure 5-22. Effect of Exit Area Variation on Thrust Moment Arm
Hood Rotation Angle = 110°

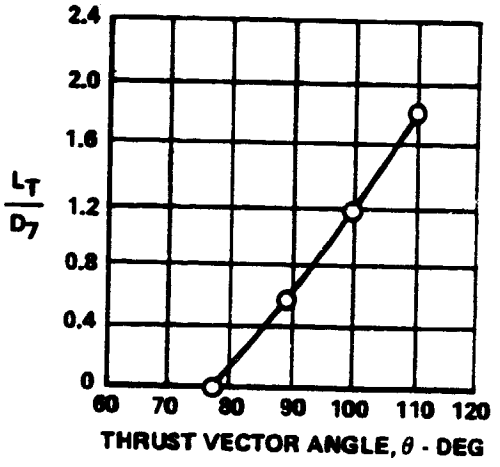

Figure 5-23. Effect of Thrust Vector Angle on Thrust Moment Arm

5.3.5 WALL PRESSURE AND TEMPERATURE MEASUREMENTS - Static wall pressure taps were installed in the fan duct, at the nozzle entrance, and along the "D" nozzle walls, as illustrated in Figure 5-24. Figures 5-25 through 5-30 illustrate the internal wall radial pressure distributions from the fan exit through to the nozzle exit for each of the hood rotation angles tested. In general, the pressure distributions do not change significantly in character as the vector angle is varied. The pressure levels do vary in a manner consistent with the change in nozzle flow rate with vector angle. The static

pressure increases and then decreases in the fan duct as the flow diffuses and then accelerates. Then the pressure distributions show the characteristic increase in wall pressure to near stagnation values as the flow proceeds through the rotating hoods and then a decrease toward ambient at the nozzle exit.

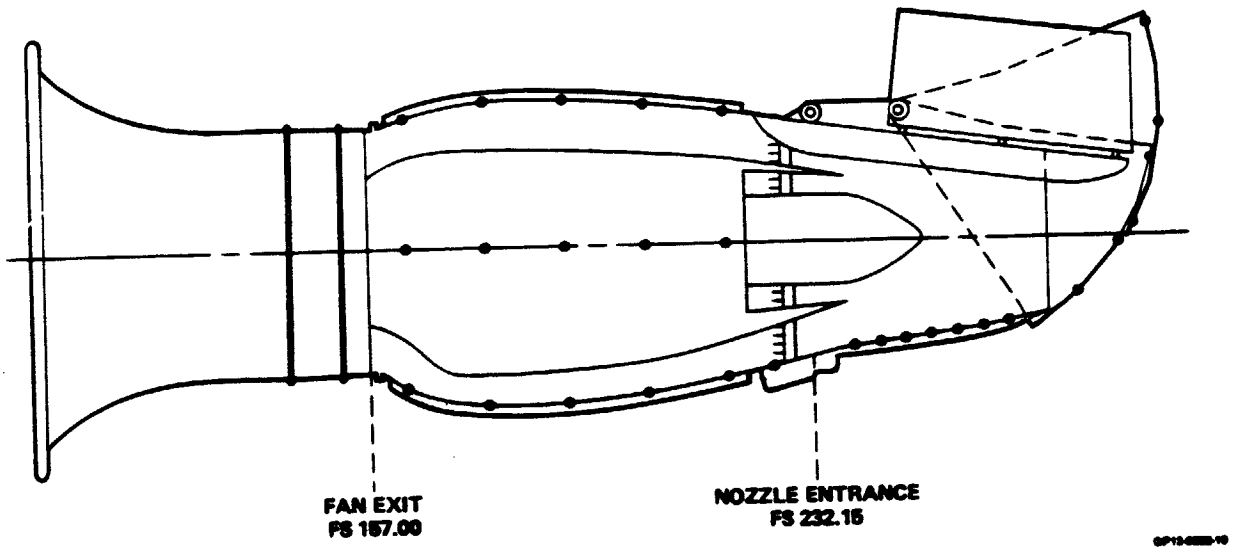

Figure 5-24. TF34/"D" Vented Nozzle Wall Pressure Instrumentation

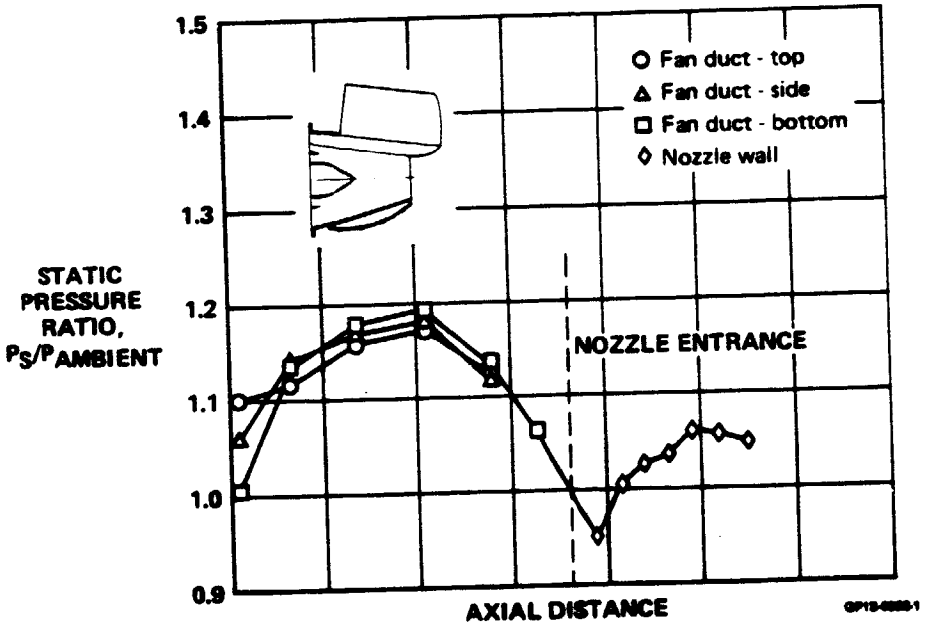

Figure 5-25. Radial Wall Pressure Distributions
Hood Rotation Angle = 35°

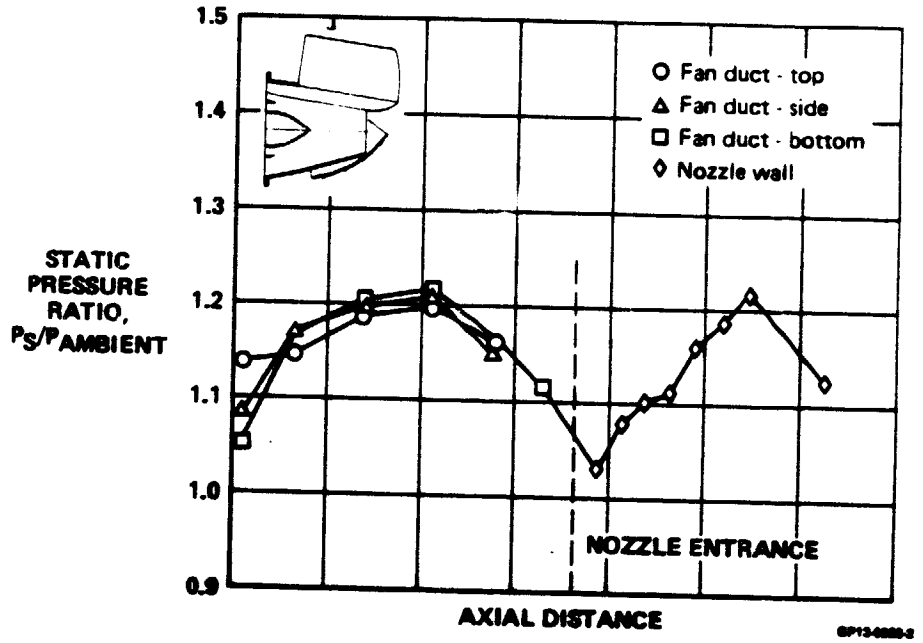

Figure 5-26. Radial Wall Pressure Distributions
Hood Rotation Angle = 60°

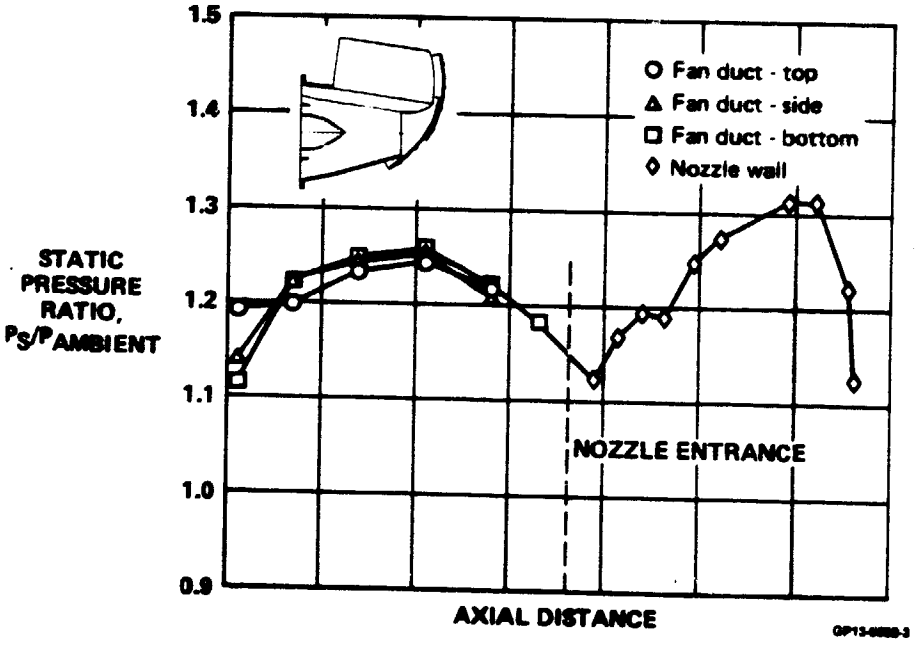

Figure 5-27. Radial Wall Pressure Distributions
Hood Rotation Angle = 100°

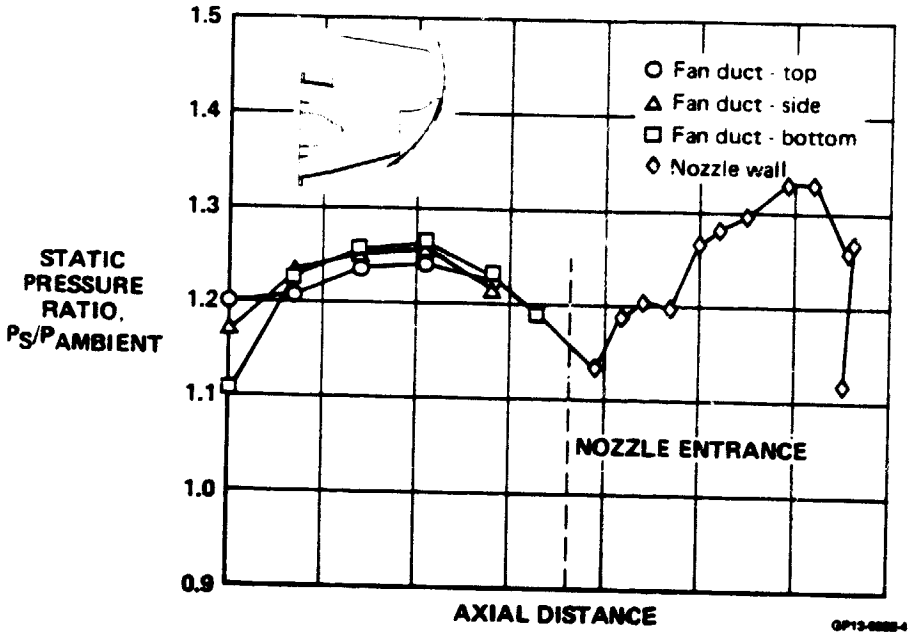

Figure 5-28. Radial Wall Pressure Distributions
Hood Rotation Angle = 110°

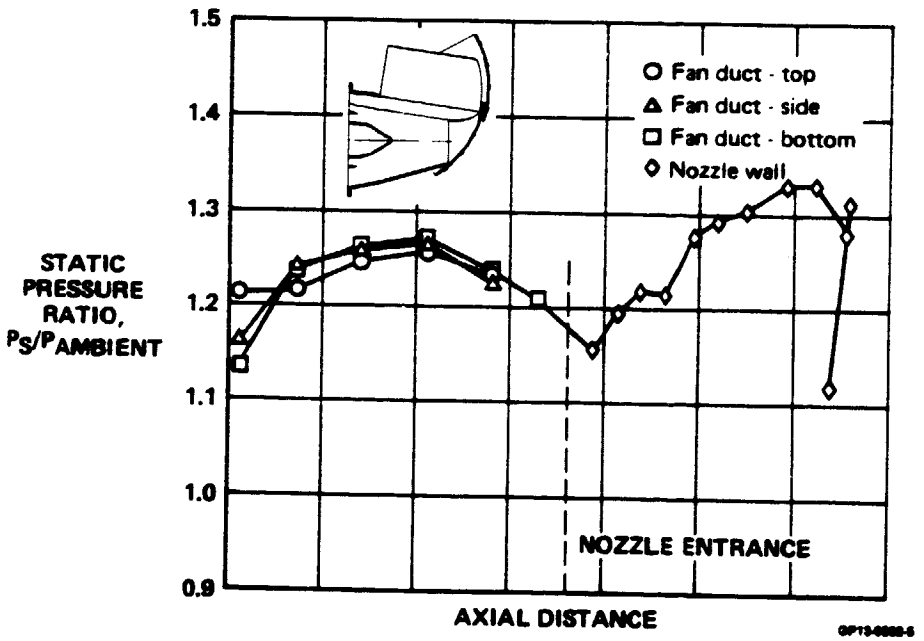

Figure 5-29. Radial Wall Pressure Distributions
Hood Rotation Angle = 120°

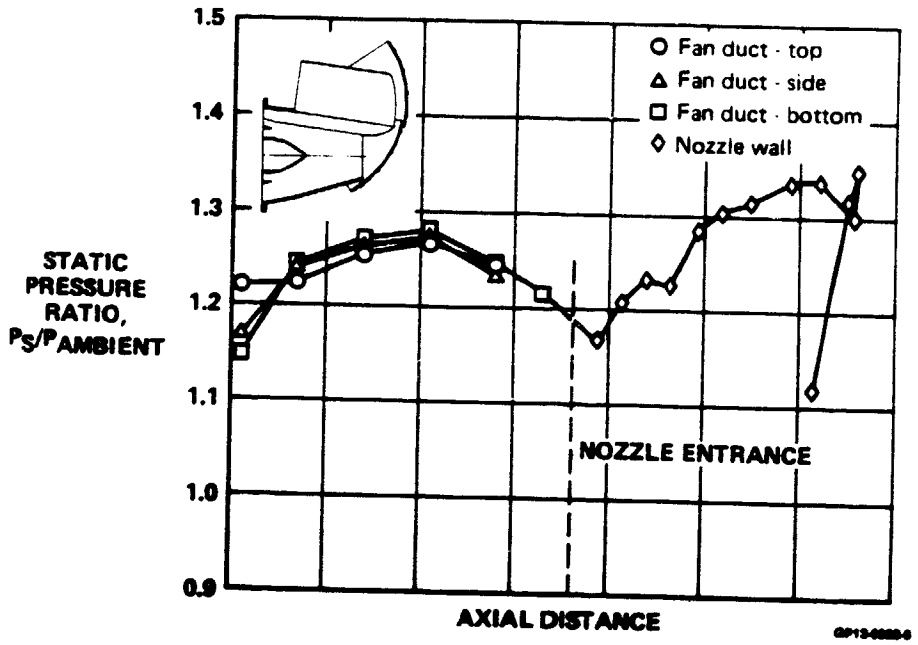

Figure 5-30. Radial Wall Pressure Distributions Hood Rotation Angle = 130°

The nozzle entrance circumferential pressure distributions are shown in Figures 5-31 through 5-36 for each of the hood rotation angles tested. In general, a circumferential gradient from the bottom to the top (reversed in aircraft installation) exists which is indicative of a net upward turning of the flow at this station in the same direction as the deflected flow. The static pressure taps at ϕ = 75° and 135° on the fan stream outer wall measured slightly lower than expected pressures during all of the "D" vented nozzle testing. This was because the flexible seals attached to the adapter section just upstream of these two pressure taps were slightly bent and extended a short distance into the flow stream. This apparently caused some local flow separation which resulted in a lower static pressure in this portion of the nozzle entrance station.

The corresponding cruise nozzle and rotating hood temperature distributions are shown in Figure 5-37. There were 16 thermocouples imbedded in the "D" vented nozzle walls. At all test conditions, even with core temperatures as high as 540°C, the temperature at the walls did not exceed approximately 50°C.

Since 50°C is the temperature of the fan stream air, these data indicate that the core stream does not penetrate the fan stream during the turn in the nozzle. Hence, mixing of the fan and core streams is incomplete. The low temperatures measured at the walls also mean that neither high temperature materials nor cooling air will be required for a production "D" vented nozzle. Therefore, the weight and cost of a production nozzle can be reduced from previous estimates.

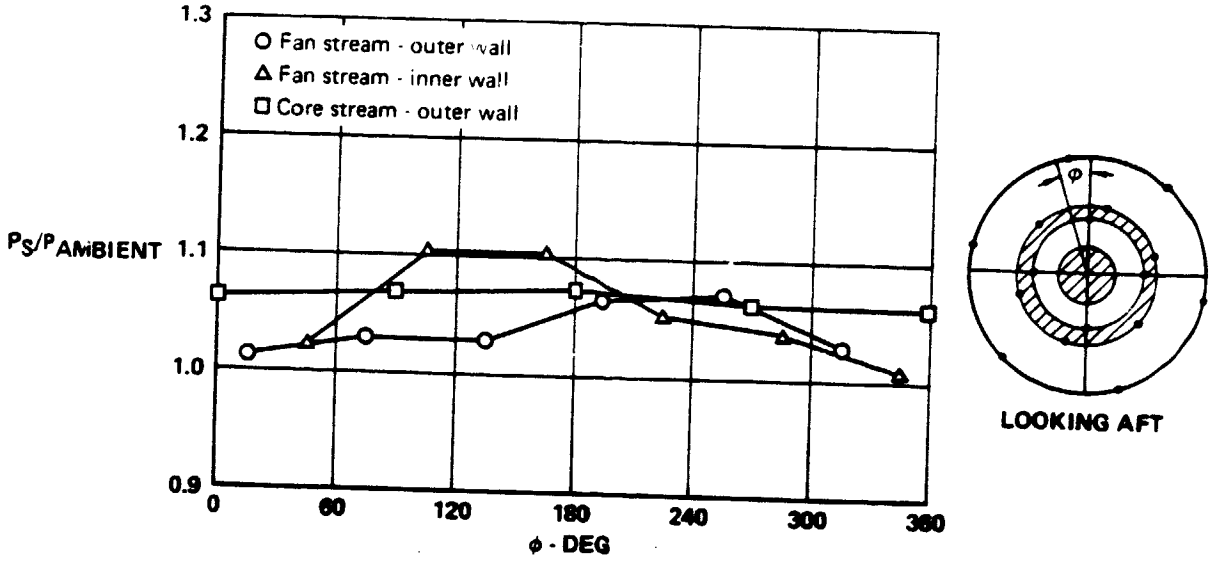

Figure 5-31. Circumferential Wall Pressure Distributions
Nozzle Entrance Station Hood Rotation Angle = 35°

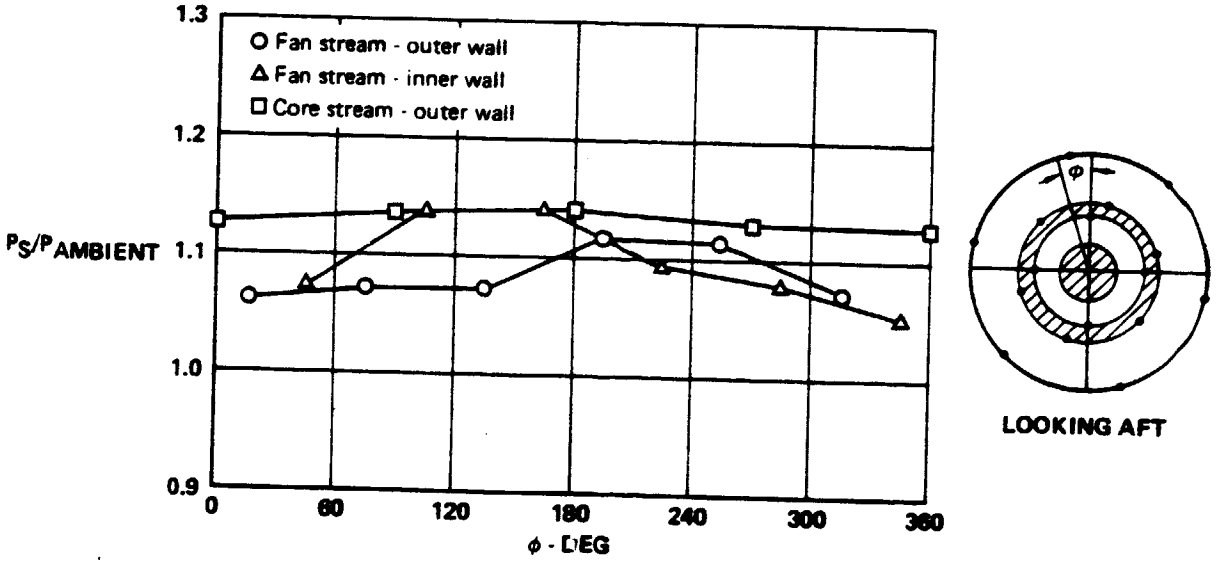

Figure 5-32. Circumferential Wall Pressure Distributions
Nozzle Entrance Station Hood Rotation Angle = 60°

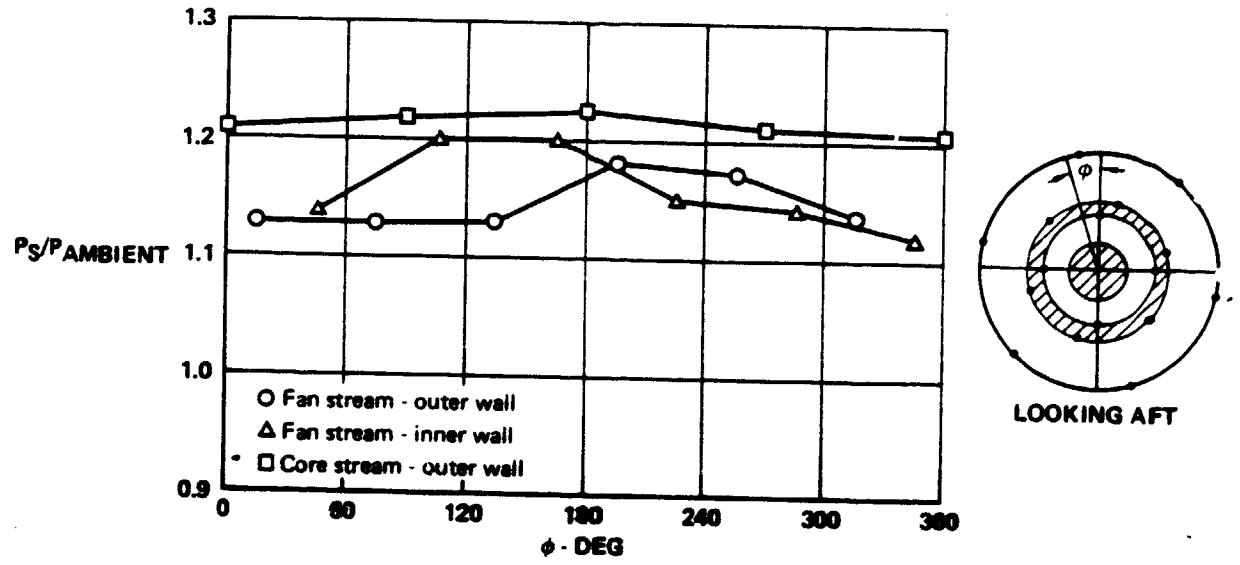

Figure 5-33. Circumferential Wall Pressure Distributions
Nozzle Entrance Station Hood Rotation Angle = 100°

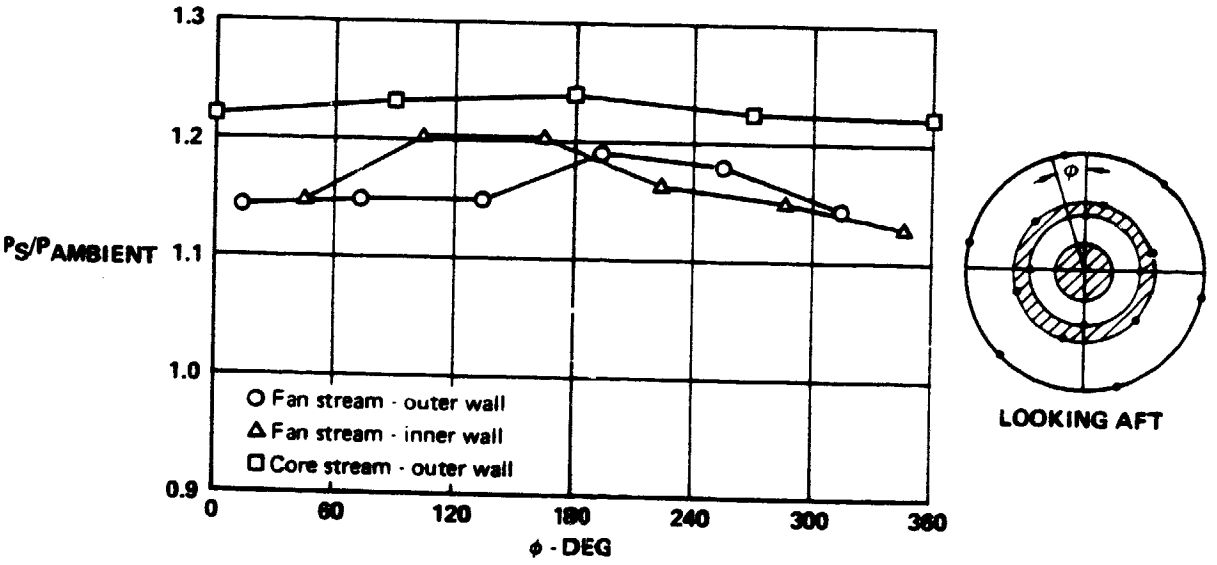

Figure 5-34. Circumferential Wall Pressure Distributions
Nozzle Entrance Station Hood Rotation Angle = 110°

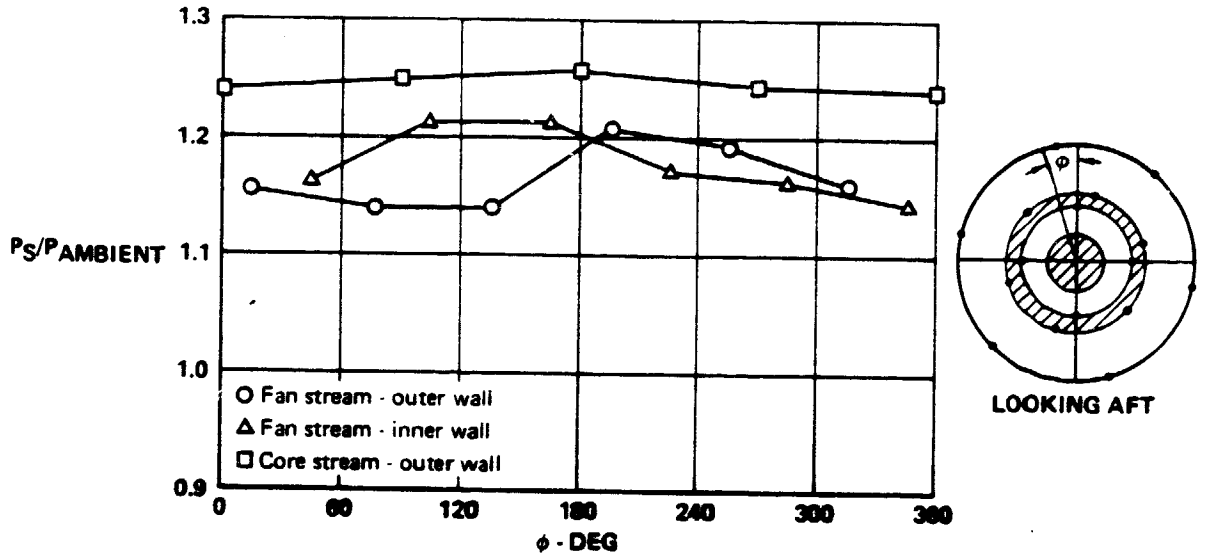

Figure 5-35. Circumferential Wall Pressure Distributions
Nozzle Entrance Station Hood Rotation Angle = 120°

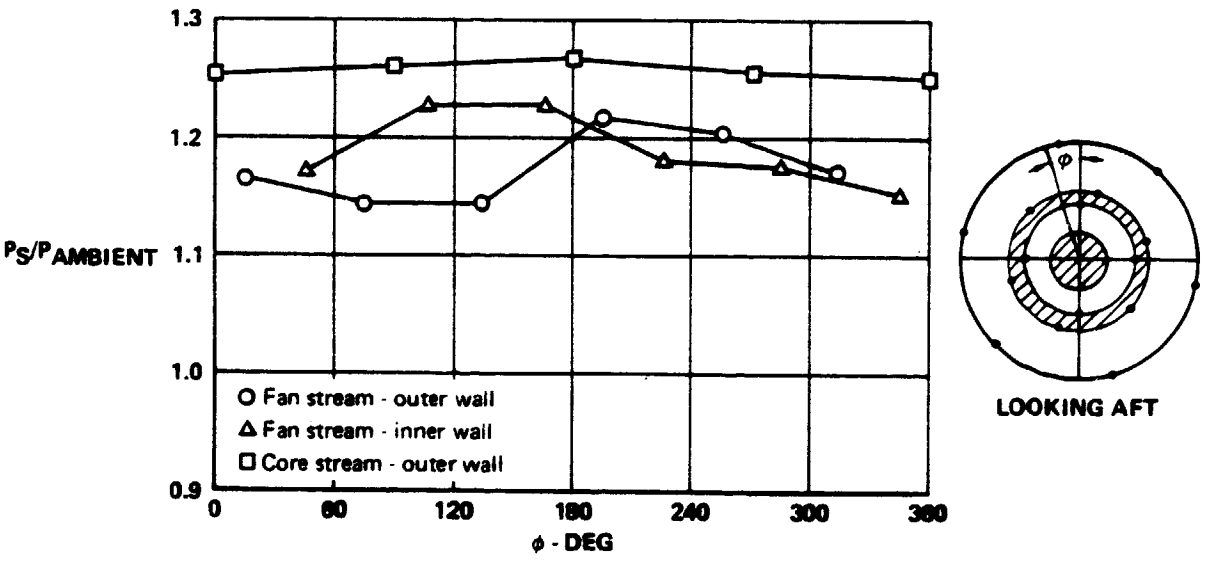

Figure 5-36. Circumferential Wall Pressure Distributions
Nozzle Entrance Station Hood Rotation Angle = 130°

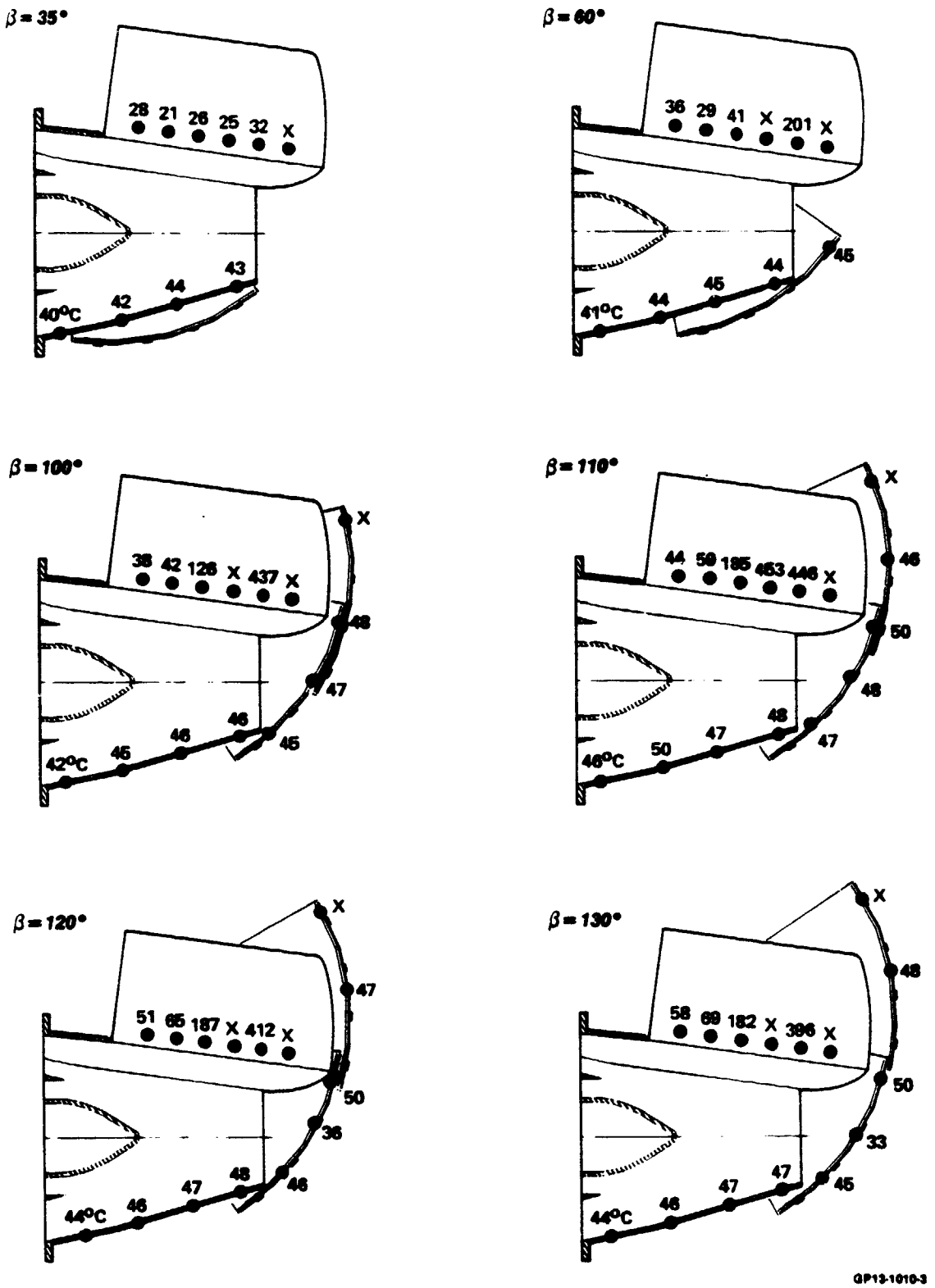

Figure 5-37. Wall Temperature Distributions
"D" Vented Nozzle

Also shown in Figure 5-37 are the temperatures recorded on the yaw vane. Even though one or two thermocouples were not working at each vector angle, the general location of the core stream can be identified. As with the nozzle wall thermocouples, these data indicate a low level of mixing of the fan and core streams.

5.3.6 YAW VECTORING PERFORMANCE - The lateral vectoring capability of the single yaw vane was investigated during the test program. Vane deflection angles of 10°, 18° and 25° were tested. The results are illustrated in Figure 5-38 in terms of the variation of vane deflection angle, velocity coefficient, and specific corrected flow with lateral vector angle. At the VTO position, 24 degrees of vane deflection were required to produce 8 degrees of lateral vectoring. Also, at this 24 degree yaw vane setting, a 4.6 percent decrease in velocity coefficient was recorded.

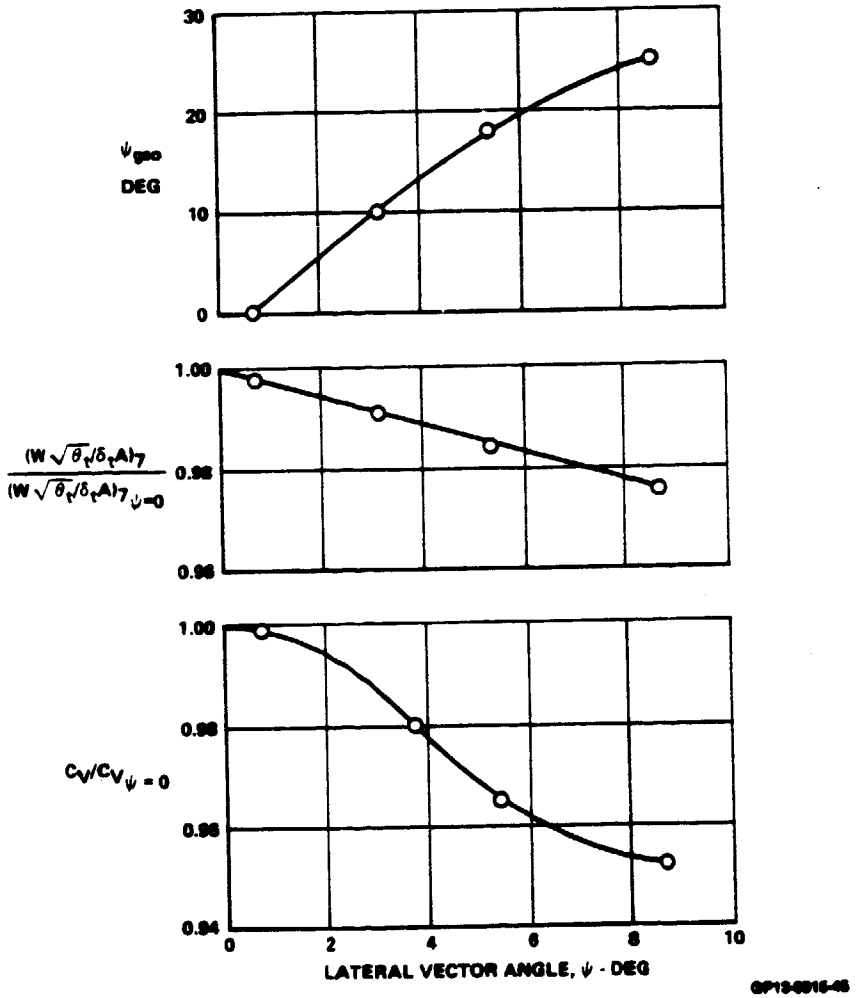

Figure 5-38. Yaw Vectoring Performance
Hood Rotation Angle = 110°
NPR = 1.35

5.3.7 YAW VANE AND BEAM REMOVAL - An alternate "D" vented nozzle concept under investigation does not require a yaw vane. To evaluate this configuration, the yaw vane and beam were removed and the nozzle was tested in the 110° hood rotation position. The results of these tests are shown in Figure 5-39 in the form of a VTO performance map. Nozzle performance with the yaw vane removed appears to be less sensitive to exit area changes. Overall, the performance improved at the larger exit areas and decreased slightly at the smallest exit area, relative to the "vane in" configuration. This latter result is unexpected because removal of the beam and vane eliminates a source of total pressure loss.

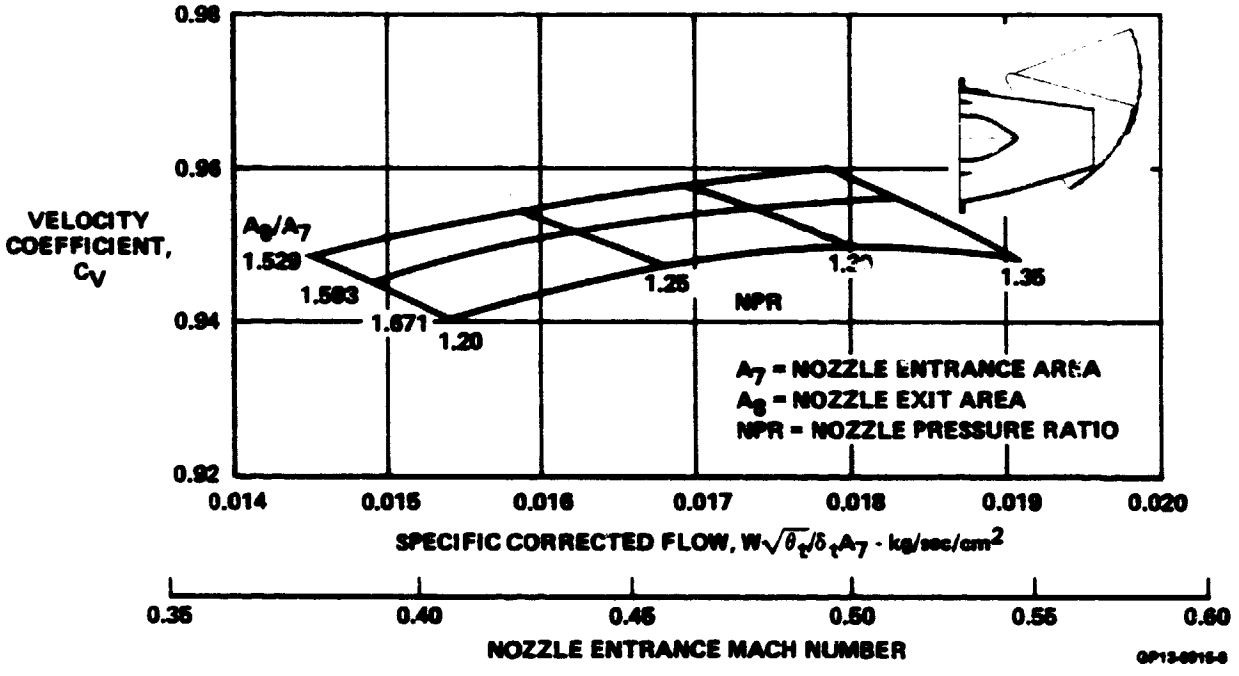

Figure 5-39. VTO Performance Map
Yaw Vane and Beam Removed
90° Thrust Vector Angle

5.3.8 PERFORMANCE IN GROUND EFFECTS - Tests were conducted with the nozzle in the 110° geometric position (VTO) and the ground plane at heights of 47.5 inches, 78 inches, and 102 inches. The ground plane height was measured from the hood pivot point on the "D" vented nozzle. When put in the form of a ratio of height from the ground plane to nozzle equivalent exit diameter (H/D), the three values tested were 1.03, 1.70, and 2.22.

The influence of the presence of the ground plane on nozzle performance appeared to be minimal. Figure 5-40 shows corrected thrust and corrected fan flow versus corrected fan speed. There appears to be a slight increase in thrust with decreasing H/D, while the fan flow rate remains essentially constant. Corrected thrust versus nozzle corrected flow, included in Figure 5-41, also shows essentially no variation with H/D. From Figures 5-40 and 5-41 we can conclude that no degradation in nozzle performance in ground effect was observed on this test.

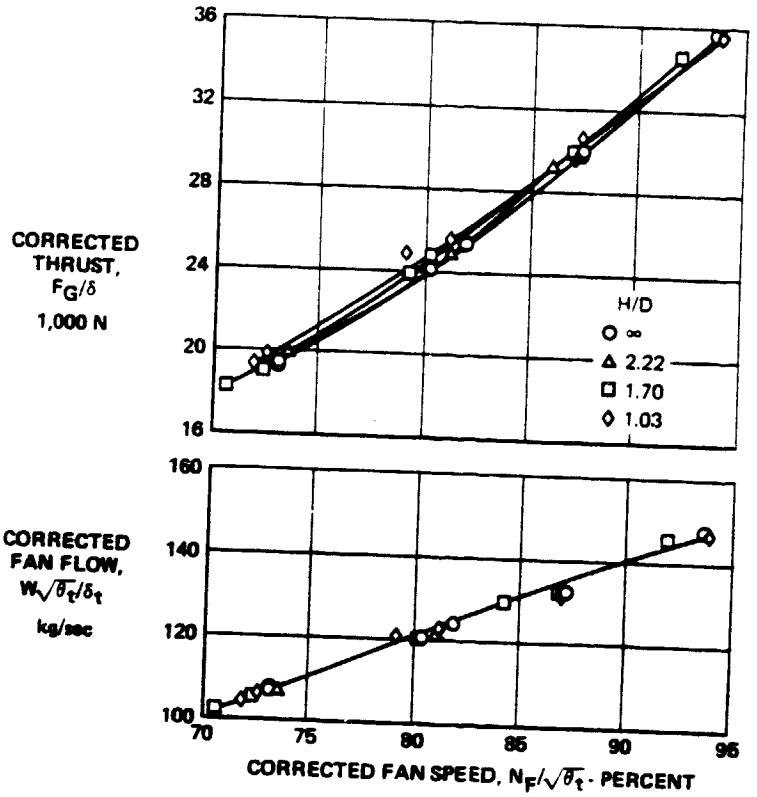

Figure 5-40. Performance in Ground Effect
Thrust and Flow vs Fan Speed Characteristics
Hood Rotation Angle = 110°

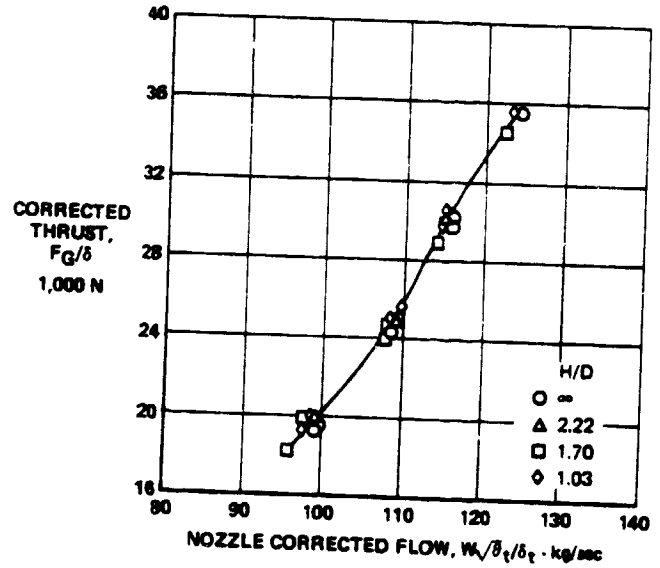

Figure 5-41. Performance in Ground Effect
Corrected Thrust vs Nozzle Corrected Flow
Hood Rotation Angle = 110°

The total pressure and temperature characteristics of each component flow and the percentage of the total flow deflected in each direction along the ground plane were determined from the four, twelve-probe rakes. A summary of these data is presented in Figure 5-42, including average total pressure ratio, average total temperature, and percent mass flow in each direction. The data indicate that the largest percentage of the flow exhausts to the rear at H/D's of 1.70 and 2.22, and exhausts forward at the lowest ground height, an H/D of 1.03. This latter result may be due to the non-uniform velocity profile at the nozzle exit. The exhaust flow at the back of the hood exits the nozzle at 110°, while the flow at the front of the nozzle leaves at less than 90°. Normally, the overturned flow at the rear of the nozzle would be strongly influenced by the underturned flow in the forward portion of the nozzle and would be turned back to approximately 90°. However, at low ground heights the overturned flow is intercepted by the ground plane before it is fully influenced by the underturned flow. This situation results in more of the exhaust flow being forced forward.

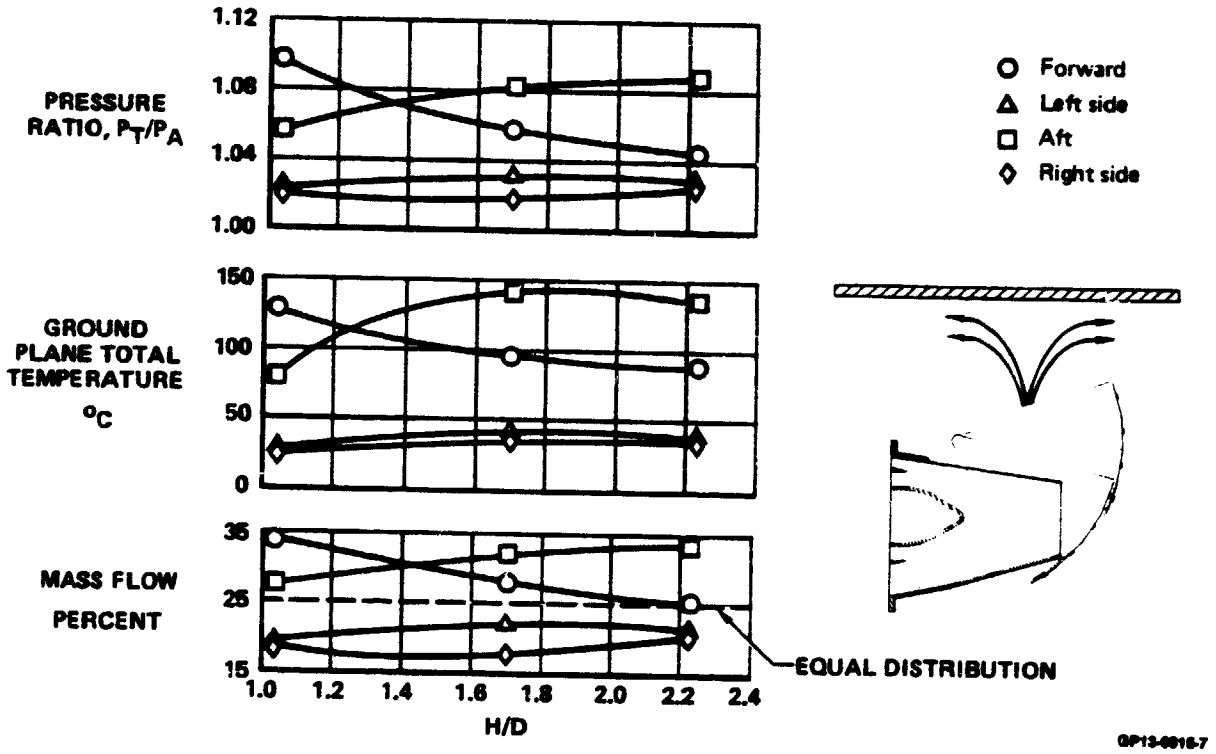

Figure 5-42. Performance in Ground Effect
Nozzle Exhaust Flow Characteristics
Hood Rotation Angle = 110°

5.4 LARGE SCALE - SMALL SCALE DATA COMPARISONS

The results from the current NASA-Ames large scale test program can be compared with data from a previous MCAIR 10% scale "D" vented nozzle test, Reference 4. Before making these comparisons, it should be noted that several differences exist between the large and small scale models. The three major differences in the small scale model, shown schematically in Figure 5-43, were that (1) it used an air supply rather than a real engine, (2) both fan and core streams were at ambient temperature, and (3) it contained no core hub. Comparisons of the VTO performance and vectoring efficiencies of the large and small scale models presented below.

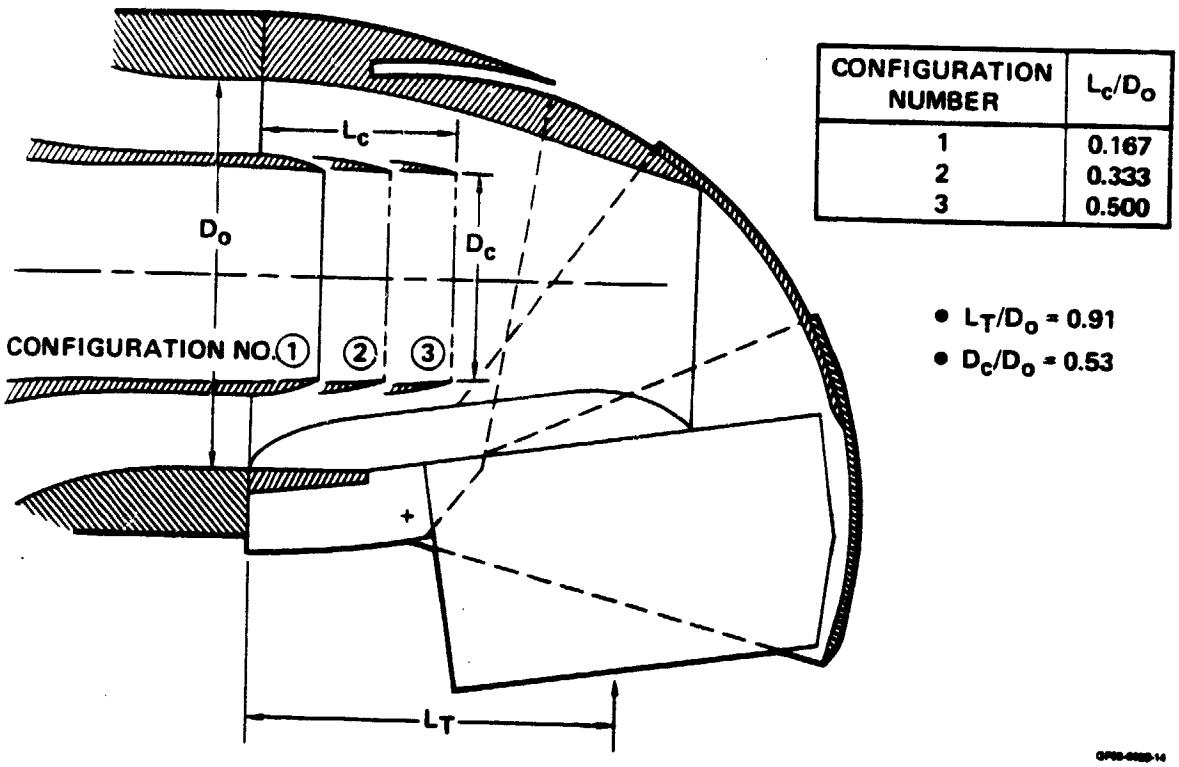

Figure 5-43. 10% Scale "D" Vented Nozzle Model
Dual Flow Turbofan Geometry

5.4.1 VTO PERFORMANCE - Figure 5-44 presents a VTO performance map from the MCAIR 10% scale model test, along with VTO performance data from the current test program. The large and small scale data agree within 1/2% at an area ratio of 1.526. However, the data from the large scale test exhibit a greater sensitivity of velocity coefficient to nozzle exit area (nozzle entry Mach number) than do the small scale data. This results in increased differences between the two sets of data as exit area is increased, with the large scale data having the lower performance. There is also a difference in the slope of the constant NPR lines. The much steeper slopes of the large scale data, together with the greater sensitivity to nozzle area changes, may be due to the presence of the core hub. The total pressure losses across the hub increase rapidly with increasing Mach number and, therefore, affect the relationship between the velocity coefficient and Mach number.

It should be noted that the "D" vented nozzle aerodynamic design point for aircraft applications generally lies in the 0.4-0.5 Mach number range and above nozzle pressure ratios of 1.3. In this region of interest, also illustrated in Figure 5-44, the large and small scale data exhibit similar performance levels.

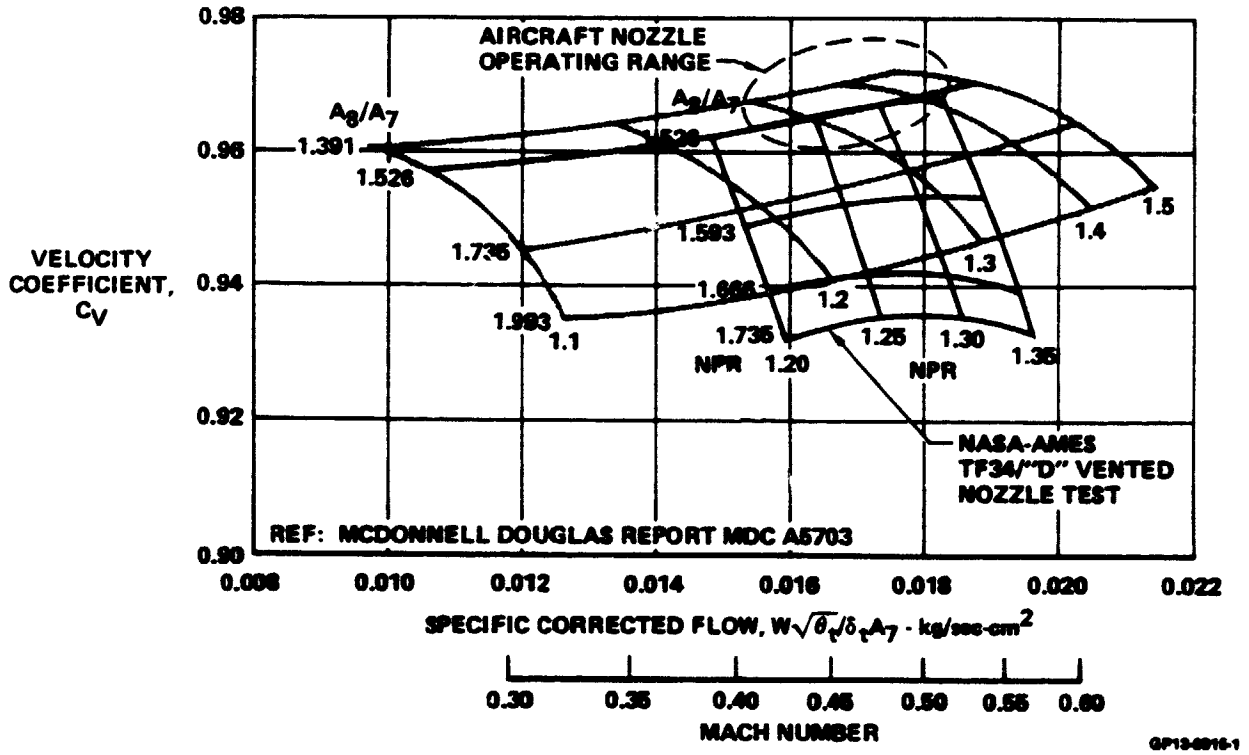

Figure 5-44. "D" Vented Nozzle VTO Performance Comparison
90° Thrust Vector Angle

5.4.2 VECTORING EFFICIENCY - Vectoring performance from the current test can also be compared with previous small scale data. Comparisons of longitudinal and lateral vectoring efficiency are included in Figures 5-45 and 5-46, respectively. The data are presented in the form of vector angle versus deflection angle. In both cases, the large and small scale data are in good agreement.

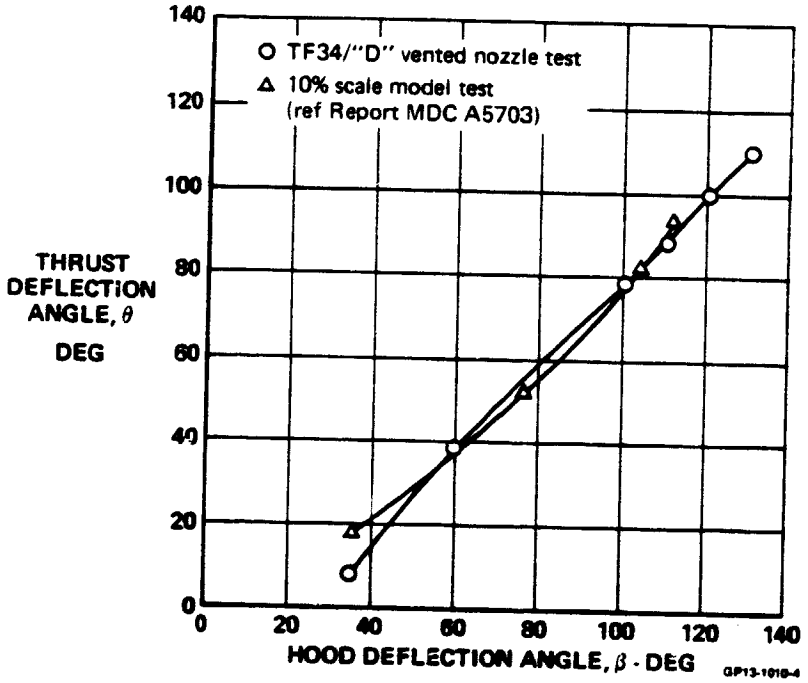

Figure 5-45. Comparison of Large and Small Scale Longitudinal Vectoring Efficiency

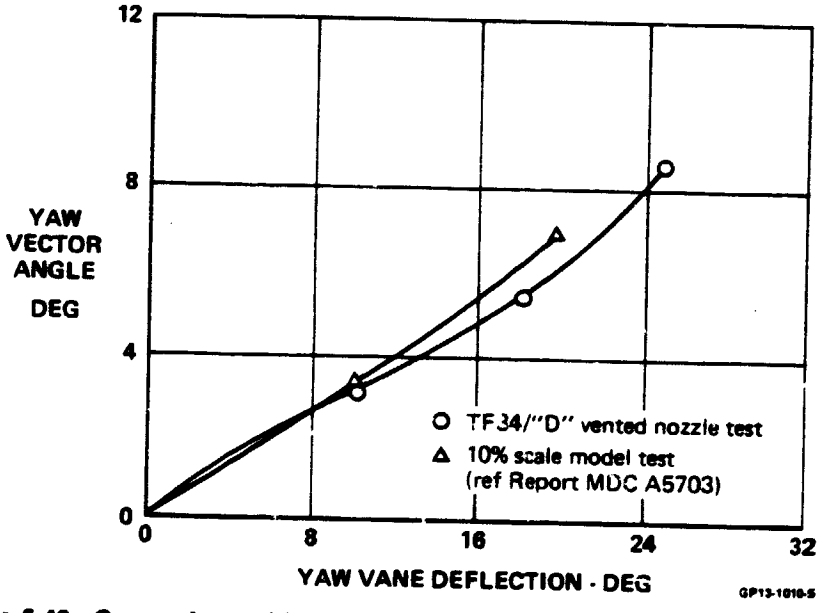

Figure 5-46. Comparison of Large and Small Scale Yaw Vectoring Efficiency

6. CONCLUSIONS

A large scale "D" vented thrust deflecting nozzle was successfully tested with a GE YTF-34-F5 turbofan engine. The test was conducted to obtain nozzle performance characteristics, demonstrate the compatibility of the nozzle with a turbofan engine, obtain pressure and temperature distributions on the surface of the "D" vented nozzle, and establish a correlation of the nozzle performance between large scale and small scale models. As stated previously in the Summary, significant test results included:

- Compatibility between the YTF-34-F5 turbofan engine and the "D" vented nozzle was demonstrated. Total pressure distortion levels were approximately the same for both the calibration nozzle and the vectored "D" nozzle. No significant effects of nozzle vectoring on engine operation were observed.

- A high level of VTO nozzle performance ($C_V \geq .96$) was obtained with a boilerplate nozzle. The "D" vented nozzle was shown to be a highly efficient thrust vectoring device for subsonic V/STOL aircraft applications, and the nozzle concept is now ready for in-flight demonstration.

- The "D" vented nozzle walls remained cool ($\leq 50°C$) during all test conditions. This indicates that mixing of the fan and core streams is incomplete. As a result of the low wall temperatures, production nozzles will not require high temperature materials.

- Good agreement was found between the current large scale data and previous small scale data in the expected aircraft nozzle operating range. Larger differences in the two sets of data were noted outside of this range. Good large scale-small scale agreement was demonstrated for both longitudinal and yaw vectoring efficiencies.

- No degradation of engine/nozzle performance in ground effect was observed. Both thrust and mass flow were insensitive to operation in the ground effect region.

Additional results obtained during the test program showed that:

- The ability of the yaw vane to provide lateral vectoring was successfully demonstrated.

- The baseline (forward core) configuration displayed the highest performance of the various core configurations tested. Moving the core exit closer to the "D" vented nozzle reduced performance, as did increasing or decreasing the core nozzle exit area from the baseline position.

7. REFERENCES

1. Rosenberg, E. W. and Esker, D. W., "Development of the "D" Vented Thrust Deflecting Nozzle", AIAA-80-1856, August 1980.

2. Watson, T. L., "Tests of a "D" Vented Thrust Deflecting Nozzle Behind A Simulated Turbofan Engine", McDonnell Douglas Report MDC A6930, May 1981.

3. Esker, D. W. "Ground Test of the "D" Shaped Vented Thrust Vectoring Nozzle", NASA CR-137959, October 1976.

4. Esker, D. W., "D" Vented Nozzle Thrust Vectoring Performance Tests Using a 10% Scale Dual Flow Model", McDonnell Douglas Report MDC A5703, June 1979.

APPENDIX A

Data Analysis Procedure

Nozzle performance was evaluated in terms of velocity coefficient, C_V, and discharge coefficient C_W. Ideal thrust and ideal flow rate were calculated assuming separate (unmixed) fan and core streams. The nozzle sizing parameter is specific corrected flow, from which nozzle entrance Mach number can be calculated using isentropic relationships. A definition of the model station designations is presented in Figure A-1.

Key performance parameters were calculated from the expressions below.

Mass averaged nozzle entrance total pressure ratio

$$NPR = \frac{NPR_{16} * W_{16} + NPR_{56} * W_{56}}{W_{16} + W_{56}} \quad (1)$$

Mass averaged nozzle entrance total temperature

$$TT_7 = \frac{TT_{16} * W_{16} + TT_{56} * W_{56}}{W_{16} + W_{56}} \quad (2)$$

The ideal gross thrusts for the fan and core stream are

$$F_{G_{I_x}} = \frac{W_x}{g} * \sqrt{T_{T_x}} \left(\frac{2\gamma R^{\frac{1}{2}}}{\gamma-1}\right) [1-(NPR_x)^{\frac{-(\gamma-1)}{\gamma}}]^{\frac{1}{2}} \quad (3)$$

where x = 16 - denotes fan stream

x = 56 - denotes core stream

Then the velocity coefficient is computed from

$$C_V = \frac{F_G}{F_{G_{I_{16}}} + F_{G_{I_{56}}}} \quad (4)$$

where F_G = measured resultant gross thrust

To determine the nozzle discharge coefficient we need to calculate both fan and core stream effective exit areas. These are computed from

$$AE_{8_x} = \frac{W_x \sqrt{T_{T_x}}}{g \left[\frac{2\gamma}{R(\gamma-1)}\right]^{\frac{1}{2}} \left\{(NPR_x)^{\frac{\gamma-1}{\gamma}} \left[(NPR_x)^{\frac{\gamma-1}{\gamma}} - 1\right]^{\frac{1}{2}}\right\}} \quad (5)$$

where x = 16 - denotes fan stream
x = 56 - denotes core stream

The flow coefficient then becomes

$$C_W = \frac{AE_{8_{16}} + AE_{8_{56}}}{A_8} \quad (6)$$

The expression for the nozzle sizing parameter, specific corrected flow, is

$$W\sqrt{\theta_t}/\delta_t A_7 = \frac{(W_{16} + W_{56}) * \sqrt{T_{T_7}}}{NPR * P_a * (A_{16} + A_{56})} * \frac{P_{std}}{\sqrt{T_{std}}} \quad (7)$$

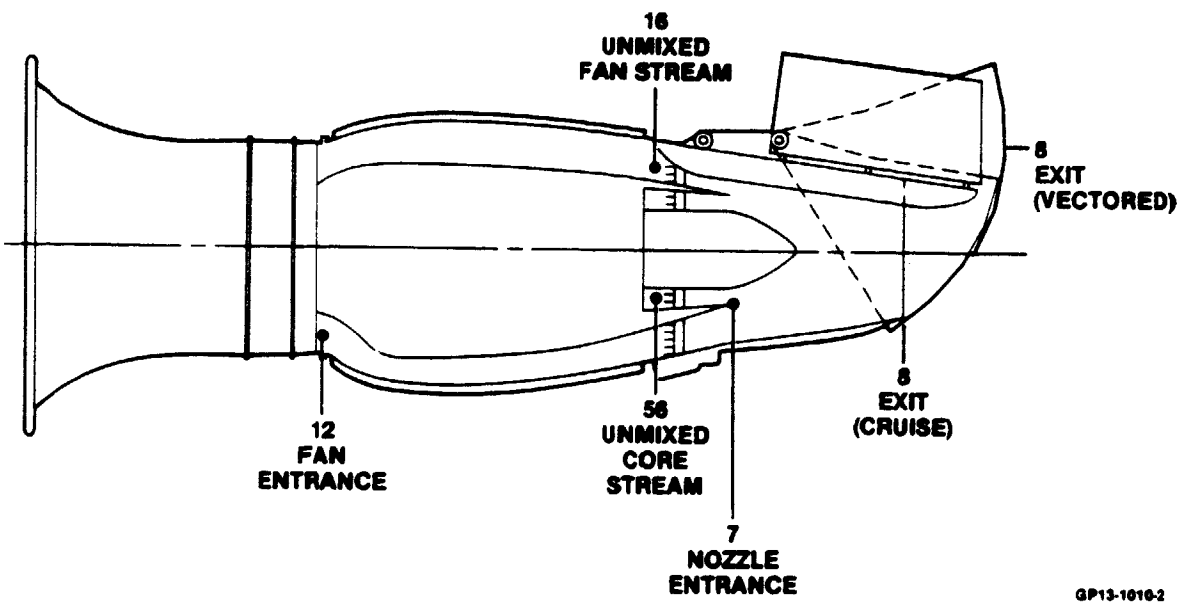

Figure A-1 Model Station Designations

END

DATE

FILMED

MAY 24 1982